GRK 1782

"Functionalization of Semiconductors"

Seminar 2015

Schloss Bettenburg, Hofheim/Unterfranken, 07.10.2015 – 09.10.2015

Research Summaries

supported by: DFG Deutsche Forschungsgemeinschaft

Graduiertenkolleg 1782

„Functionalization of Semiconductors“

Seminarzentrum Schloss Bettenburg, Hofheim

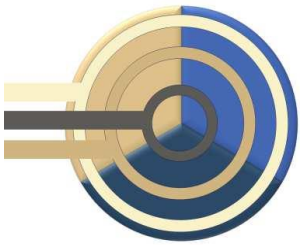

Program Seminar 07. – 08.10.2015

Wednesday, 07.10.2015

till 11:30	Arrival
12:00 – 12:30	Welcome Snack
13:00 – 13:10	**Introduction**: *Kerstin Volz*
	Session I Chair: *Andreas Stegmüller*
13:10 – 13:30	*Benjamin Ringler:* Novel interpnictogenes as possible group 15 single source MOVPE precursors
13:30 – 13:50	*Eduard Sterzer:* Novel precursor for Ga(NAs) MOVPE growth with high efficient N incorporation
13:50 – 14:10	*Lukas Nattermann:* MOVPE growth of dilute Bi containing III/V materials for efficient optoelectronics application
14:10 – 14:30	Break
	Session II Chair: *Phil Rosenow*
14:30 – 14:50	*Lars Finger:* Ionic Liquids with Chalcogenide Anions and their Application for the Synthesis of Amorphous MoS_2
14:50 – 15:10	*Jens Eußner:* Functional Organotetrel Chalcogenide Clusters
15:10 – 15:30	*Susanne Pulz:* Substituted Amidines, Guanidines and Formazanes: Hydrazine-Based Ligands for the Synthesis of MOVPE-Precursors
15:30 – 16:00	Coffee Break
	Session III Chair: *Philip Springer*
16:00 – 16:20	*Sebastian Gies:* Optical and Electronic Properties of Ga(N,As,P) Quantum Wells on Silicon for Laser Application
16:20 – 16:40	*Christian Lammers:* Time resolved photoluminescence spectroscopy on Ga(NAsP)/Si MQWs
16:40 – 17:00	*Nils Rosemann:* Nonlinear optical properties of adamantane-like functionalised semiconductor clusters
17:00 – 17:20	Break

Session IV Chair: *Marcel Reutzel*

17:20 – 17:40 *Phillip Springer:* Consequences of Anisotropic Electron Masses on THz Absorption

17:40 – 18:00 *Phil Rosenow:* Structural and chemical effects on the electronic structure of semiconductor alloys

18:00 – 18:20 *Andreas Stegmüller:* Insight into GaP-Si semiconductor interfaces from DFT

19:00 Dinner

Thursday, 08.10.2015

08:00 – 09:00 Breakfast

Session V Chair: *Jan Oliver Oelerich*

09:00 – 09:20 *Alexandra Ostapenko:* Surface etching of single crystalline ZnO by phosphonic acid based SAMs

09:20 – 09:40 *Paul Rotter:* Molecules on Rails: Coupling of Diffusion and Orientation for Pentacene on an Organic Surface

09:40 – 09:50 Break

Session VI Chair: *Andreas Beyer*

09:50 – 10:10 *Lennart Duschek:* Structural formation processes of III/V semiconductors in HAADF STEM

10:10 – 10:30 *Katharina Werner:* Chemical vapor deposition and physical characterization of gallium, and carbon-related structures on Si (001) and GaP/Si (001) templates for the growth of graphene layers

10:30 – 10:50 *Marcel Reutzel:* Binding Energy and Dissociation Barrier - Experimental Determination of the Key Parameters of the Potential Energy Curve of Diethyl Ether on Si(001)

10:50 – 11:00 Break

Session VII Chair: *Sebastian Gies*

11:00 – 11:20 *Lars Kraft:* An introduction to NMR at surfaces

11:20 – 11:40 *Martin Wiemer:* Theory to generation, transport, and recombination of carriers in disordered materials

11:40 – 12:00 *Nadeem Sabir:* Manganese doped semiconductor quantum dot structures

12:00 – 13:30 Lunch Break

13:30 – 16:00 **Poster Session**

1. *Andreas Beyer:* Quantitative Determination of Chemical Composition of Multinary III/V Semiconductors with Sublattice Resolution using Aberration Corrected HAADF-STEM
2. *Florian Dobener:* Gain Measurements of Ga(NAsP)/(BGa)(AsP) Heterostructures
3. *Lars Finger:* Low Temperature Synthesis of MoS_2 from Tetrathiomolybdate and Sulfide Ionic Liquids
4. *Lars Kraft:* Tailoring specimens for nuclear double resonance experiments on single crystal surfaces
5. *Christian Lammers:* Generation of high power THz pulses by tilted-pulse-front excitation
6. *Jan Oliver Oelerich:* Computer Simulation of Growth Kinetics of Compound Semiconductors
7. *Andre Pick:* Site-selective deposition of perylene and polymorph-selective growth of single-crystals
8. *Christian Prinzisky:* Absorption and Photoluminescence Spectroscopy of Anthraquinone Dyes
9. *Susanne Pulz:* New MOCVD-Precursors with Application in the Synthesis of Group III/V Semiconductor Compounds
10. *Marcel Reutzel:* Adsorption Dynamics of Organic Molecules on Si(001) - Control of Reactivity
11. *Niklas Rinn:* Binary and Ternary Orgaotin Selenide Clusters
12. *Johannes Röder:* Optical and Magnetic Studies of MBE-grown Ferromagnetic CrSe and CrS-layers in Zincblende Structure
13. *Phil Rosenow:* On the interplay of the spatial and electronic structure in ternary and quarternary III/V semiconductors
14. *Nadeem Sabir:* ZnO nanoparticles
15. *Phillip Springer:* On optical properties of nitride containing quantum wells
16. *Mikko Wilhelm:* Energy transfer characteristics in Mn doped CdS/ZnS quantum dots
17. *Johannes Völkner:* Towards Spatially Resolving Photoelectrochemical Sensors

Workshop

Chemical Contributions to Semiconductor Development – in Vitro and in Silicio

Program Workshop 09.10.2015

Friday, 09.10.2015

09:00 – 10:00	*Prof. Dr. Andreas Schnepf*, Institut für Anorganische Chemie der Eberhard Karls Universität Tübingen Cryochemistry
10:00 – 11:00	*Dr. Ralf Tonner*, FB Chemie, Philipps-Universität Marburg Bonding analysis
11:00 – 11:30	Coffee
11:30 – 12:30	*Prof. Dr. Axel Schulz*, Institut für Anorganische Chemie der Universität Rostock und Leibnitz-Institut für Katalyse, Rostock [(Un)usual] Reaction Media
12:30 – 13:30	Lunch Break
13:30 – 14:30	*Prof. Dr. Andreas Schnepf*, Institut für Anorganische Chemie der Eberhard Karls Universität Tübingen Chemistry With Outer Space Molecules: Insights into the borderland between molecules and the solid state of (semi-)metals
14:30 – 15:30	*Dr. Ralf Tonner*, FB Chemie, Philipps-Universität Marburg In silico functionalization - from precursor chemistry to surface reactions with quantum chemical methods
15:30 – 16:00	Coffee
16:00 – 17:00	*Prof. Dr. Axel Schulz*, Institut für Anorganische Chemie der Universität Rostock und Leibnitz-Institut für Katalyse, Rostock Pnictogen Chemistry: Ions, Rings, Radicals, Biradicals and more

Novel Interpnictogenes as Possible Group 15 Single Source Precursors

Benjamin Ringler, Carsten von Hänisch

Faculty of Chemistry and Material Sciences Center, Philipps-Universität Marburg

Introduction

In our working group we synthesize and characterize novel interpnictogenes and study their chemical properties. Furthermore we investigate the application as group 15 single source precursor for metal organic vapor phase epitaxy (MOVPE) together with the working group of professor Volz.

Results

In 1969 Scherer and Janssen described the preparation of tBu$_2$AsNH$_2$ briefly.[1] We expected this compound to have the optimal requirements serving as precursor for MOVPE: It has bulky *t*butyl groups on arsenic that lead to stable radicals during the decomposition in the MOVPE reactor. This and the absence of a nitrogen carbon bond both result in a low carbon incorporation, which is vital for semiconductor layers. Therefore we synthesized tBu$_2$AsNH$_2$ at a large scale by first preparing tBu$_2$AsCl and subsequent passing of ammonia into the solution.

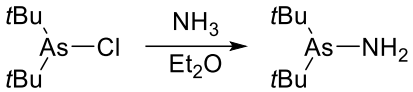

Fig.1: Preparation of tBu$_2$AsNH$_2$.

Our cooperation partner, the working group of professor Volz, used tBu$_2$AsNH$_2$ (DTBAA) as single source precursor (SSP) for nitrogen and arsenic to grow nitrogen containing gallium arsenic semiconductor layers. Following studies confirmed that high quality Ga(NAs) were grown with good structural and optoelectronic properties using tBu$_2$AsNH$_2$.[2]

These results motivated us to design novel compounds containing two group 15 elements, called interpnictogenes, that could be used as SSP. Firstly we prepared the starting material tBu$_2$SbCl. Based on the preparation developed by Hartmann, Kühl and Issleib in the 1960s, we improved the synthesis and were able to prepare the product in large quantities.[3,4] A lithium chloride salt elimination lead us to several novel stibano amines (figure 2).

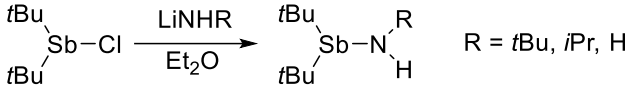

Fig.2: Preparation of stibano amines via lithium chloride salt elimination.

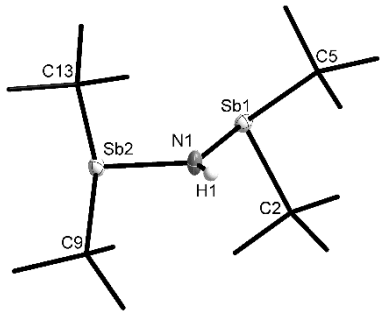

Fig.3: Molecular structure of (tBu$_2$Sb)$_2$NH in the crystal.

Among them we achieved the antimony analog of tBu$_2$AsNH$_2$. The purification of the *t*butyl and *i*propyl substituted amines was done by distillation. tBu$_2$SbNH$_2$ cannot be purified under these conditions because the condensation to a colorless solid of (tBu$_2$Sb)$_2$NH occurred. Its molecular structure in the crystal is shown in figure 3.[5]

The reaction of tBu$_2$SbNH$_2$ with MEt$_3$ (M = Al, Ga, In) lead to the formation of the four membered rings containing alternating nitrogen and the group 13 metal. They are the first examples of antimony substitution among the otherwise well-known M_2N_2 rings.[5]

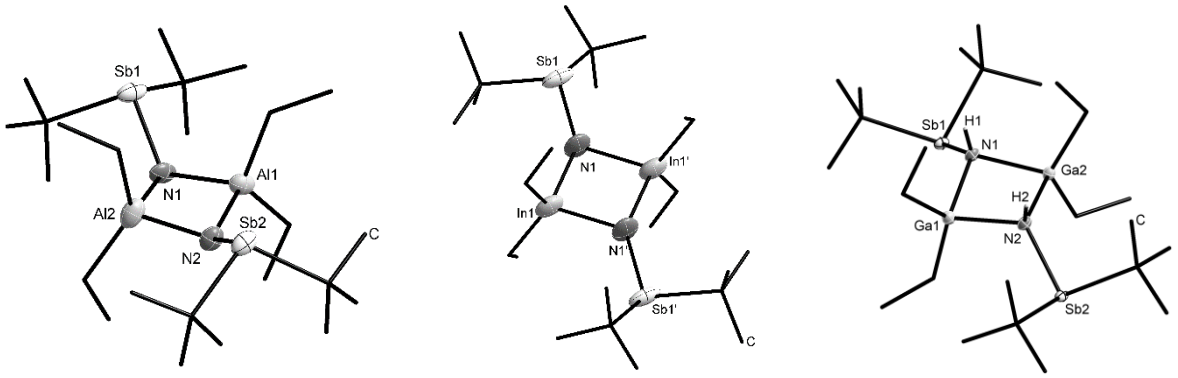

Fig.4: Molecular structures of [tBu$_2$SbN(H)MEt_2]$_2$ (M = Al, Ga, In) in the crystal.

Recently, we began investigations for disubstituted *t*butyl stibanes. As starting material we chose *t*BuSbCl$_2$ and nearly doubled the yield of its synthesis compared to the original literature.[6] Subsequent reactions with different amines lead to *t*butyl amino chloro stibanes. They can be converted to di-amino substituted stibanes by reacting them with lithiated amines. Additionally, the molecular structure of *t*BuSbCl(NH*t*Bu) in the crystal was determined (figure 5).

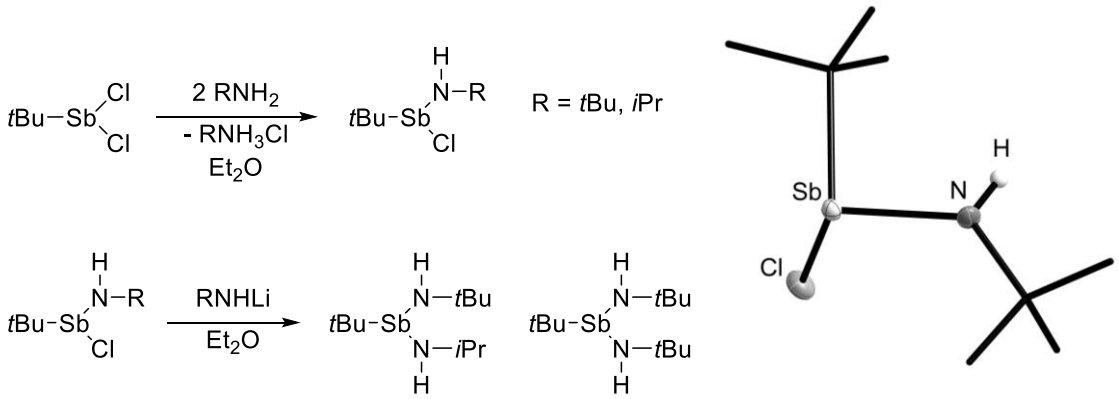

Fig.5: Preparation of di-amino substituted stibanes and molecular structure of tBuSbCl(NHtBu) in the crystal.

Conclusions and Outlook

We investigated the synthesis of tBu$_2$AsNH$_2$ and its application in the MOVPE process. Motivated by the results we developed new synthesis strategies to obtain novel inter-pnictogenes which are bearing favorable substituents for MOVPE. We are planning to expand our field of research towards arsenic containing interpnictogenes to achieve molecules like *t*BuAs(NH$_2$)$_2$, *t*BuAs(N(H)*t*Bu)$_2$ and *t*BuSb(NH$_2$)$_2$ as well as phosphorous containing molecules.

References

[1] O. J. Scherer, W. Janssen, *J. Organomet. Chem.* **1969**, *16*, 69–70.

[2] E. Sterzer, A. Beyer, B. Ringler, L. Duschek, R. Tonner, C. von Hänisch, W. Stolz, K. Volz, *manuscript in preparation* **2015**.

[3] H. Hartmann, G. Kühl, *Zeitschrift für Anorg. und Allg. Chemie* **1961**, *312*, 186–194.

[4] K. Issleib, B. Hamann, L. Schmidt, *Zeitschrift für Anorg. und Allg. Chemie* **1965**, *84*, 298–303.

[5] B. Ringler, Synthese und Charakterisierung Organisch Substituierter Interpnictogene, *Masterarbeit*, Universität Marburg, **2014**.

[6] H. J. Breunig, W. Kanig, *Chemiker-Zeitung* **1978**, *7/8*, 263–264.

Novel precursors for highly efficient N-incorporation in III/V semiconductors by MOVPE

E. Sterzer, A. Beyer, B. Ringler*, C. von Hänisch*, W. Stolz, K. Volz

*Material Sciences Center and Faculty of Physics/ *Faculty of Chemistry, Philipps-Universität Marburg, Germany*

Introduction

III/V semiconductors containing small amounts of Nitrogen are discussed in the context of several solar cell and laser applications. Such applications are typically hampered by the large amount of Carbon incorporation into the layers, which either stems from the Nitrogen precursor or from the group III-sources, where the Nitrogen – due to the high strength of the C-N bond – leads to the incorporation of C from the organic ligands of the other precursors. Furthermore, in the growth of these materials, a large excess of the N-precursor has to be offered in the gas phase in order to incorporate only small amounts of N. Conventionally UDMHy (unsymmetric dimethyl hydrazine) is used as a nitrogen precursor in MOVPE (metal organic vapour phase epitaxy) growth of dilute nitrides. We synthesized and purified a novel precursor (Di-tert-butyl-arsano-amin) for use in dilute nitride growth. This precursor has the advantage that no C-N bond exists in the molecule, which could reduce the C incorporation and increase the efficiency of semiconductor devices. We used this molecule – together with TEGa (triethylgallium) and, in some experiments, also with TBAs (tertiarybutylarsine) and/or TMIn (trimethylindium) – in low temperature growth of Ga(NAs) and (GaIn)(NAs).

Results

We observe an extremely high efficient N-incorporation from this molecule. It is also observed that the surface is smooth even in experiments without TBAs. The layer structures grown using DTBAA exhibit high structural quality, as shown in figure 1. Also, the quantum well structures exhibit room temperature photoluminescence at a position that would be expected from the N-content measured from HRXRD. The (GaIn)(NAs) experiments revealed a slightly increased N incorporation if into (GaIn)As compared to GaAs, which is different from the UDMHy experiments where a significant decrease of N incorporation was observed in (GaIn)(NAs) using with increasing In incorporation. This behavior was explained with a higher desorption rate of N in combination with In (ref.1). SIMS experiments showed C incorporation in the in region of 10^{18} Atoms/cm^3, which is the same magnitude as we observed in Ga(NAs) and (GaIn)(NAs) grown with UDMHy. Apart from C incorporation SIMS-measurements revealed also O incorporation which could stem from solvent used for synthesizing of DTBAA.

Conclusions

The newly synthesized and characterized N precursor DTBAA is a highly promising candidate for dilute N growth. The extraordinary high N incorporation efficiency makes the precursor preferable for dilute nitrides, as we don't have to float the reactor with N precursor, which affects strongly the growth conditions. The increase of N incorporation in (GaIn)(NAs) compared to Ga(NAs) makes the precursor even more interesting. We could not observe a lower C incorporation using DTBAA, but as also O is incorporating we expect impurities in the precursor, which are also incorporated during epitaxy.

Outlook

Next step is to synthesize a larger amount of DTBAA and to have it purified by an industry partner to be able to grow a significant amount of (GaIn)(NAs) and Ga(NAsP) samples for a detailed study of optical and electrical properties.

References

[1] Volz, K., Koch, J., Höhnsdorf, F., Kunert, B., & Stolz, W. (2009). MOVPE growth of dilute nitride III/V semiconductors using all liquid metalorganic precursors. *Journal of Crystal Growth*, *311*(8), 2418–2426. doi:10.1016/j.jcrysgro.2008.09.210

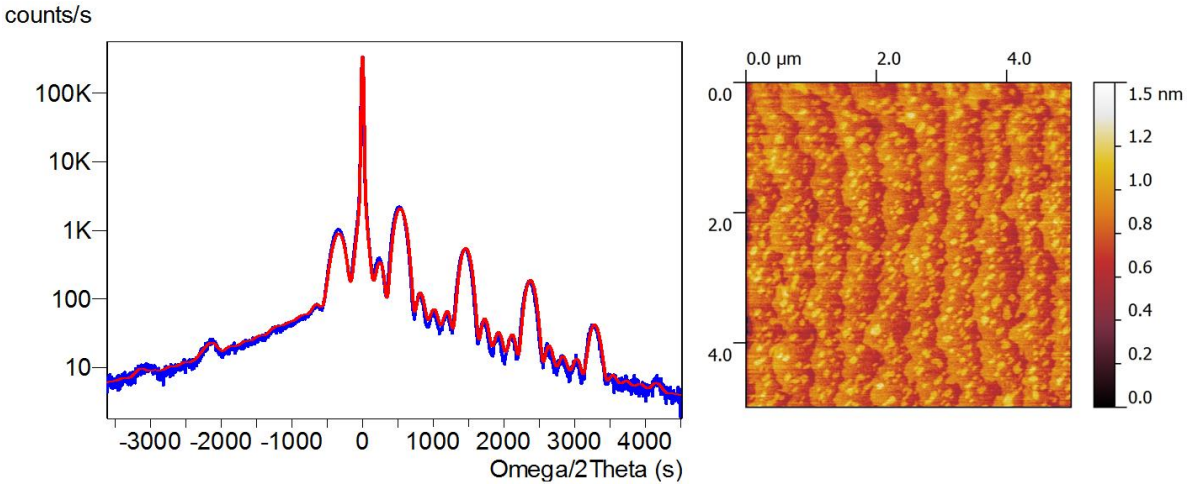

Fig.1: HRXRD profile of a Ga(NAs) sample on the left and an AFM picture of a Ga(NAs) surface.

MOVPE growth of Ga(PAsBi)/GaAs and Ga(NAsBi)/GaAs at low temperatures for infra-red light applications

L. Nattermann*, P.Ludewig, N. Knaub, E. Sterzer, W. Stolz, K. Volz

Faculty of Physics and Material Sciences Center, Philipps-Universität Marburg

Introduction

The incorporation of bismuth (Bi) in III/V semiconductors can play an important role in addressing the development of the new generation of highly efficient optoelectronic devices [1]. A major problem of most of the currently used telecom lasers is their low efficiency, which is around 20 % [2]. Cooling effort decreases the efficiency again by an order of magnitude. Bi leads to a strong reduction of the band gap by 80 meV per % Bi in GaAs and simultaneously shifts the spin orbit split off band to lower energies. Hence, loss processes could be suppressed for Bi fractions above 11 % Bi in GaAs [1], [3]–[5]. Furthermore, a decreased sensitivity of band gap energy to temperature has been observed which increases the efficiency of Bi containing devices additionally [6]. Nevertheless, the metal organic vapour phase epitaxy (MOVPE) growth of dilute Bi containing materials is challenging, as significant amounts of Bi are required. In previous studies it has been reported about a saturation level of the Bi incorporation in GaAs and that the saturation level depends on temperature and As/Ga ratio [7]–[10]. Indeed the Bi incorporation in high quality Ga(AsBi) using MOVPE is still limited to a Bi fraction of 7 %. Only in MBE grown samples Bi fractions of up to 20% have been realized, but temperatures as low as 200°C are required. The growth of Ga(AsBi) above the saturation level leads to the formation of Bi- and GaBi-droplets at the surface [11]. The mechanisms of Bi incorporation and the droplet formation are not literally understand yet. These mechanisms are subject of investigation in this work.

In previous studies we and others have already reported on the influence of hydrocarbon groups and the Bi surface coverage on the Bi incorporation [7], [8]. However we found that the usage of different kind of Bi sources with different hydrocarbon rest groups does not influence the growth of Ga(AsBi) [7]. Hence Ga(PAsBi) samples were realized in order to figure out what kind of effect the increasing compressive strain with increasing Bi incorporation has [12]. Recently we found that the Bi incorporation can be increased by increasing the P fraction, while the offer of Bi is kept constant, as long as the growth takes place in the saturation region. To err on the side of caution that the dependency between the offer of P and increasing Bi incorporation is strain induced, Ga(PAsBi) and Ga(NAsBi) layers were deposited and compared in this work. By growing two different kind of quaternary Bi structures, both with a smaller group V elements (P and N), it can be demonstrated that the by P and N compensated local strain leads to an increasing Bi incorporation.

Beside from that, both material systems, Ga(PAsBi) and Ga(NAsBi), are promising candidates for a 1 eV sub-cell in multi junction solar cells, as the band gap and the lattice constant can be tuned independently from each other. Hence the growth and a comparison of these structures is of interest for solar cell applications.

Results

Different Ga(AsBi), Ga(PAs), Ga(PAsBi) and Ga(NAsBi) layers are grown at 400°C on exact GaAs (001) substrates using Triethylgallium (TEGa), Tertiarybutylarsine (TBAs), Tertiarybutylphosphorous (TBP), Trimethylbismuth (TMBi) and unsymmetrical Dimethylhydrazine (UDMHy). The crystaline quality, growth rate and Bi incorporation were investigated using HR-XRD, transmission electron microscopy (TEM), secondary ion mass

spectrometry (SIMS) and atomic force microscopy (AFM) in order to understand the growth of the dilute bismide material systems.
We found that not only strain is a limiting factor for Bi incorporation but also the gas phase composition and related interactions between molecules and growth surface are important for the understanding of the growth process and to grow high quality crystals in a wide range of band gaps.
Figure 1 displays the dependency of strain induced by P, Bi and N in Ga(PAs), Ga(AsBi) and Ga(NAs) on the fraction of P, Bi and N. Following the addition of P and N, a tensile strain results, whereas the addition of Bi leads to a compressive strain in GaAs. In figure 1 the Bi incorporation in quaternary Ga(PAsBi) and Ga(NAsBi) is plotted versus the strain from P and N in ternary Ga(PAs) and Ga(NAs). The circular data points show the Bi fraction in the saturation region. The rhombical data points mark the Bi fraction below the saturation. It is obvious that in both cases, for Ga(PAsBi) and Ga(NAsBi), the strain compensation by the smaller group V atoms leads to the same increase in Bi incorporation. This indicates that beside of hydrocarbon groups at the growth surface and the Bi surface coverage, strain is an important parameter, which is responsible for the limitation of Bi incorporation in GaAs based crystals.
The empty circles in figure 1 are depicting the Bi fraction for a higher Pp(TMBi). The increase of the Bi fraction with increasing Pp(TBP) is even higher for higher Pp(TMBi). Hence, the effect of strain compensation increases for the growth further in the saturation region, as more Bi is at the growth surface that can be incorporated.
The rhombical data illustrate that below the saturation domain already in Ga(AsBi) all Bi is incorporated into the crystal. The introduction of P or N does not have an effect on the Bi incorporation, except for a slight decrease of the Bi fraction due to an enormous change of the gas phase and growth surface, due to the high partial pressures of TBP or UDMHy.

Conclusions

By the usage of the two smaller group V atoms P and N, the effect of local strain compensation was investigated. The comparison of Bi incorporation in the two quaternary material systems proved the importance of local strain for the limitation of Bi incorporation, beside other effects like Bi surface coverage and hydrocarbon groups at the growth surface.

Outlook

Further investigations on the formation of clusters in Ga(PAsBi) and Ga(AsBi) will be done in order to get a more comprehensive understanding of the growth of dilute bismuth containing materials, to realize the long-term goal, the realization of optoelectronic devices.

References

[1] S. J. Sweeney and S. R. Jin, “Bismide-nitride alloys: Promising for efficient light emitting devices in the near- and mid-infrared,” *J. Appl. Phys.*, vol. 113, no. 4, p. 043110, 2013.

[2] S. J. Sweeney, A. F. Phillips, A. R. Adams, E. P. O’Reilly, and P. J. A. Thijs, “The effect of temperature dependent processes on the performance of 1.5-μm compressively strained InGaAs(P) MQW semiconductor diode lasers,” *IEEE Photonics Technol. Lett.*, vol. 10, no. 8, pp. 1076–1078, Aug. 1998.

[3] K. Alberi, J. Wu, W. Walukiewicz, K. M. Yu, O. D. Dubon, S. Watkins, C. Wang, X. Liu, Y.-J. Cho, and J. Furdyna, “Valence-band anticrossing in mismatched III-V semiconductor alloys,” *Phys. Rev. B*, vol. 75, no. 4, p. 045203, Jan. 2007.

[4] M. Usman, C. A. Broderick, A. Lindsay, and E. P. O'Reilly, "Tight-binding analysis of the electronic structure of dilute bismide alloys of GaP and GaAs," *Phys. Rev. B*, vol. 84, no. 24, p. 245202, Dec. 2011.

[5] C. A. Broderick, P. E. Harnedy, R. J. Manning, E. P. O'Reilly, P. Ludewig, Z. L. Bushell, and K. Volz, "Determination of band offsets in dilute bismide GaBix As 1 - x quantum wells using polarization-resolved photovoltage spectroscopy and 12-band kp calculations," 2015.

[6] K. Oe and H. Okamoto, "New Semiconductor Alloy GaAs1-xBix Grown by Metal Organic Vapor Phase Epitaxy," *Jpn. J. Appl. Phys.*, vol. 37, no. Part 2, No. 11A, pp. L1283–L1285, Nov. 1998.

[7] P. Ludewig, N. Knaub, W. Stolz, and K. Volz, "MOVPE growth of Ga(AsBi)/GaAs multi quantum well structures," *J. Cryst. Growth*, vol. 370, pp. 186–190, Jul. 2013.

[8] L. Nattermann, P. Ludewig, L. Meckbach, B. Ringler, D. Keiper, C. von Hänisch, W. Stolz, and K. Volz, "MOVPE growth of Ga(AsBi)/GaAs using different metalorganic precursors," *J. Cryst. Growth*, vol. 426, pp. 54–60, 2015.

[9] K. Forghani, Y. Guan, A. W. Wood, A. Anand, S. E. Babcock, L. J. Mawst, and T. F. Kuech, "Self-limiting growth when using trimethyl bismuth (TMBi) in the metal-organic vapor phase epitaxy (MOVPE) of GaAs 1 À y Bi y," *J. Cryst. Growth*, vol. 395, pp. 38–45, 2014.

[10] I. Moussa, H. Fitouri, A. Rebey, and B. El Jani, "Atmospheric-pressure metalorganic vapour phase epitaxy optimization of GaAsBi alloy," *Thin Solid Films*, vol. 516, no. 23, pp. 8372–8376, 2008.

[11] E. Sterzer, N. Knaub, P. Ludewig, R. Straubinger, A. Beyer, and K. Volz, "Investigation of the microstructure of metallic droplets on Ga(AsBi)/GaAs," *J. Cryst. Growth*, vol. 408, pp. 71–77, Dec. 2014.

[12] K. Forghani, Y. Guan, M. Losurdo, G. Luo, D. Morgan, S. E. Babcock, A. S. Brown, L. J. Mawst, and T. F. Kuech, "GaAs1−y−zPyBiz, an alternative reduced band gap alloy system lattice-matched to GaAs," *Appl. Phys. Lett.*, vol. 105, no. 11, p. 111101, 2014.

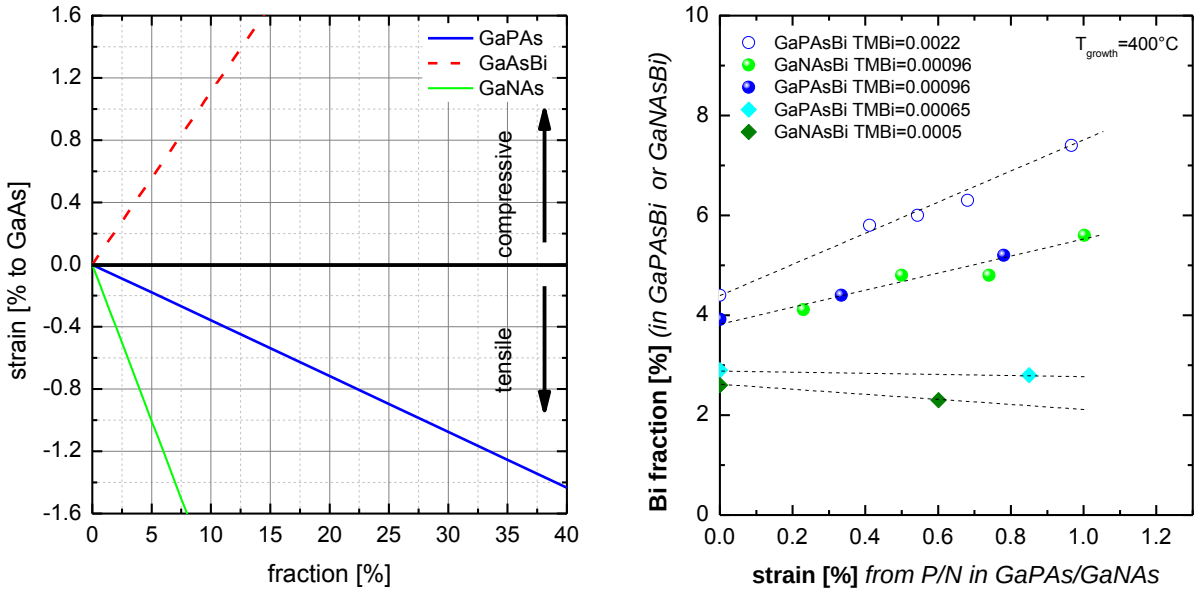

Fig.1: Relation between strain compensation and Bi incorporation in quaternary dilute Bi containing materials.

Ionic Liquids with Chalcogenide Anions: Highly Volatile Salts, Reagents for the Synthesis of Polysulfide Redox Shuttles and MoS_2 Semiconductor Materials

Lars Hendrik Finger

AK Sundermeyer, FB Chemie, Philipps-Universität Marburg

The recent focus of my research within the GRK 1782 lay in the synthesis and detailed characterization of ionic liquids (ILs) and low melting organic salts with chalcogenide anions. We were able to develop a halide, metal and water free access to hydrochalcogenide salts by introducing the corresponding hydrogen chalcogenide gas (H_2E, E = S, Se, Te) into solutions of methyl carbonate based ILs (scheme 1). Those are easily accessible themselves from the appropriate nucleophiles (*e.g*. *N*-butylpyrrolidine) and dimethyl carbonate.[1] H_2Se and H_2Te were generated *in situ* from the respective bis(trimethylsilyl)chalcogenide and methanol.

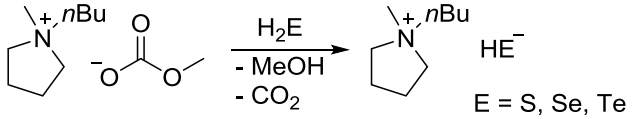

Scheme 1. Halide free synthesis of hydrochalcogenide based ionic liquids.

Imidazolium hydrochalcogenides (E = S, Se) show an astonishingly high volatility for cation-aprotic ILs, which allows their sublimation below 100 °C in fine vacuum and actually resulted in single crystal growth (figure 1). The sublimation can be employed as high end purification. In Cooperation with the Groups of Prof. Roling and Prof. Berger the vaporization and decomposition characteristics were investigated by isothermal TGA measurements and DFT calculations.[2]

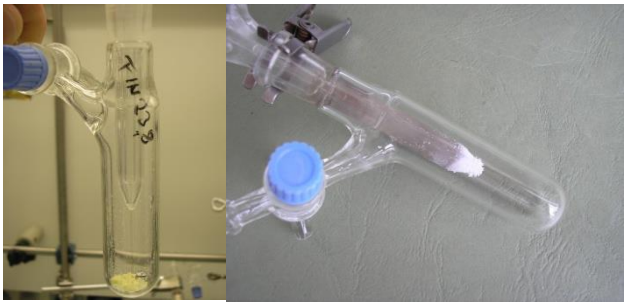

Figure 1. The IL (T_m= 92 °C) 1-ethyl-3-methyl-imidazolium hydrosulfide before (left) and after sublimation (right).

Furthermore we were able to extend the synthetic procedure to the preparation of trimethylsilylchalcogenolate salts by reacting methylcarbonate ILs with the bis(trimethylsilyl)chalcogenides (E = S, Se, Te) under strictly aprotic conditions (scheme 2). This constitutes a novel reaction behavior of methylcarbonate ILs, acting as nucleophilic desilylating agent and Lewis base instead of as Brønstedt base. Thus prepared silylchalcogenolate salts represent an activated form of the multifunctional TMS_2E reactant series. The desilylation reaction can be transferred to other silyl bearing synthons such as trimethylsilylazide and trimethylsilylcyanide.[3]

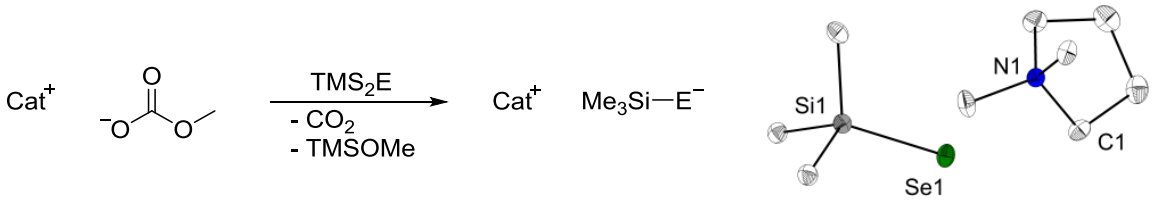

Scheme 2. Synthesis of trimethylsilylchalcogenolate based organic salts (E = S, Se, Te; left) and molecular structure of N,N-dimethyl-pyrrolidinium trimethylsilylselenolate (right).

On the one hand pyrrolidinium TMS-S salts have proven as excellent precursors for the synthesis of pyrrolidinium hexasulfides. Those were recently investigated as redox mediators in e.g. quantum dot sensitised solar cells.[4] On the other hand the hydro- and silylchalcogenide salts are sure to expand the starting material basis for many chemists working in the topical areas of metal chalcogenido clusters, (silyl)chalcogenidometallates, metal chalcogenide semiconductor materials and polychalcogenide redox mediators. In the group of Prof. Dehnen the hydrosulfide and hydroselenide salts are investigated as ionothermal pseudo-flux media in the synthesis of chalcogenido mercurates.[5]

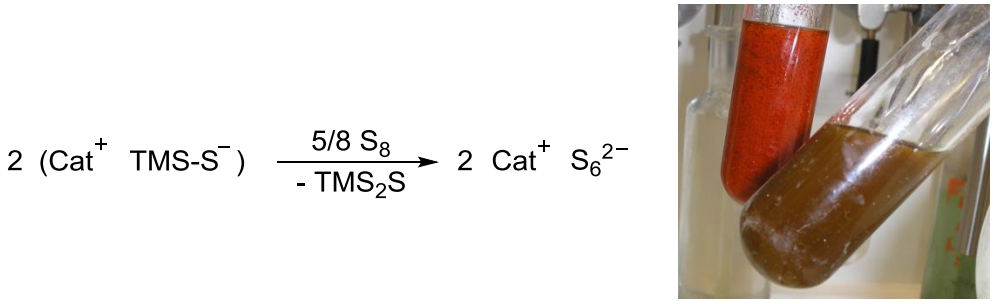

Scheme 3. Synthesis of pyrrolidinium hexasulfides from trimethylsilylthiolates (left), and bis(N-butyl-N-methyl-pyrrolidinium)hexasulfide precipitating during the reaction (red).

We are further examining the potential of the sulfide salts as starting materials for the synthesis of molybdenum disulfide. While MoS_2 acts as an indirect semiconductor in the bulk material, monolayers exhibit highly promising direct bandgap characteristics.[6] We were able to generate spherical MoS_2 micro and nano particles by combining a molybdenum chlorido precursor complex with a variety of hydro and silylsulfide salts.[7] We are now investigating the potential of this method to form MoS_2 thin films for electronic applications.

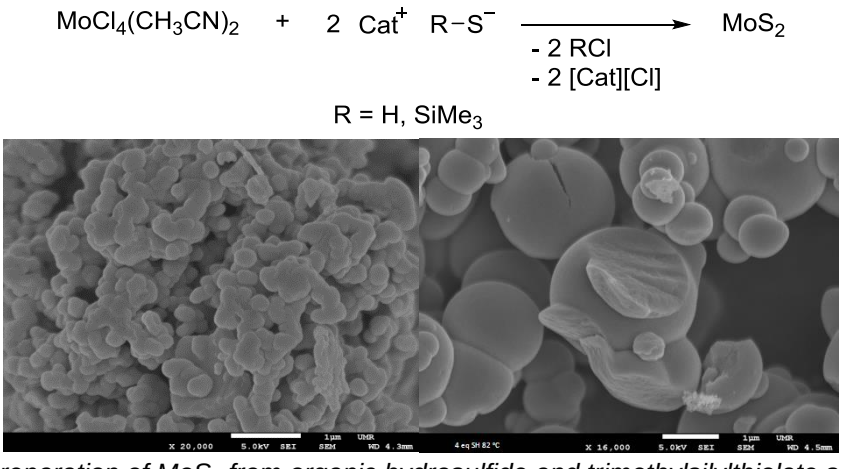

Scheme 4. Preparation of MoS_2 from organic hydrosulfide and trimethylsilylthiolate salts (top) and REM pictures of the so generated MoS_2 particles (bottom).

References:

1. R. Kalb (PROIONIC), *PCT Int. Appl.,* WO2008/052861, **2008**; G. Degen, C. Stock (BASF), WO2009/040242, **2009**.
2. L. H. Finger, F. Wohde, E. I. Grigoryev, A. K. Hansmann, R. Berger, B. Roling, J. Sundermeyer, *Chem. Commun.* **2015**, 10.1039/C5CC06224A.
3. L. H. Finger, B. Scheibe, J. Sundermeyer, *Inorg. Chem.* **2015**, 10.1021/acs.inorgchem.5b01665.
4. V. Jovanovski, V. González-Pedro, S. Giménez, E. Azaceta, G. Cabañero, H. Grande, R. Tena-Zaera, I. Mora-Seró, J. Bisquert, *J. Am. Chem. Soc.* **2011**, *133*, 20156-20159.
5. G. Thiele, H. Borkowski, L. Finger, J. Sundermeyer, S. Dehnen, $K_2Hg_6Se_7$ – A new Mercurate from Ionothermal Synthesis: A Pseudo-Flux Reaction, *In Preparation.*
6. a) K. K. Kam, B. A. Parkinson, *J. Phys. Chem.* **1982**, *86*, 463-467; b) K. F. Mak, C. Lee, J. Hone, J. Shan, T. F. Heinz, *Phys. Rev. Lett.* **2010**, *105*, 136805-1-136805-4; c) T. Li, G. Galli, *J. Phys. Chem. C* **2007**, *111*, 16192-16196.
7. B. Scheibe, *Bachelors Thesis*, Philipps-Universität Marburg, **2014**, Supervisor: L. H. Finger.

Derivatization of Functionalized Organotin-Chalcogenide Clusters

Jens. P. Eußner, S. Dehnen

Faculty of Chemistry and Material Sciences Center, Philipps-Universität Marburg

The chemistry of inorganic-organic hybrid compounds combines the chemical and physical properties of inorganic and organic materials on the nanoscopic level. The versatile material properties allow for the development of tailored functional materials. These materials often exhibit new material properties. Inorganic-Organic hybrid compounds have potential applications as (photo-)catalyzers, (opto-)electronic switches or coating materials.[1]

Organotetrel-chalcogenide clusters of the general formula $[(RT)_xE_y]$ (R = organic ligand; T = tetrel atom = Si, Ge, Sn, Pb; E = chalcogen atom = S, Se, Te) represent discrete chemical hybrid compounds. The organic component is covalently attached via tetrel–carbon-bonds to the inorganic cluster core. The variation of the composition, organic ligands, tetrel- and chalcogen atoms (as well as additional transition metal atoms) allows for the design of fine-tunable properties and structures.[2,3]

Systematic experimental and theoretical investigations of reactions of R^1SnCl_3 (R^1 = $CMe_2CH_2C(Me)O$) with $(Me_3Si)_2Te$ allowed for the stepwise formation and single-crystalline isolation of the first tin sesquitelluride clusters with functional organic ligands, like $[(R^1Sn)_4Te_6]$ (**1**, see Fig. 1). Subsequent derivatization reactions afforded clusters with complex hybrid architectures. With increasing cluster size a significant decrease of the band gap was overserved [4]

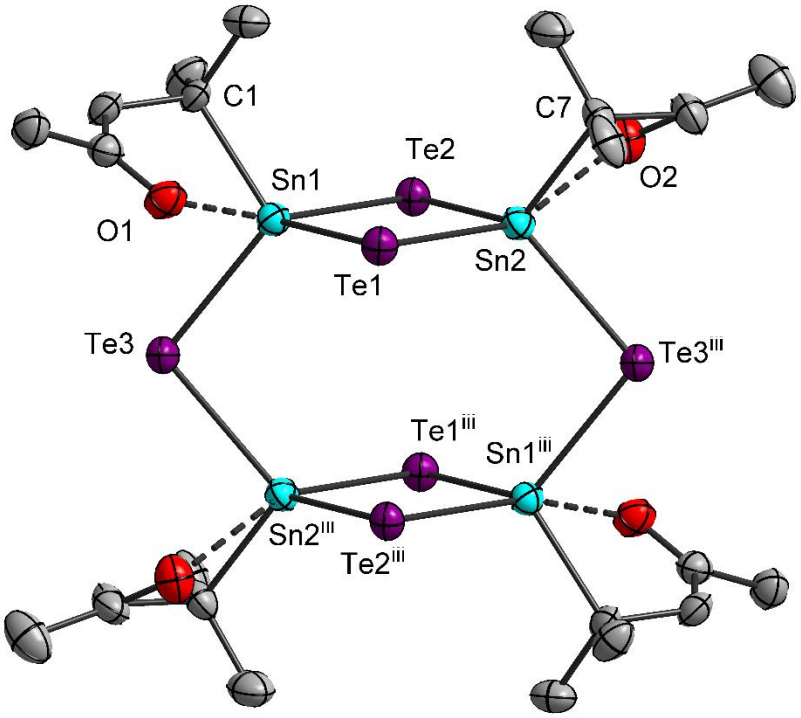

*Fig.1: Molecular structure of **1** without H atoms. Ellipsoids are drawn at 50%.[4]*

Investigations of the photophysical properties of $[(RT)_xE_y]$ cluster materials were performed with N. W. Rosemann and S. Chatterjee.[5] $[(R^3Sn)_4S_6]$ (**2**, R^3 = $CH_2CHC_6H_4$, see Fig. 2) shows extreme nonlinear optical properties. It acts as nonlinear medium in a highly directional white light emitter driven by a continuous wave IR-Laser diode.[6]

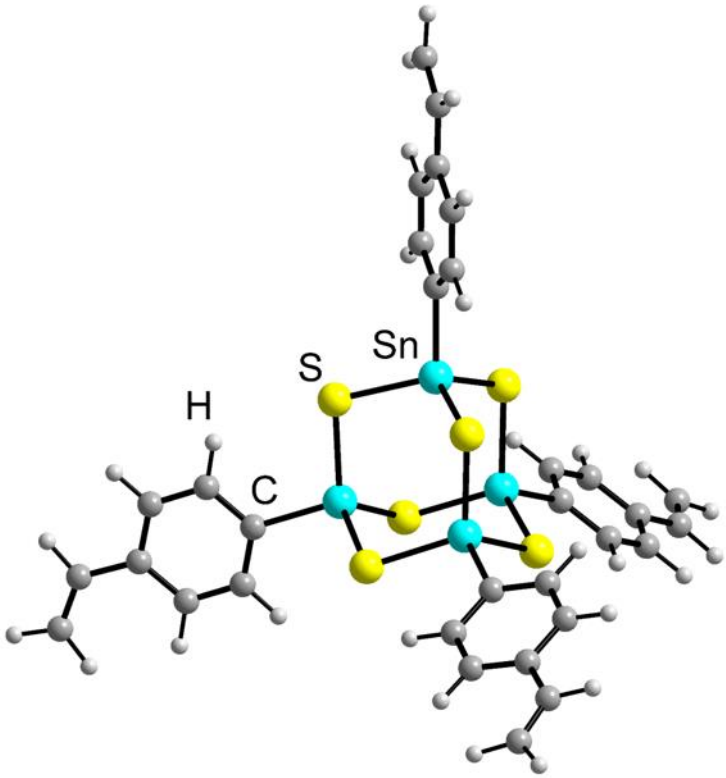

*Fig.2: Molecular structure of **2** according to DFT-calculations.*[7]

Further studies will focus on the systematic variation of photophysical properties of $[(RT)_xE_y]$ cluster materials and their use in highly directional white light emitters.

[1] L. Nicole, C. Laberty-Robert, L. Rozes, C. Sanchez, *Nanoscale* **2014**, *6*, 6267–6292.
[2] J. P. Eußner, B. E. K. Barth, E. Leusmann, Z. You, N. Rinn, S. Dehnen, *Chem. Eur. J.* **2013**, *19*, 13792–13802.
[3] J. P. Eußner, S. Dehnen, *Chem. Commun.* **2014**, *50*, 11385–11388.
[4] J. P. Eußner, R. O. Kusche, S. Dehnen, *Chem. Eur. J.* **2015**, *21*, 12376−12388.
[5] J. P. Eußner, B. E. K. Barth, U. Justus, N. W. Rosemann, S. Chatterjee, S. Dehnen, *Inorg. Chem.* **2015**, *54*, 22–24.
[6] J. P. Eußner, N. W. Rosemann, A. Beyer, K. Volz, S. Dehnen, S. Chatterjee, *submitted*.
[7] J. P. Eußner, *dissertation*, Marburg 2015.

Substituted Amidines, Guanidines and Formazanes: Hydrazine-Based Ligands for the Synthesis of MOVPE-Precursors

Susanne Pulz

AK Sundermeyer, FB Chemie, Philipps-Universität Marburg

Introduction

Within the GRK research project we are aiming to design and synthesize highly volatile N-rich group III precursor molecules for use in MOVPE processes. The new precursors combine typical group III MOVPE sources (EH_3 or EMe_3, E = B, Al, Ga, In) and the classical N-source, 1,1-dimethylhydrazine, in volatile low molecular weight ring systems. The key to success are newly designed amidine and guanidine chelate ligands (Figure 1). In collaboration with the STOLZ and VOLZ groups, the joint goal is to optimize the efficient casting of nitrogen into silicon lattice adapted III/V semiconductor materials Ga(NAsP). Conventional precursors, for example thermally highly stable NH_3 or the mentioned hydrazine should be replaced by single-source precursors to optimize the process.

The precursor design idea

For efficient N-casting and a high incorporation rate, the nitrogen atom should be prebonded to the group III metal (blue). Furthermore, N-N bonds of the two hydrazine units (red) – thermodynamically less stable and labile compared to N-C bonds - will readily dissociate with low barriers during the MOVPE process (dissociation 1). Traditional group III sources contain alkyl groups X (green), which are cleaved either via a radical or β-H elimination process (dissociation 2). With X = H, the first room-temperature long-term stable liquid [$GaH_2(L)$] was introduced. While the M-N bond (3) is weak due to its donor acceptor character, the focus of the research has been the optimization of dissociation of N-C bond (4). The instability of this bond (4) is directly related to the stabilization of the generated C radical or C cation by the substituent R_1. So the high barrier of decay into [M-N] (dark green oval) should decrease from formamidines (R_1 = H) via acetamidines (R_1 = Me) to guanidines (R_1 = NMe_2). In order to prove this concept, the different precursor classes were prepared within the last 2-3 years.

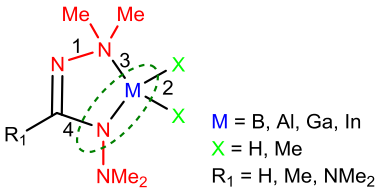

Results

The investigated ligand classes which can be divided into two groups – the *N*-amino-amidines and the *N*-amino-guanidines − are obtained via condensation of 1,1-dimethylhydrazine and electrophilic acetic acid, formic acid or carbonic acid synthons.[1-4]

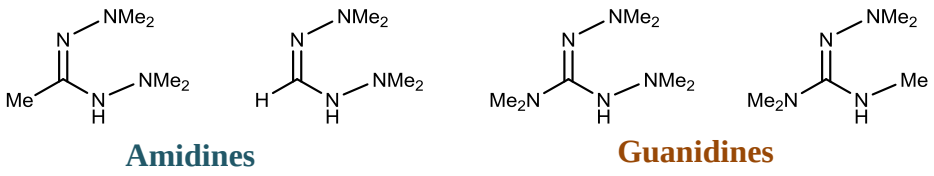

Figure 1: Developed ligand systems, N-amino-amidines and N-amino-guanidines.

The ligands are able to stabilize boranes, alanes, galanes and indanes MX_3 (X = H, Me) in group III methyl and hydrido precursors. The absence of any covalent M-C bond in some of these molecules minimizes the risk of undesired carbon incorporation.

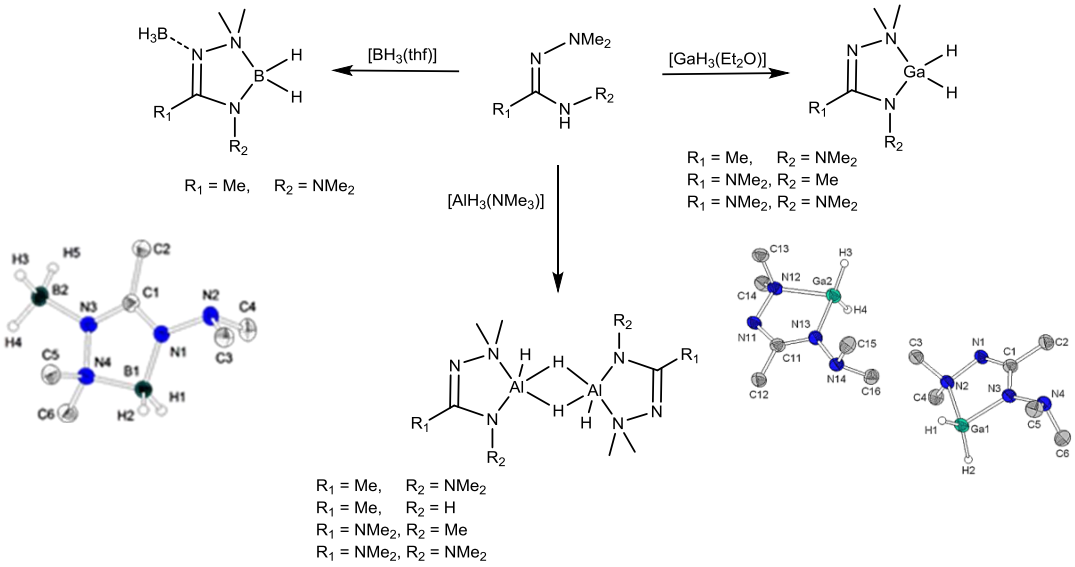

Scheme 1: Synthesis of complexes of the type $[MH_2(L)]$ with selected crystal structures: molecular structure of frozen liquid $[GaH_2(bdma)]$ at -100 °C (right).

Outlook

The previously investigated precursors are based on the N-source 1,1-dimethylhydrazine. So the focus of the subsequent research is to design new volatile group III precursor molecules based on the other established N-source *tert*-butylhydrazine. This includes N-*tert*-butyl substituted formazanes, triazenido species and highly volatile *tert*-butylhydrazine-MX_3 adducts (X = H, Me) and their condensation ring products.

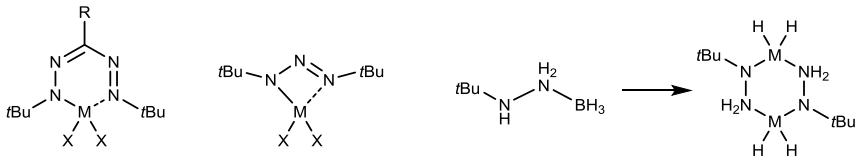

Scheme 2: Formazanes (left), triazenido (middle) or tert-Butylhydrazine complexes (right).

Another fundamental investigation with impact on the cost of III/V semiconductor fabrication and highly suitable for academic research training is the mechanistic investigation of reaction fundamental steps in a newly discovered direct synthesis of prominent TMG and TMI starting from the metals, methylchloride and halide acceptors.[5]

References

[1] Dissertation W. Schorn, Marburg **2012**.
[2] W. Schorn, J. Sundermeyer, R. Karch, WO**2012**113761 (A1).
[3] K. Schlechter, J. Sundermeyer, R. Karch, Eur. Patentantrag, Az: 14195515.3, **2013**.
[4] Inorganic Chemistry, in Vorbereitung: W. Schorn, K. Schlechter, E. Sterzer, K. Volz, W. Stolz, J. Sundermeyer.
[5] W. Schorn, J. Sundermeyer, patent pending.

Optical and Electronic Properties of Ga(N,As,P) Quantum Wells on Silicon for Laser Application

Sebastian Gies[1], Sarah Karrenberg[1], Martin Zimprich[1], Tatjana Wegele[1], Carsten Kruska[1], Andreas Beyer[1], Wolfgang Stolz[1], Kerstin Volz[1], and Wolfram Heimbrodt[1]

[1]*Faculty of Physics and Material Sciences Center, Philipps-University Marburg*

Introduction

In today's optoelectronics the monolithic integration of suitable light sources on silicon is an important goal. Realizing such a device enables one to combine the advantages of silicon microelectronics and optical data transfer. The quaternary material Ga(N,As,P) is a promising candidate for the realization of such a device and successful laser operation on Si substrate has already been demonstrated. [1]

On the one hand, N is a crucial part of the luminescent Ga(N,As,P) quantum well (QW), as it enables lattice matched growth on silicon. On the other hand, N introduces a huge disorder that can influence the device performance negatively.

Here, we present a comprehensive analysis of monolithically integrated Ga(N,As,P) QWs on silicon substrate, in order to improve the device performance and understand the interplay of N-induced disorder and optical and structural properties.

Results

The samples under investigation were grown in a horizontal reactor by metal-organic vapor phase epitaxy (MOVPE). The substrate for growth was a GaP/Si template consisting of a 100 nm thick GaP nucleation layer on exactly oriented Si substrate [2,3]. On this substrate a multi-quantum well (MQW) was grown. It consists of three units of Ga(N,As,P) QWs separated by barriers of 5.6 nm GaP and 33 nm (B,Ga)P. The boron containing layers are introduced to reduce the strain in the sample, while the GaP interlayer prevents the formation of non-radiative B-N centers. The MQW region is embedded in an optical confinement region of (B,Ga)(As,P).

To analyze the influence of N on optical and structural properties two different sample series were grown. In the first series the samples were grown at $T_{gr.}$= 575°C and annealed via rapid thermal annealing (RTA) at temperatures between $T_{a.}$= 850°C and $T_{a.}$= 1000°C. The second set of samples was grown at various growth temperatures between $T_{gr.}$= 525°C and $T_{gr.}$= 700°C. The following RTA was performed at $T_{a.}$= 925°C for all samples.

In both series the N-content in the Ga(N,As,P) QWs was kept constant at x_N= 7%.

The room temperature photoluminescence (PL) of the samples with varying annealing temperature is depicted in Fig. 1. The room temperature

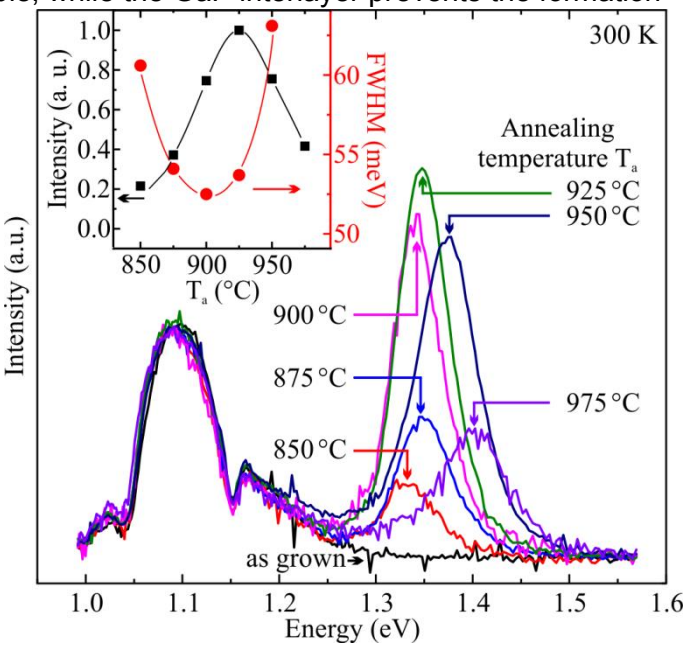

Fig. 1: PL spectra of the Ga(N,As,P) MQWs measured at room temperature. The spectra are labled according to the annealing temperature during the RTA. The inset shows the integrated intensity of the PL (squares) and the FWHM (circles) as a function of T_a. The solid lines are only a guide to the eyes.

PL in Fig. 1 is normalized to the silicon emission at 1.09 eV. At low temperatures the Si emission vanishes and the Ga(N,As,P) PL gains more than a magnitude of intensity. The complex interplay of structural and optical properties can be seen here. On the one hand, the emission properties such as full width at half maximum (FWHM) and integrated intensity (see inset of Fig. 1) are optimal around $T_{a.}$= 925°C . On the other hand, there is a monotonous blueshift of the Ga(N,As,P) PL with increasing Ta., indicating severe structural changes. A similar behavior is found for varying growth temperature yielding an optimal $T_{gr.}$ In the range of 585°C to 605°C.

Furthermore, we studied the disorder in the samples using temperature dependent PL. A two scaled disorder, typical for the Ga(N,As,P) material system [4-7], is found and quantized. In terms of disorder the optimal growth and annealing temperatures found in the 10 K PL are confirmed. To connect the disorder parameter to the structural properties of the samples X-ray diffraction (XRD) and high angle annular dark field transmission electron microscopy (HAADF-TEM) is employed. Here, we find that the long ranged disorder is caused by fluctuations in the quantum well width. These get gradually worse with increasing $T_{a.}$ Or $T_{gr.}$, respectively. Furthermore, the analysis of intensity profiles of the TEM images allows revealing changes in the samples' composition. Together with Raman spectroscopy we find that there is an inevitable As-P exchange between Ga(N,As,P) QWs and barriers upon increasing the annealing temperature.[7] Finally, this exchange could be quantized by utilizing the Ga(N,As,P) PLs excited states, found by photoluminescence excitation spectroscopy, as input parameter for a quantum well calculation. The calculation takes strain and the band anticrossing between N-impurities and the Ga(As,P) conduction band into account. This model yield an As-P-exchange of 5-10% for increasing $T_{a.}$ from 850°C to 1000°C.[7]

Conclusions

The complex interplay of N-induced disorder and optical and structural properties of Ga(N,As,P) MQWs on silicon substrates was analyzed. Utilizing PL and PLE the optical properties of the samples were studied and connected to the structural properties investigated by XRD and TEM. Thus, optimal parameter for growth and annealing were found and an inevirtable As-P-exchange upon annealing could be revealed and quantized.

Outlook

Using pressure dependent PL we aim to analyze the complex band anticrossing of N-impurities and Ga(As,P) conduction band. Furthermore, we will be able to precisely determine the hetero-offests between Ga(N,As,P) QW and the barriers and therefore gain important insights in the electronic structure of this material. This will allow to further optimize the parameters for manufacturing monolithically integrated light sources for optoelectronic integration on silicon.

References

[1] S. Liebich, et al., Appl. Phys. Lett. **99** (2011) 071109.
[2] K. Volz, et al., J. Cryst. Growth **315** (2011) 37.
[3] B. Kunert, et al., Thin Solid Films **517** (2008) 140.
[4] C. Karcher, et al., J. Lumin. **133** (2015) 125.
[5] K. Jandieri, et al., Phys. Rev. B **86** (2012) 125318.
[6] C. Karcher, et al., Phys. rev. B **82** (2010) 245309.
[7] S. Gies, et al., J. Cryst. Growth **402** (2014) 169.

Carrier dynamics in (BGa)(NAsP)-materials on silicon

C. Lammers, M. Stein, R. Woscholski, K.M. Shafka, S. Gies, A. Rahimi-Iman, W. Stolz, W. Heimbrodt, M. Koch

Faculty of Physics and Material Sciences Center, Philipps-Universität Marburg

Introduction

The goal of my work performed in the framework of the GRK functionalization of semiconductors is to investigate the carrier dynamics of metastable nitrogenous and boracic III/V semiconductors on Silicon, fabricated in the framework of the GRK.

Results

Due to its quaternary nature this material system is very prone to disorder. Compositional fluctuations and nitrogen related clusters as well as imperfect interfaces and varying quantum well width can raise the disorder potential. This can affect the carrier dynamics of the semiconductor and, hence, its performance in devices applications. The disorder in a material is determined by its growth conditions, composition and the annealing process. During the last year I have been investigating by means of time-resolved photoluminescence (TR-PL) spectroscopy both, the effects of different temperatures during rapid thermal annealing (RTA) and the effects of different growth temperatures, on the optical properties and carrier dynamics in Ga(NAsP) Multi-Quantumwells (MQWHs) grown on silicon substrate. The measurements for the samples annealed at different temperatures in the range of 850°C to 975 °C show an enhancement in the PL efficiency when the annealing temperature is increased up to 925 °C. However, when the annealing temperature is further raised, the PL intensity dramatically decreases. This is explained by the variation of the disorder degree in the studied structures. The analysis of the low-temperature emission-energy-dependent PL decay time can be used to characterize the disorder in the Ga(NAsP) MQWHs with the (very much simplified) model suggested by Gourdon and Lavallard. The theoretically extracted energy-scales of disorder confirm the experimental observations.

The use of different growth temperatures leads to different As and P contents in the QW material, while the N content stays nearly constant at 8% between 565°C - 650°C. The variation in composition leads to a blueshift of the PL maximum. The optimal growth temperature with respect to high PL intensity, small linewidth and small disorder energy scale was found between 575°C - 605°C. The disorder-energy-scale parameters were extracted from the characteristic temperatures of the s-shape for the short range disorder, which is mainly due to compositional fluctuations, and from the rise of the exponential slope of the lower-energy side of the PL spectrum for the long-range disorder which is attributed to interface imperfections.

Conclusions and Outlook

The time resolved photoluminescence measurements reveal a strong connection between the carrier dynamics on the one hand and the sample composition as well as the disorder energy scale on the other hand. For a better understanding, different scattering processes and carrier loss channels must be taken into account. Further TR-PL-measurements are planned to identify the influence of the nitrogen content, as well as pump-probe measurements on GaNAsP QW structures to observe the carrier dynamics by means of transient-absorption.

References

(1) B. Kunert, K. Volz, W. Stolz, Dilute nitride Ga(NAsP)/GaP- heterostructures: toward a material development for novel optoelectronic functionality on Si-substrate, Phys. Status Solidi B 244 (2007) 2730

(2) S. Liebich, M. Zimprich, A. Beyer, C. Lange, D.J. Franzbach, S. Chatterjee, N. Hossain, S. J. Sweeney, K. Volz, B. Kunert, W. Stolz, Laser operation of Ga(NAsP) lattice-matched to (001) silicon substrate Appl. Phys. Lett. 99 (2011) 071109.

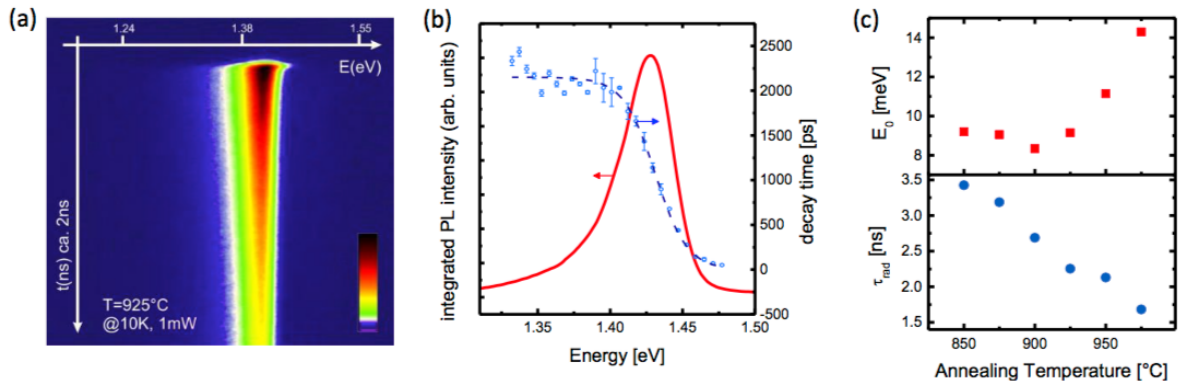

Fig. 1: (a) time resolved photoluminescence spectrum, (b) emission energy dependence of the decay time, (c) theoretically extracted parameters from the model suggested by Gourdon and Lavallard for different annealing Temperatures: E_0 is a characteristic energy for the density of states and t_{rad} is the radiative recombination lifetime

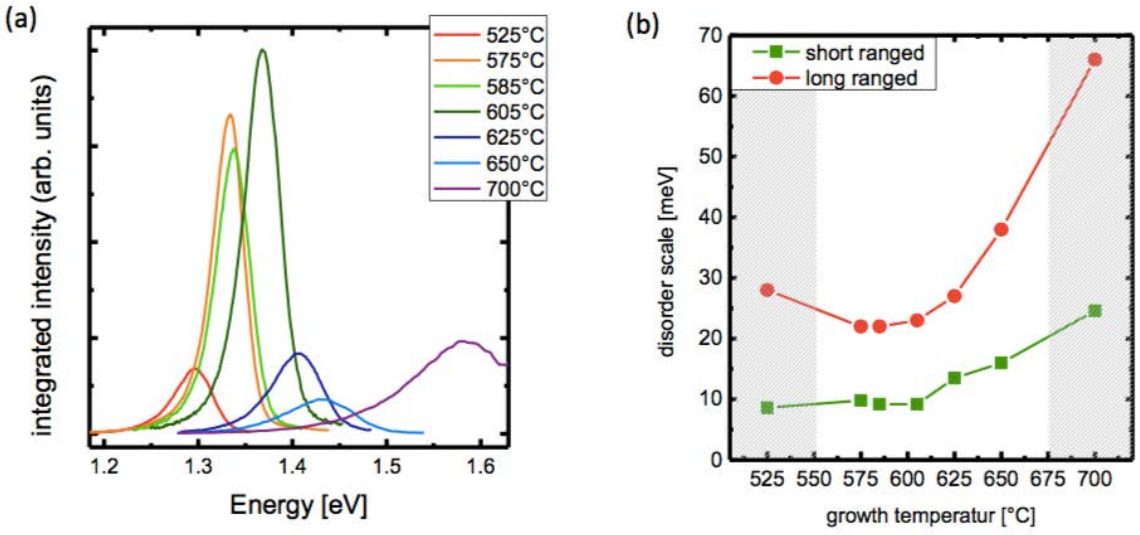

Fig. 2: (a) time integrated photoluminescence spectrum for different growth temperatures, (b) disorder energy scales for different growth temperatures, (b) disorder energy scales for different growth temperatures

Extreme nonlinear optical properties of adamantane-like functionalized semiconductor based clusters

Nils W. Rosemann and Sangam Chatterjee

Optics & Laser Spectroscopy Group – Faculty of Physics, Philipps-Universität Marburg

Tin/Sulphur crystals usually form complex crystal structures, due to these structures they exhibit pronounced nonlinear optical properties. The most common example is second-harmonic generation (SHG), expected in non-centrosymmetric structures. Additionally higher-order effects can occur, of which supercontinuum generation is the most interessting. These nonlinear processes usually exhibit high electric field threshold, which is why they are usually driven by pulsed laser sources.

Here we present a novel class of semiconductor based cluster that features extreme nonlinearities and enables white light supercontinuum generation with a continuous wave low cost laser pump source.

The clusters were grown in the group of Prof. Dr. Stefanie Dehnen. The archetype of this class of clusters is based on an inorganic Sn_4S_6 core that is surrounded by 4 styryl ligands (Fig. 1a). It forms a fine amorphous white powder that is non-volatile and air-stable.

As this powder is amorphous and no crystal could be grown, we performed reflection measurement to determine the band gap energy.

The reflectance is shown in Fig. 1b. It exhibits a broad featureless shoulder starting at 3eV (413nm) and rising up towards 3.7eV (335nm), indicating a band gap of around 3.7eV.

Next we performed standard photoluminescence (PL) measurements to obtain the linear optical response. When pumped with an energy close to the band gap the cluster shows a broad PL up to a wavelength of 550nm (Fig 2a,c). The transient of this PL resembles a double exponential decay, as it is well known for this sort of cluster[1] (Fig 2b).

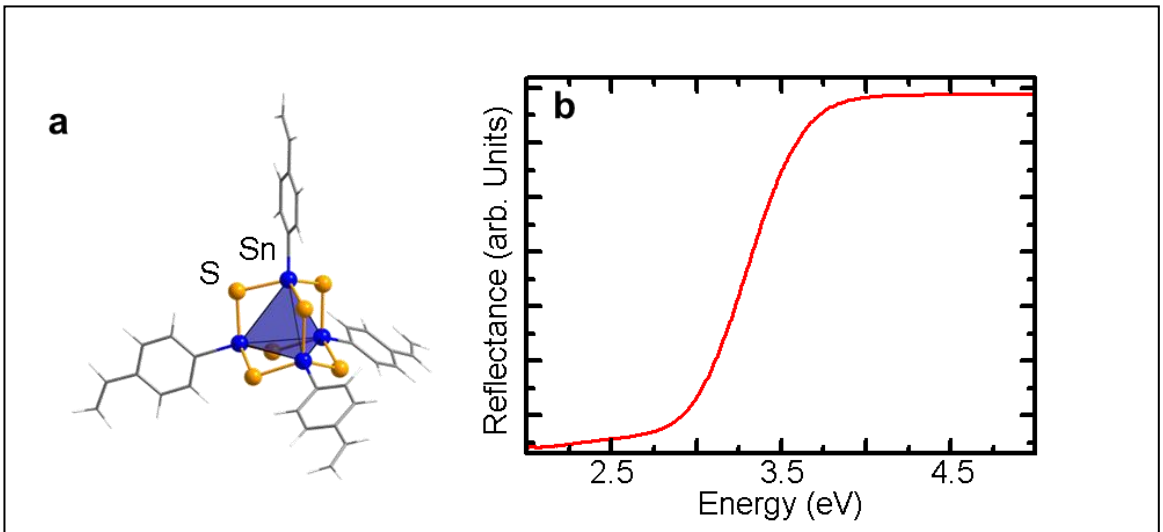

Fig. 1: a, molecular structure of the cluste. Tin (blue) and sulphur (yellow) atoms are indicated by spheres, carbon (grey) and hydrogen (white) atoms are drawn as wires. b, solid state UV/VIS spectrum in reflectance mode.

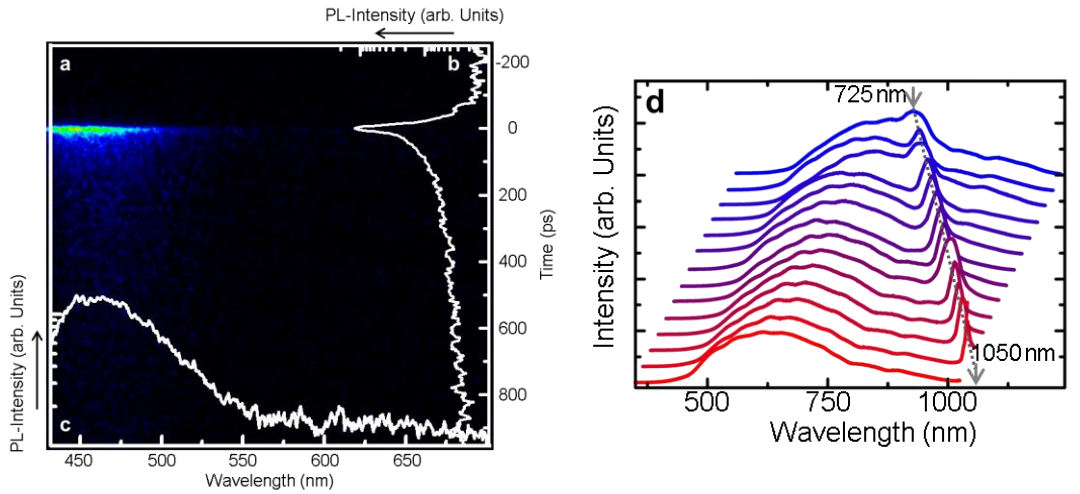

Fig. 2: a, false color image of the photoluminescence of the cluster, excitation wavelength was 410nm. b, luminescence transient integrated over the whole spectral region. c, spectrum integrated over the whole temporal range. d, supercontinuum spectra for pump wavelength varied from 725nm to 1050nm.

To investigate the nonlinear optical response, non-resonant excitation conditions were chosen. Pumped by an energy smaller than the band gap, the cluster no longer shows PL but a broad supercontinuum peaked at ~700nm (Fig. 2b). This broad spectrum has a warm white appearance to the eye and is independent of pump wavelength, at least in the range accessible by the used Ti:Sa laser.

To get more insight into the underlying processes we investigated the input-output characteristics of the supercontinuum. The pump power dependency shows a highly nonlinear behavior that scales to the power of 8.5 and thus excludes any classical recombination mechanism (Fig. 3a).

Further characterization was performed by checking the spatial distribution of the supercontinuum; here we found that the white light almost retains the spatial profile of the laser (Fig. 3b).

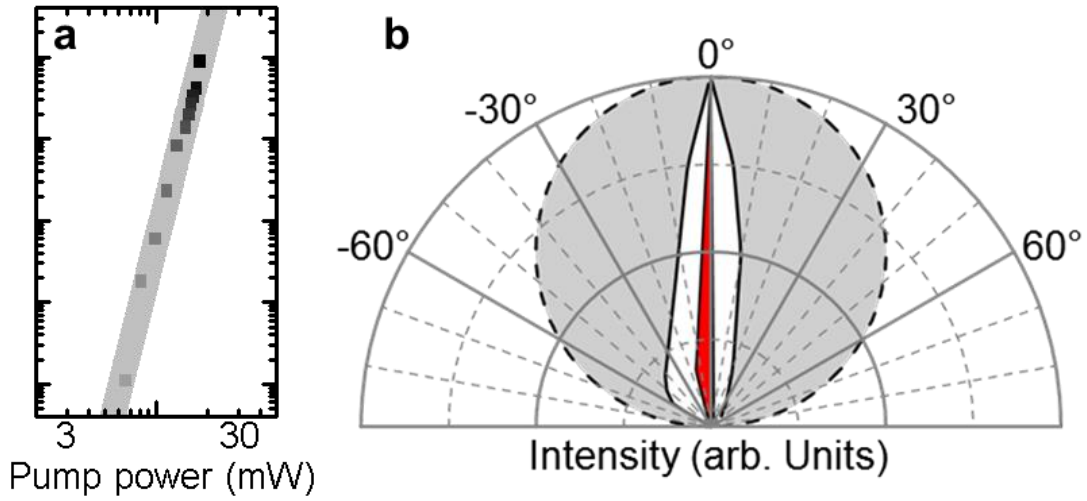

Fig. 3: a, double-logarithmic plot of the input-output characteristics of the supercontinuum. b, spatial emission characteristics. Angle-dependent intensity distribution for the white light-spectrum integrated in the range from 350-800 nm (white), the excitation laser at 940 nm (red) and a perfect Lambertian emitter (grey).

In summary, we found extreme nonlinear optical properties of novel semiconductor based clusters with organic ligands. These nonlinearities enable the generation of a warm white supercontinuum using a low cost laser-diode while retain the spatial emission characteristics of the laser.
Further studies include changing the size of the ligand (i.e. changing it to naphthyl, phenyl or methyl), thus changing the π-electron systems which should influence the efficiency of the nonlinear processes. In addition changing the core to Ge_4S_6 and Si_4S_6 should change the band gap and thus the high energy flank of the supercontinuum.

[1] Leusmann, Eliza, et al. *"Synthesis, Crystal Structure, and Photoluminescence Studies of a Ruthenocenyl-Decorated Sn/S Cluster."* Inorganic chemistry **53.8** (2014): 4228-4233.

Optical properties of nitride containing heterostructures

P. Springer and S. W. Koch

Faculty of Physics and Material Sciences Center, Philipps-Universität Marburg

The components of common III-V semiconductor compounds such as GaAs, GaP or AlSb are relatively well matched with respect to atom size, electronegativity or ionicity. The substitution of just a few percent of the group V atoms by N leads to unusual large bowing of the band gap. If only 1 % of the As is replaced by N in GaAs, the band gap reduced by ≈150 meV. This rapid decrease has attracted the interest of the research community with a strong focus on device applications, since it allows an elevated level of band gap engineering besides composition and strain variations [1, 2].

Regarding the unification of micro- and optoelectronic devices, a promising material systems is Ga(N,As,P), since it can be grown pseudomorphically on Si, the most important element used in telecommunication systems. However, in contrast to Ga(N,As,P), Si is unsuitable for lasing purposes since it is an indirect semiconductor. Therefore, integrating Ga(N,As,P) with existing microelectronics based on Si opens up new possibilities for the functionalization of semiconductor devices. Together with the enhanced possibilities to define the lasing properties via the band gap makes this material system appealing to further research [3, 4].

The bowing of the band gap of dilute nitride containing semiconductors have been successfully described within a band anti crossing (BAC) model. It models the interaction of isolated and localized N impurities with the resonant conduction band edge in terms of 3 parameters (V, α, and γ), which ultimately have to be provided by experiments. The conduction band splits up into two bands according to the single-impurity Anderson model with the band edges $E_{\pm}$, the fundamental band edge E_{c}, and the N related impurity level E_{N} [5]:

$$E_{\pm}(x) = \frac{1}{2}\left[E_{\mathrm{c}}(k=0,x) + E_{\mathrm{N}}(x) \pm \sqrt{\left[E_{\mathrm{c}}(k=0,x) - E_{\mathrm{N}}(x)\right]^2 + 4V^2 x}\right],$$

$$E_{\mathrm{c}}(k=0,x) = E_{\mathrm{c}}(k=0,x=0) - \gamma x - \Delta E_{\mathrm{c,strain}},$$

$$E_{\mathrm{N}}(x) = E_{\mathrm{N}}(x=0) - \alpha x - \Delta E_{\mathrm{N,strain}}.$$

To obtain a full band structure of multi quantum well structures, this model is well suited as an extension of a fully coupled Luttinger Hamiltonian including a conduction, heavy-, light-hole and split-off band (each twice spin degenerate). The resulting ***k·p*** Hamiltonian describes the near-band gap states and it's solution is used to calculate the multi band single-particle energies as well as Coulomb and dipole matrix elements [6]. These in turn are used within the semiconductor luminescence and Bloch equations to obtain the photoluminescence (PL) and photo modulated reflectivity (PR) spectra of semiconductor heterostructures.

We used our fully microscopic many-body theory to compare the obtained PL and PR spectra to the experimental data from Ga(N,As,P)/GaP samples [7]. Both the P and N content of the available samples varied over a large range. The PL spectra of one sample is shown in Fig. 1 (a) as a function of excitation power. The figure also shows the energetic position of the PL peak as a function of N (frame (b)) and P composition (frame (c)) for both the experiment and the theoretical prediction. All comparisons show a remarkable agreement

confirming the predictive power of our theory. A key feature to obtain this degree of agreement was to include strain effects for the nitride impurity level.

In a current project, we characterize and examine double quantum well structures with type II band alignment as shown in Fig. 2 (a). Since one of the quantum well is constituted by Ga(N,As), the same theory applies for these samples. We can already reproduce the gradual transit of a type-I to a type-II optical transition in samples that vary the spacer layer between

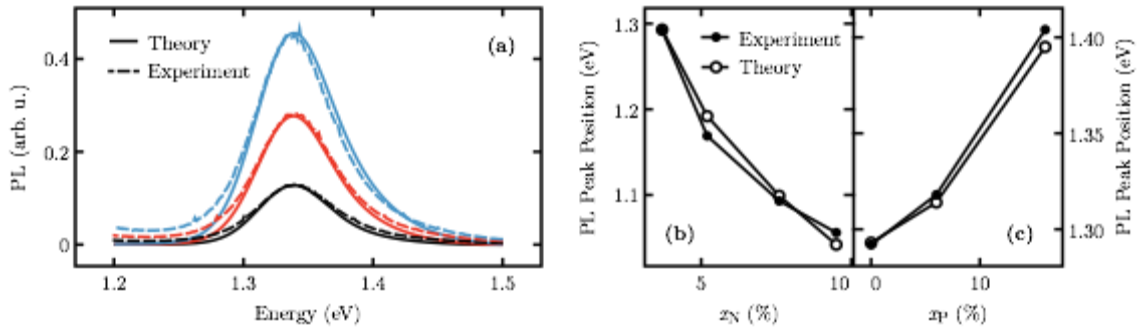

Fig.1: The PL spectra from experiments (dashed) compared to the theoretically obtained (solid) for one specific sample is shown in frame (a). Shown are 3 different excitation powers which correspond to three excitation densities. The extracted PL peak position is shown in frame (b) as a function of N content for a series of samples with a fractional P content of x_P=0%. Similarly, frame (c) shows the PL peak position as a function of P content while the nitrogen fraction is x_N=3.7%.

the two quantum wells, see Fig. 2 (b). However, a major source of controversy is the valence band offset of Ga(N,As)/GaAs quantum wells [2, 6, 8]. Such a double quantum well structure may allow us to determine the band alignment because the potential of the non-nitride quantum well is well established in the literature. Further investigations are needed to confirm the evidence we have obtained from preliminary studies that strongly favors a type-II alignment of the valence bands.

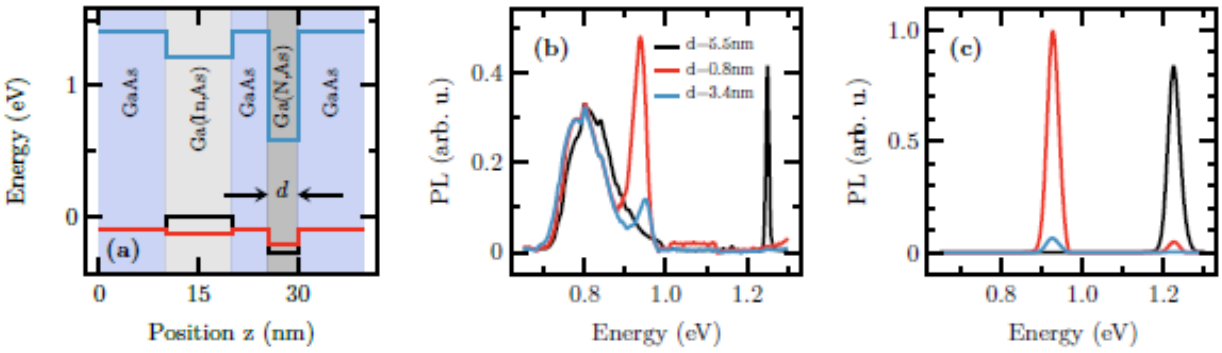

Fig.2: The double quantum well structure with a type-II alignment of the Ga(N,As)/GaAs sub structure is shown in frame (a). The thickness d is varied for the different samples. The experimental (a) and theoretical (b) PL spectra showing a transition between the type-I and type-II carrier recombination with decreasing spacing layer thickness d.

References

[1] C. A. Broderick, M. Usman, S. J. Sweeney, and E. P. O'Reilly, Semicond. Sci. Technol. **27**, 094011 (2012).

[2] J. Wu, W. Shan, and W. Walukiewicz, Semicond. Sci. Technol. **17**, 860 (2002).

[3] S. Borck, S. Chatterjee, B. Kunert, K. Volz, W. Stolz, J. Heber, W. W. Rühle, N. C. Gerhardt, and M. R. Hofmann, Appl. Phys. Lett. **89**, 3 (2006).
[4] N. Koukourakis, C. Bückers, D. A. Funke, N. C. Gerhardt, S. Liebich, S. Chatterjee, C. Lange, M. Zimprich, K. Volz, W. Stolz, B. Kunert, S. W. Koch, and M. R. Hofmann, Appl. Phys. Lett. **100**, 72 (2012).
[5] S. Tomić, E. P. O'Reilly, P. J. Klar, H. Grüning, W. Heimbrodt, W. M. Chen, and I. A. Buyanova, Phys. Rev. B - Condens. Matter Mater. Phys. **69**, 1 (2004).
[6] J. Hader, S. W. Koch, J. V. Moloney, and E. P. O'Reilly, Appl. Phys. Lett. **76**, 3685 (2000).
[7] K. Jandieri, P. Ludewig, T. Wegele, A. Beyer, B. Kunert, P. Springer, S. D. Baranovskii, S. W. Koch, K. Volz, and W. Stolz, J. Appl. Phys. **118**, 065701 (2015).
[8] I. A. Buyanova, G. Pozina, P. N. Hai, W. M. Chen, H. P. Xin, and C. W. Tu, Phys. Rev. B **63**, 033303 (2000).

A computational study on the structural and electronic properties of III/V semiconductor alloys

Phil Rosenow, Ralf Tonner

Faculty of Chemistry, Philipps-Universität Marburg

Introduction

The integration of III/V semiconductor alloy based laser emitters in silicon based electronic devices is a promising approach to improve computer technology and other optoelectronic applications. In order to model and predict the optical properties of quantum well laser devices free from any empirical input, the properties of the alloy materials must be computed in a reliable and consistent fashion. Density functional theory (DFT) can provide good accuracy for reasonable computational cost. Within DFT, a plethora of functionals is available, from which a suitable method must be chosen. Ultimately, band parameters within the **kp** theory will be extracted from computed band structures and used for the computation of optical properties of semiconductor quantum wells. Here, some results regarding the band gap of semiconductor alloys will be presented.

Results

Several methods have been used on the binary semiconductors GaAs, GaP and GaN in order to assess their accuracy. All structures (lattice constants) have been determined with the dispersion-corrected PBE-D3(BJ) functional within a plane wave formalism as implemented in the VASP code. The band gaps were determined with the GGA functional PBE, the global hybrid functional PBE0, the range-separated hybrid functional HSE06, the meta-GGA functional TB09 and the many-body perturbation method G_0W_0. Results are shown in Table 1.

Tab.1: Computed band gaps at the Γ-point for binary semiconductors in zinc blende structure. All values are given in eV.

	PBE	PBE0	HSE06	TB09	G_0W_0	Exp.[1]
GaAs	0.32	1.71	1.11	1.44	1.41	1.52
GaP	1.74	3.31	2.66	2.95	2.86	2.86
GaN	1.58	3.48	2.78	3.03	3.09	3.28

PBE shows its well-known gross underestimation of band gaps. The hybrid functionals exhibit different tendencies: PBE0 computes overestimated, while HSE06 slightly underestimated band gaps. TB09 and G0W0 produce reasonable band gaps. Since the computational cost of the former is much lower than that of the latter, TB09 has been chosen for studies of alloy systems.

The extension to the ternary systems $Ga(As_{1-x}P_x)$ and $Ga(N_xAs_{1-x})$ has shown a strong dependence between lattice distortions and the computed band gap. The band gaps for $Ga(As_{1-x}P_x)$, where alloying distorts the lattice only slightly, agree well with reference values from a virtual crystal approximation (VCA).[1] In $Ga(N_xAs_{1-x})$ on the other hand, the lattice distortion is much stronger and the band gap is grossly underestimated when compared to a band anticrossing model (BAC) which agrees well with measured gaps.[2] Also, the effect of the atomic configuration of a supercell with more than one guest atom is stronger Ga(NAs) than for Ga(AsP). Results from both systems are shown in Figure 1.

The TB09 functional contains a parameter *C*, which is usually determined self-consistently but can also be fixed. Since the band gap of an alloy can be strongly determined by the

minority component and this parameter varies significantly between GaAs and GaP on the one hand and GaN on the other hand, it was fixed to the value obtained for GaN in order to test its effect on the band gap of $Ga(N_{0.037}As_{0.963})$. While this led indeed to a slight improvement of the band gap, the deviation to the reference values is still too large.
The effect of the lattice relaxation was tested by setting the lattice constant of the alloy supercell to the value for the alloy, but keeping the atomic position of an ideal, undistorted lattice. This led to a perfect agreement with reference values for Ga(NAs). For Ga(AsP), this effect is much less pronounced, the band gaps being hardly affected by lattice relaxation.

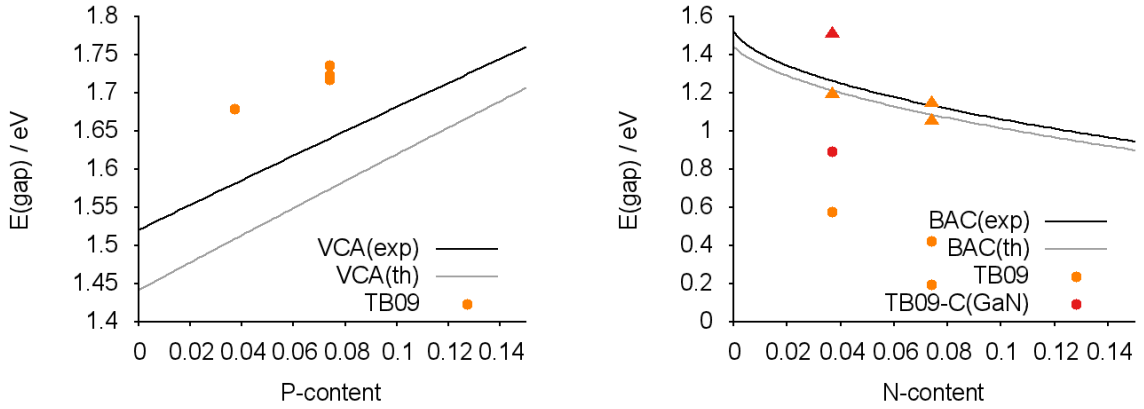

Fig.1: Computed band gaps of (left) $Ga(As_{1-x}P_x)$ and (right) $Ga(N_xAs_{1-x})$ in comparison with reference models based on experimental (exp) and computed (th) component band gaps. Triangles denote an unrelaxed lattice. Several values for one composition come from different configurations of the supercell.

Conclusions & Outlook

An in principle reliable approach for computing band gaps of semiconductor alloys from first principles has been found with the TB09 density functional. In further studies not mentioned here, it has also shown good results for other band parameters for **kp** theory. However, the fact that until now accurate band gaps of dilute nitrides can only be computed for unrelaxed structures is deeply disturbing and requires further investigations. Thus, the interplay of chemical, structural and electronic factors in this class of materials will be studied in more detail. Specifically, the relation between lattice relaxations and electronic band gap and the role of chemical bonds in this will be investigated. Once the issues described herein have been addressed, the procedure will be extended to full band structure calculations and quartenary semiconductor alloys like Ga(NAsP).

References

[1] I. Vurgaftman, J. R. Meyer, L. R. Ram-Mohan, *J. Appl. Phys.* **89**(11), 5815 (2001).
[2] I. Vurgaftman, J. R. Meyer, *J. Appl. Phys.* **94**(6), 3675 (2003).

GaP-Si interface formation and properties studied by DFT

Andreas Stegmüller and Ralf Tonner

Faculty of Chemistry and Material Sciences Center, Philipps-Universität Marburg

Introduction

It recently has been found that the morphology of the interface of gallium phosphide (GaP) grown on a silicon (Si) substrate is not flat but rather atomically intermixed and facetted across eight atomic layers.[1] This was concluded from the results of experimental growth and structure analysis of the semiconductor materials by transmission electron microscopy, kinetic Monte Carlo modelling of the growth as well as density functional theory (DFT) investigations on surface-adatom mobility and interface stabilities.

Based on these findings, the origin of stability differences found for interfaces at varied crystal orientation and structural configuration was investigated. Local and film-wide features were determined for characteristic chemical properties such as atomic structure, charge distribution and electrostatics, respectively. Reasoning for the preference of specific interface configurations was based on those properties and the findings were discussed applying the criteria of older models predicting III/V interface formations.[2,3] Those models were found to be insufficient to quantitatively predict the stability of complex interface configurations.

In Figure 1, the orientations and configurations of GaP-Si interfaces investigated are presented including the number of non-octet bonds between interface Si and Ga / P atoms. Ga- and P-terminated configurations were modelled explicitly for the complete set.

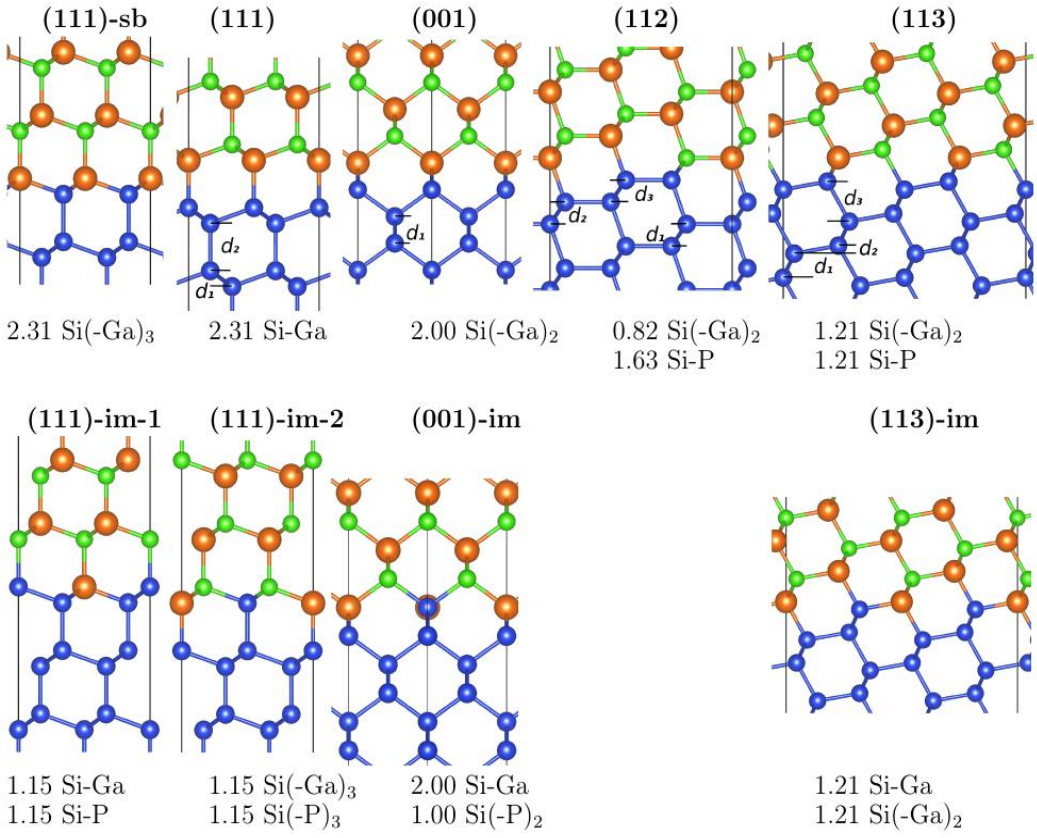

Fig.1: GaP-Si interface configurations investigated (Ga-terminations shown). Below the structural models, the number of direct contacts of Ga (P) (non-octet bonds) with Si are provided normalized to the area $A_{(001)}$. P-terminated configurations and bond counts can be derived by interchanging Ga and P element symbols.

Results

The minimization of non-octet bonds provides stabilization which is in quantitative agreement with the formation energies calculated from DFT for GaP-Si interfaces with exclusively Ga- or P-Si direct contacts. For more complex configurations with both III/V elements at the interface, other effects dominate the stabilization.

As GaP and Si exhibit almost identical lattice dimensions only small strain energies were determined, but local stress was found to be dominating the stability of some interface configurations. However, the ideal, unrelaxed supercell models applied in periodic DFT calculations are sufficient to reproduce the correct order of stabilities of the configurations examined (with the exception of the P-terminated, flat interface at (111), which is exceptionally stabilized by structural relaxation).

Partial charges from the natural bond orbital scheme were determined as projected from the periodic wavefunction onto local Gaussian functions. Irrespective of interface configuration or orientation, atomic charges inside the GaP and Si films show constant values within the applied slab- and bulk-type cells. Local interface charges, on the other hand, deviate from this value but converge within only two atomic layers towards the bulk values.

Based on the wavefunctions derived by the PBE functional, averaged local electrostatic potentials across the films and interfaces were calculated. Those show film-wide polarization fields along growth direction (Z) caused by GaP's polarity. Locally, the potentials resolve atomic layers indicating charge neutralization within GaP in some crystal orientations. At the interfaces, transitions can be recognized showing the convergence of the potential towards to bulk energy levels and providing a measure for the energy offset between the films.

Conclusions

Chemically motivated argumentation including the atomic structure of GaP-Si interface configurations and the minimization of non-octet contacts allows qualitative stability prediction. However, some interfaces are stabilized by multiple effects and, thus, models based exclusively on charge neutrality or bond counts are insufficient to quantitatively predict the stabilities of the GaP-Si interface configurations modelled. Apart from potential strain effects (lattice mismatch), the conclusions obtained can be applied to other III/V-IV semiconductor interfaces as most trends are dominated by electrostatics and, thus, chemical arguments.

Outlook

In order to further investigate the electronic structure at the interface and gain extensive insight into the chemical bonding situation of the individual configurations, the following studies on this system will involve partial densities of states analysis and periodic energy decomposition analysis with natural orbitals of chemical valence [4].

Furthermore, new methodology for geometry optimization and ab initio molecular dynamics will be introduced which will enable the exploration of further structural features on interface formation and surface reactivity. The latter is important to complement the understanding of growth including the activation of the silicon surface and decomposition of adsorbed precursors.

References

[1] A. Beyer, A. Stegmüller, J. O. Oelerich, K. Jandieri, K. Werner, W. Stolz, S. D. Baranovskii, R. Tonner, K. Volz, submitted, 2015.

[2] W. A. Harrison, E. A. Kraut, J. R. Waldrop, R. W. Grant, Phys. Rev. B, 18, 1978.

[3] M. Pashley, Phys. Rev. B, 40, 1989.

[4] M. Raupach and R. Tonner, J. Chem. Phys. 142, 194105, 2015.

Surface etching of single crystalline ZnO by phosphonic acid based SAMs

Alexandra Ostapenko, Gregor Witte

Molekulare Festkörperphysik, Philipps-Universität Marburg, Renthof 7, 35032 Marburg, Germany
alexandra.ostapenko@physik.uni-marburg.de

The development of organic-inorganic hybrid systems has already found broad application in transparent electrodes in light emitting devices or in dye-sensitized photovoltaic cells [1]. The key is the interface between semiconducting metal oxide and organic semiconductor, since it determines the resulting injection barrier of charge carriers at electrodes. The quality of an interface, the resulting molecular orientation and film morphology, depends critically on the roughness and chemical termination of the substrate and is crucial for the device performance. Pretreating electrodes by covalently bound self-assembled monolayers (SAMs) has proven to be an effective way of tuning electronic interfacial properties or specifically link dye-molecules to transparent substrates. The system of SAMs on metals such as organothiols on gold has been already comprehensive investigated [2], [3]. In contrast only little is known about the film formation and structure of SAMs on metal oxides. Covalent attachment of organic molecules in hybrid systems based on metal oxides is typically achieved through other anchoring groups such as phosphonic acids (PAs). Moreover, it was shown, that PA-based SAMs form well-defined monolayers with distinct molecular orientation within the layer [4-7]. However, real devices utilize polycrystalline metal oxide powder or nanostructured oxides with ill-defined interfaces [8], [9]. In order to explore the interrelation between microstructure of the interface and dissociation of photo-excited states as well as the subsequent charge transfer dynamic well defined model systems are required. One promising substrate for this purpose is zinc oxide single crystal (ZnO), since it has several surface terminations (polar and non-polar), that makes it versatile for surface experiments. Owing the simplest aromatic backbone, phenylphosphonic acid (PPA) has been chosen for the present model study. Though the adsorption of similar molecules has already been studied, a microscopic understanding of the binding mechanism as well as limitations of the approach has not been achieved. Here we report on additional complications caused by substrate etching during the thin film preparation by immersion.

In contrast to thiole-based SAMs on gold substrates, where the immersion preparation procedure yields monolayer formation, we observed an unexpected side-effect for the system of ZnO and organic molecules with phosphonic acid anchoring units. A surface damage is caused by formation of “star shaped” surface defects and crystalline needles (Fig.1a). Using atomic force microscopy measurements (AFM) we identified individual steps on the surface of single needles (Fig.1b-d), which is typical for crystalline materials. With increasing immersion time the formation of large lamellas on the surface was observed. To exclude the crystallization of pure PPA thermal desorption was examined. Complementary measurements have shown, that PPA multilayer desorption takes place at 420 – 440 K and a chemisorbed monolayer on ZnO is stable till 690 – 720 K. By contrast the newly found precipitations are thermally stable even after extensive annealing up to 900 K and remain on the surface, indicating their metal-organic origin. The mechanism of metal-organic surface structures has been attributed as dissolution-precipitation of ZnO, where surface Zn atoms can be extracted from the surface matrix by a strong acid and chemically react with it. Corresponding energy-dispersive (EDX) X-ray spectroscopy, revealed a relative content for P and Zn of 1:1, hence suggesting zinc-phenylphosphonate ($Zn(O_3PC_6H_5)\cdot H_2O$)

as the possible material of precipitations. To verify this assumption we have conducted X-ray diffraction (XRD) on surface precipitations as well as on single separated lamellas that were peeled off from the ZnO crystals. XRD patterns exhibit additional to ZnO signatures which are in a good agreement with the spectra for the pure zinc-phenylphosphonate reported in the literature. In particular, the increasing intensity of (010) peak followed by longer immersion time indicates the top face of formed crystalline lamellas oriented according to the [010] crystallographic direction. Moreover, the extracted interlayer distance for the compound is in a good agreement with the height of discreet steps found in AFM.

After the experimental determination of surface precipitations as zinc-phenylphosphonate crystals, we examined the influence of different surface terminations of ZnO on the dissolution efficiency as well as the surface morphology. Apparently, the ZnO surface dissolution takes place for both polar and non-polar surfaces equally strong. However, the surface roughness influence the resulting surface deformation, since the dissolution primary takes place at the surface step edges and defects. Another important aspect is the influence of the pH-value of the immersion solution upon SAMs preparation on the ZnO stability. We have shown that the etching rate can be tuned by variations of pH-value in the experiment. To complement experimental results a theoretical analysis was carried out in the group of Prof. Dr. Bernd Meyer (Uni Erlangen). In addition to detailed information on the binding mechanism it was found that the formation of zinc-phenylphosphonate phase is indeed energetically favored.

[1] Hagfeldt A. et al., Chemical Reviews, **110** (2010) 6595
[2] D.Käfer, G.Witte, P.Cyganik, A.Terfort, C.Wöll, J. Am. Chem. Soc. **128** (2006) 1723
[3] J. C. Love et al. Chemical Reviews **105** (2005) 1103
[4] Gupta S., Gleskova H., Organic Electronics, **13** (2013) 354-361
[5] Hubert Mutin P. et al., J. Mater. Chem., **15** (2005) 3761-3768
[6] Di Valentin C., Costa D., J. Phys. Chem., **116** (2012) 2819-2828
[7] Ma H., Acton O., H. Hutchins D. et al., Phys. Chem. Chem. Phys. **14** (2012) 14110-14126
[8] Gliboff M. et al., J. Phys. Chem. C, **117 (29)** (2013) 15139-15147
[9] Gouzman, I. et al., Surface Science, **600 (4)** (2006) 773-781

Fig. 1 Morphology of precipitations studied by scanning electronic microscopy (a) and atomic force microscopy techniques (b, c) together with the line profile (d).

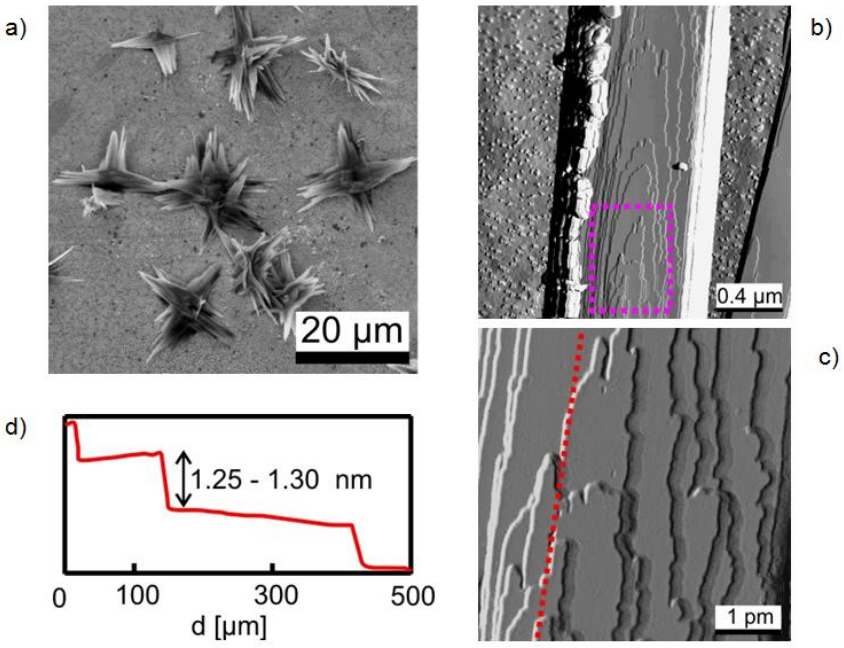

Molecules on Rails: Coupling of Diffusion and Orientation for Pentacene on an Organic Surface

Paul Rotter[1], Barbara A. J. Lechner[2], Antonia Morherr[1], David M. Chisnall[2], David J. Ward[2], Andrew P. Jardine[2], John Ellis[2], William Allison[2], Bruno Eckhardt[1] and Gregor Witte[1]

[1]*Department of Physics, Philipps-Universität Marburg, Germany*

[2]*Cavendish Laboratory, University of Cambridge, United Kingdom*

The realization of novel organic electronics requires the controlled preparation of molecular thin films and heterostructures. Since top-down structuring methods like lithography cannot be applied to van der Waals bound materials, surface diffusion becomes a structure determining factor that requires microscopic understanding. However, despite providing atomic resolution, traditional scanning probe techniques are limited to slow movements and therefore constrained to low temperatures. To study pentacene diffusion at room temperature, we instead used the recently developed helium-3 spin-echo (HeSE) technique[1]. This method takes advantage of the the nuclear spin of ^{3}He atoms to detect a small energetic Doppler broadening upon scattering from moving adparticles. By preparing coherent wave packets and measuring their dephasing rate depending on surface correlation in time and space, both picosecond time and nanometer spatial resolution are achieved.

To obtain a stable and well-ordered organic surface, which is not affected by disorder or pre-melting which often occur already at room temperature, we used a pentacene monolayer chemisorbed on Cu(110) (cf. Fig. 1a inset). A small coverage of pentacene admolecules diffuse on top of this overlayer. Since HeSE detects only motion projected onto one chosen azimuthal direction, measurements along two directions were performed to map two-dimensional diffusion.

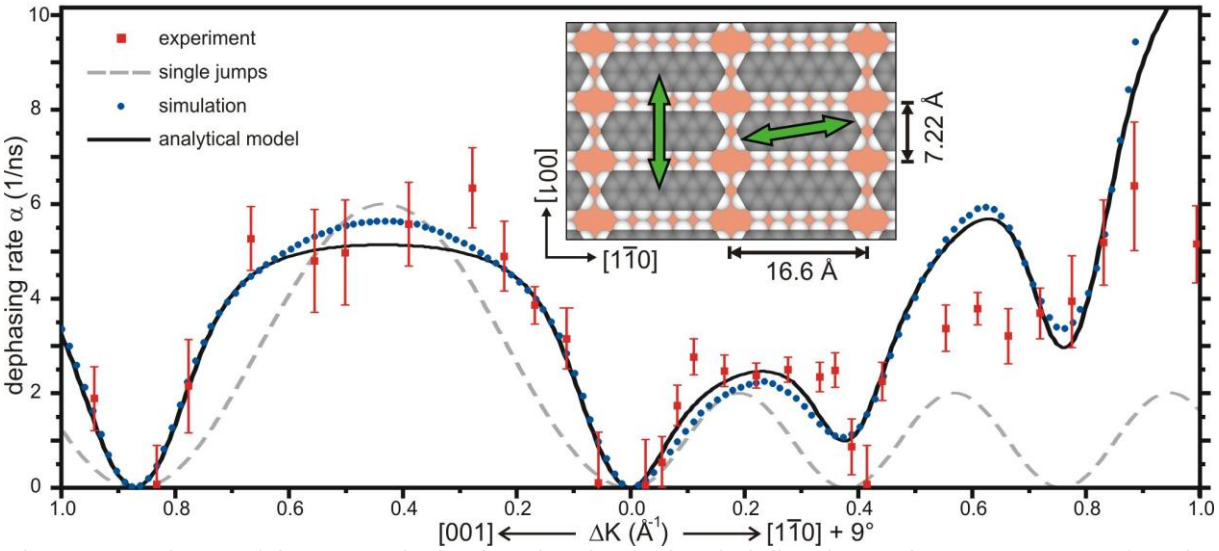

Fig.1: Dependence of the HeSE dephasing signal on azimuthal direction and momentum transfer. The pentacene on Cu(110) model surface (inset) illustrates the HeSE measurement directions (green arrows). Experimental data (red squares) was measured at T = 300 K. The simulation (blue circles) agrees with the experimental data. Squared sinusoids (dashed gray lines) are expected for Chudley-Elliot single jump diffusion. Solid black lines illustrate an analytical model which was developed based on the given microscopic explanation of pentacene on pentacene diffusion. The overall rise on the rhs is a consequence of the small offset angle.

As a scattering technique, HeSE provides detailed ensemble properties of adparticle motion. Information about individual diffusion processes, can be extracted by computer simulation of trajectories and comparison of the corresponding calculated HeSE results to the experimental data (cf. Fig. 1). To obtain an *a priori* potential energy surface (PES) for the simulation, we describe the forces between the immobile pentacene molecules (within the well-defined surface lattice) and the diffusing pentacene using the MM3 force field[2]. The global minimization of all six molecular degrees of freedom (three rotations and three translations) results in a planar admolecule orientation with two different minimum energy configurations as illustrated in Fig. 2a: the pentacene long axis is aligned either parallel or perpendicular to the surface molecules. The uniformly oriented surface molecules form effective rails which guide the admolecule motion. Sideways diffusion without rotation is supressed by a barrier exceeding 300 meV, whereas the potential energy required for rotation of the long axis is only 175 meV. This leads to combinations of the diffusion processes which appear as long jumps. Those apparent long jumps explain the broadening of the observed curve in comparison to the expected shape for single hops between adjacent sites (Chudley-Elliot model[3], cf. Fig. 1 gray line).

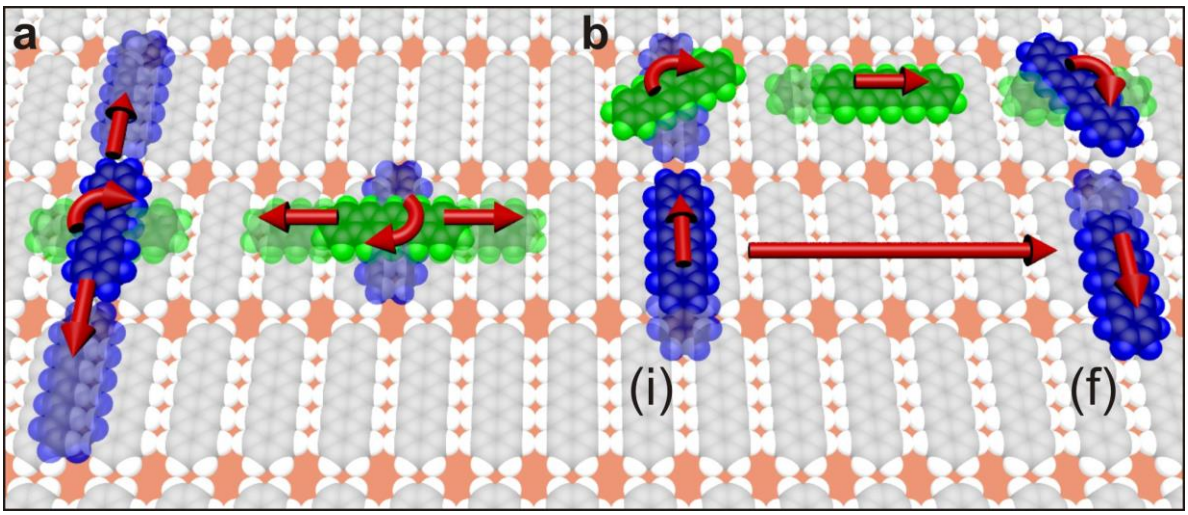

Fig.2: ***a****, Single pentacene admolecules in their potential energy minimum positions together with the corresponding elementary diffusion processes. Admolecules preferentially move along the direction of their long axis but sometimes turn 90°.* ***b****, A molecule that turns 90° from its initial (i) diffusion direction moves perpendicularly and finally (f) turns back appears to perform a long jump in the intermediate direction (long red arrow) covering multiple lattice distances (6-fold jump illustrated).*

In summary, we presented the first observation of molecular scale diffusion in complex organic systems at room temperature. Diffusion of pentacene molecules on a pentacene surface highlights the pivotal role of molecular orientation, which leads to unexpected diffusion dynamics. Our findings enable the first experimental validation of a PES constructed from force field schemes and will serve as an important benchmark for future *ab initio* approaches. Future research includes transfer of the used approach to substituted aromatic molecules such as fluorinated pentacene.

1. Jardine, A. P., Hedgeland, H., Alexandrowicz, G., Allison, W. & Ellis, J. Helium-3 spin-echo: Principles and application to dynamics at surfaces. Prog. Surf. Sci. 84, 323–379 (2009).
2. Allinger, N. L., Yuh, Y. H. & Lii, J. H. Molecular mechanics. The MM3 force field for hydrocarbons. 1. J. Am. Chem. Soc. 111, 8551–8566 (1989).
3. Chudley, C. T. & Elliott, R. J. Neutron Scattering from a Liquid on a Jump Diffusion Model. Proc. Phys. Soc. 77, 353–361 (1961).

Investigations on defect formation during thermal annealing of Ga(NAs) and (GaIn)(NAs) using aberration corrected STEM at different angular regions

Lennart Duschek, Andreas Beyer, Eduard Sterzer, Patrick Sträßer, Wolfgang Stolz and Kerstin Volz

Faculty of Physics and Material Sciences Center, Philipps-Universität Marburg

Introduction

Growing suitable III/V laser structures for optical data transmission on silicon substrate is a highly focused goal to achieve the integration of optics on electronic devices. The quaternary material system Ga(NAsP) is a promising candidate because it can be grown lattice-matched on silicon substrate and is a direct bandgap semiconductor. Furthermore the emitting wavelength of the material can be tuned by the Nitrogen (N) & Arsenic (As) composition. Due to its metastability, Ga(NAsP) has to be grown at rather low temperatures, i.e. 575°C. Post-growth thermal annealing allows the reduction of certain types of structural defects and thus improves the optical properties. The optimal annealing temperature in this case was found at 925°C for 10 s as visualized in figure 1 [1]. Annealing at higher temperatures can cause changes in the structure of the material as can be seen in fig. 2 [1]. Circular structures build up at 925 °C (b) that are not visible in the as grown sample (a) and get more distinct at even higher annealing temperatures like 975°C (c). This also affects the optical properties of the material, depicted in fig. 1. To understand how the process of defect formation in the quaternary material system Ga(NAsP) works, this contribution concentrates on the investigation of different N containing samples, namely Ga(NAs) and (GaIn)(NAs) in GaAs via scanning transmission electron microscopy (STEM) using high angle annular dark field (HAADF) images. All the samples were grown by metalorganic vapor phase epitaxy (MOVPE) with growth temperatures of 525°C (Ga(NAs)) and 575°C ((GaIn)(NAs)). Furthermore the samples were treated thermally either post-growth (annealing at different temperatures) or in the reactor (growth interruption for different times).

Methods

All images shown were recorded with a double C_S corrected JEOL JEM-2200FS transmission electron microscope (TEM) in scanning mode (STEM), where the sample is scanned with a focused electron beam. Thus the electron-sample interaction can be described mainly by Rutherford scattering. These electrons are collected with an annular dark-field detector that has a defined inner and outer detection angle. Since the scattering mechanism in STEM is dominated by Rutherford scattering and thus the scattering angle, respectively the measured intensity I is proportional to Z^c, where $1 < c < 2$. Therefore it is possible to connect the measured intensity directly to the atomic number and obtain chemical sensitive images. Besides Rutherford scattering, also sample thickness and strain of the material can influence the HAADF intensity. Strain can be induced due to static atomic displacements that is caused by N atoms and can produce an increase of low angle scattering. The inner detector angle was changed systematically from 73 mrad down to 24 mrad to take into account the several effects.

Conclusions

Figure 3 shows a Ga(NAs) QW in GaAs, annealed at 975°C and recorded by changing the detector angle, increasing from the bottom to the top of the image. Circular structures, as already seen in Ga(NAsP) fig.1 (c) are clearly visible in the QW structure and get more prominent by decreasing the inner detector angle. This could be an indication for the presence

of Nitrogen or strain relaxation at the edges. It can also be shown that the photoluminescence intensity is not directly connected to the circular defects since the drop in intensity appears already at lower annealing temperatures (fig. 4). This formation could be a property of dilute nitrides, which is a metastable material system. To study structure formation processes in metastable materials further, (GaIn)(NAs) samples with varied growth interruptions on the QW have been examined. It can be shown, that the surface of the QWs get rougher with increasing growth interruption times however, the chemical composition stays homogeneous. This could be the same physical effect, already observed in the Ga(NAs) sample described above, resulting in a different structure.

Outlook

To see whether the observed structural formation is due to the incorporated Nitrogen or a different specific material property, further material systems with and without Nitrogen will be investigated systematically. Also an in-situ annealing procedure of dilute nitride material systems will help to understand the process of structural defect formation.

References

[1] Gies, S., et al. "Annealing effects on the composition and disorder of Ga (N, As, P) quantum wells on silicon substrates for laser application." Journal of Crystal Growth 402 (2014): 169-174.

[2] Grillo, V., et al. "Strain, composition and disorder in ADF imaging of semiconductors." Journal of Physics: Conference Series. Vol. 326. No. 1. IOP Publishing, 2011.

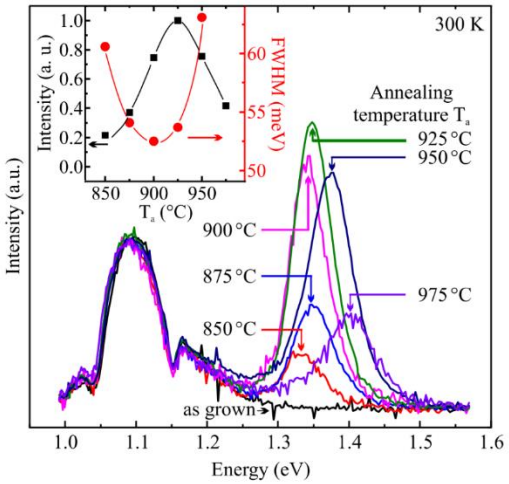

Figure 1 [1]: Photoluminescence spectra of the annealed Ga(NAsP) QW. The inset shows the integrated intensity of the luminescence (squares) and the full width half maximum (circles) as a function of the annealing temperature.

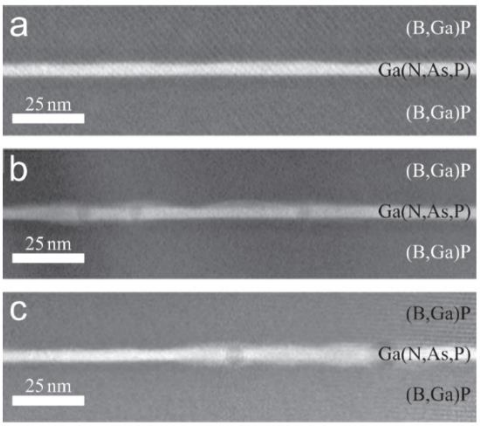

Figure 2 [1]: Low magnification HAADF-images of the as-grown sample (a) and annealed at 925°C (b) and 975°C (c).

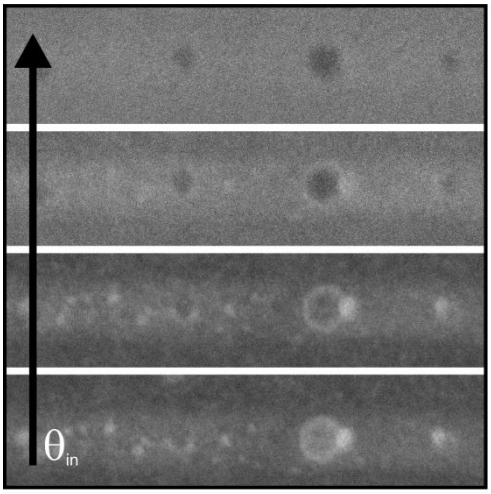

Figure 3: Low magnification HAADF-images of the Ga(NAs) QW annealed at 975 °C.

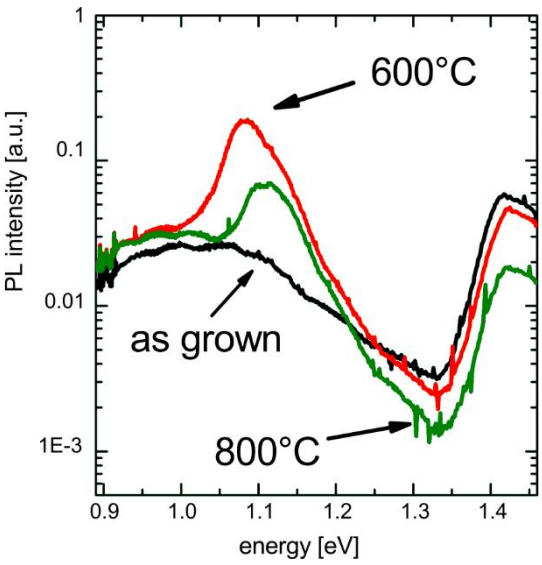

Figure 4: Photoluminescence spectra of the as grown (black) and annealed Ga(NAs) sample at 600°C (red) and 800°C (green).

Chemical vapor deposition and physical characterization of gallium, and carbon-related structures on Si (001) and GaP/Si (001) templates for the growth of graphene layers

Katharina Werner, Andreas Beyer, Kerstin Volz, Wolfgang Stolz

Material Sciences Center and Faculty of Physics, Philipps-Universität Marburg

Having remarkable physical properties as, for example, carrier mobilities as large as several thousands of cm^2/Vs, graphene has attracted great scientific interest in recent years. Researchers have found ways to produce high-quality graphene, e.g., by chemical vapor deposition (CVD) on transition metal substrates such as copper (Cu). Until now though, the production of graphene for particular devices has generally been connected to a transfer of the carbon (C) layer from a growth substrate to an appropriate target substrate. At present complementary metal-oxide-semiconductor electronics are based on silicon (Si) (001) substrates. If graphene could directly be deposited on Si (001) the advantages of graphene could be combined with these widely used devices. This study, therefore, focuses on the direct deposition of graphene on Si (001) by CVD by using the catalytic effect of gallium (Ga), a standard material in Si technology, on the growth of this two-dimensional C material. This catalytic effect was shown before under different conditions [1]. Applying this technique to the deposition of graphene on Si, however, requires a profound understanding of Ga deposition and the characteristics of Ga on Si.

All investigated samples were grown via CVD in a horizontal reactor system using molecular hydrogen (H_2) as carrier gas for most samples. For the Ga growth trimethyl gallium (TMGa) and triethyl gallium (TEGa) were used, while tert-butylethylene, tert-butylethyne, benzene and ethylene were used for C deposition. The surface conditions were investigated with atomic force microscopy (AFM). Scanning transmission electron microscopy (STEM) was applied to gain an insight into the atomic structure and, in combination with energy dispersive X-ray spectroscopy (EDX) into the composition of the grown structures. For selected samples the composition was also determined by secondary ion mass spectroscopy (SIMS). To detect ordered C structures on the samples' surfaces, Raman spectroscopy was applied.

It was reported in earlier studies that the direct deposition of Ga on Si (001) leads to a formation of Ga containing pyramidal structures in Si [2]. The size and number of these structures in Si can be tailored by adjusting the deposition parameters, such as the growth temperature and growth time or the Ga partial pressure. An intermixing of liquid Ga and Si occurs, though, which can lead to the formation of a passivating Si containing layer covering the Ga structures. This effect is also increased by an additional annealing after the Ga deposition. This Si containing layer might hinder the desired catalytic effect of the metallic Ga on the graphene growth. Therefore, the Ga deposition was subsequently performed on a gallium phosphide (GaP) interlayer on Si (001) separating liquid Ga from Si. On GaP also pyramidal Ga containing structures form in the crystalline material topped by mounds which again contain Ga. The size of these structures as well as their number depends on the characteristics of the GaP surface, such as the number of anti-phase boundaries. Additionally, as for the Ga deposition on Si, the size and number of structures forming can again be tailored by adjusting the deposition parameters.

A deposition of metallic Ga on GaP/Si is possible and an annealing at temperatures of 500°C does not seem to significantly affect these structures. This is shown in the AFM images of an as grown and an annealed sample after TEGa deposition on GaP/Si (001) in fig. 1 (a) and (b), respectively. Depositing a carbon precursor, such as benzene, on the Ga pretreated surfaces, however, leads to an etching of Ga rather than to a deposition of material. This can

be observed in fig. 1 (c), presenting a GaP/Si (001) surface after TEGa deposition and a subsequent deposition of benzene for 15 min at 500°C.

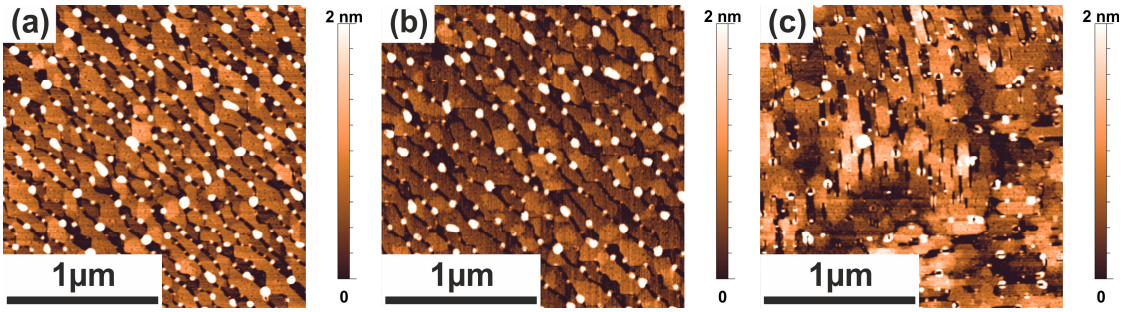

Fig.1: AFM micrographs of TEGa deposited on GaP/Si (001) as grown (a) and after 15 min of annealing (b) or benzene deposition (c) at 500°C.

As a treatment of liquid Ga with a C precursor led to an etching process, it was then approached to deposit C directly on a GaP layer on Si (001). This approach was motivated by studies of other groups proving it possible to synthesis graphene on semiconducting material, such as germanium (Ge), on Si [3]. A deposition of the C precursor ethylene using H_2 as carrier gas again led to an etching of the surface, while a deposition of ethylene using N_2 as carrier gas led to a growth of new structures. As no C related Raman signal was detected for any sample prepared it this way, it has to be assumed, though, that these structures are purely amorphous.

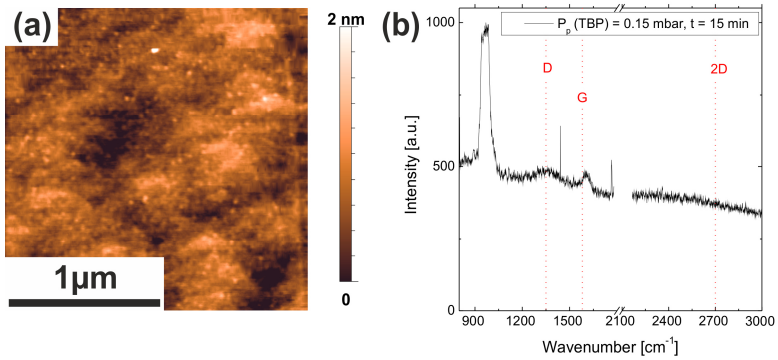

Fig.2: AFM measurement and Raman spectrum of ethylene deposited for 15 min at 800°C on GaP/Si.

High-temperature treatment of GaP with tert-butylphosphine (TBP), however, led to the deposition of considerable amounts of C. The GaP surface structure can still be observed after 15 min of TBP deposition at 800°C, as presented in the AFM measurement of the surface in fig. 2 (a). The Raman spectrum recorded at this sample, however, clearly reveals the C related so-called D and G peaks, which are generated by vibrations of the C_6-ring. As no C6-ring structures, or even sp2-bonded C atoms, exist in the TBP molecule, these must have formed during or after deposition. This could be used as a starting point for further investigations of the deposition of long-range ordered graphene on Si (001). A further investigation of the influence of the growth parameters on this formation is necessary to analyze whether graphene with a long-range order can be grown by this approach.

[1] G. Ding, et al., Carbon. 53 (2013) 321–326
[2] K. Werner, et al., J. Cryst. Growth. 405 (2014) 102–109.
[3] J.-H. Lee, et al., Science. 344 (2014) 286-9

Binding Energy and Dissociation Barrier – Experimental Determination of the Key Parameters of the Potential Energy Curve of Diethyl Ether on Si(001)

Marcel Reutzel[1], Marcus Lipponer[1], Michael Dürr[1,2], and Ulrich Höfer[1]

[1]*Fachbereich Physik und Zentrum für Materialwissenschaften, Philipps-Universität, D-35032 Marburg*
[2]*Institut für Angewandte Physik, Justus-Liebig-Universität Giessen, D-35392 Giessen, Germany*
marcel.reutzel@physik.uni-marburg.de

Introduction

A promising possibility to compete with the challenges of miniaturization in semiconductor device physics is the functionalization of inorganic semiconductor surfaces with organic molecules. In this context, it is important to understand the basic adsorption mechanisms and adsorption dynamics of organic molecules on these surfaces. Within the framework of the GRK 1782 we investigate among others the interaction of ether molecules on Si(001). In the first two years in the GRK 1782, we have studied the adsorption mechanism and dynamics of tetrahydrofuran [1,2] and diethylether (Et_2O) [3] on Si(001). In the last year, we determined experimentally the main parameters of the potential energy curve of diethyl ether on Si(001) by a combination of optical second-harmonic (SHG) and molecular beam techniques.

Results

The optical SH response of the Si(001) surface is proportional to the number of dangling bond orbitals. In Fig. 1 (left), we show that optical SHG can thus be used to follow the ether cleavage reaction of Et_2O in real-time, as the number of quenched dangling bond orbitals changes from the datively bonded intermediate state to the covalently attached final state. Prior to adsorption of Et_2O, the SH response of the clean surface is constant. At t = -155 s, the SH signal drops as Et_2O is adsorbed in the datively bonded intermediate state at T_S = 80 K. At t = -22 s, the surface temperature was increased to T_S = 293 K. Up to t = 0 s, the decrease of the signal is dominated by the temperature dependence of the surface SH response. At t = 0 s, the final temperature is reached and for t > 0 s the change in SH signal

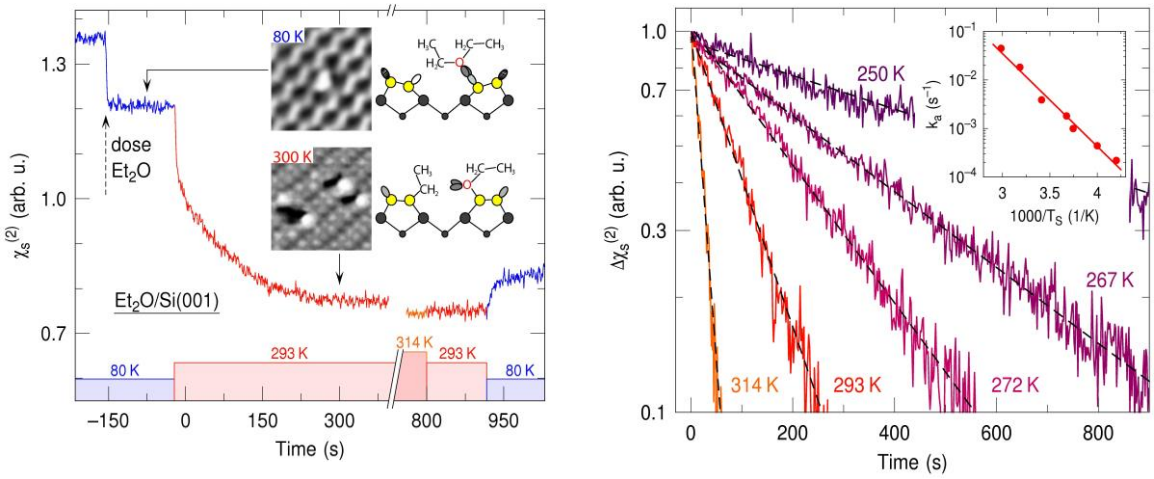

Fig. 1: *(Left) Typical measurement of the normalized nonlinear susceptibility $\chi_s^{(2)}$ for real-time monitoring of the thermally activated ether cleavage reaction which is sketched in the inset [2]. (Righ) Isothermal SH experiments monitoring the ether dissociation at different surface temperatures. The inset shows an Arrhenius plot of the deduced dissociation rate k_a.*

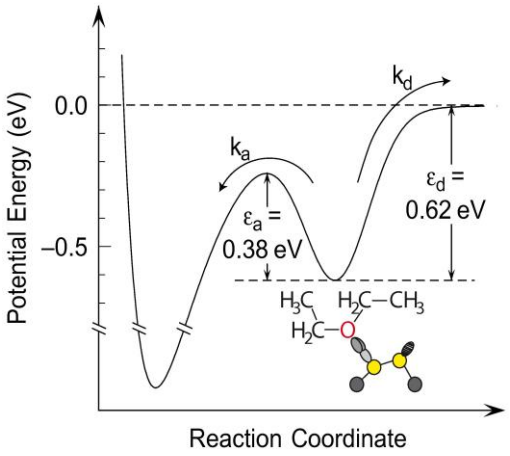

Fig. 2: *Potential energy curve of diethyl ether on Si(001). The datively bonded intermediate state is kinetically stabilized against the ether cleavage reaction by* $\varepsilon_a = 0.38$ *eV and is bonded with* $\varepsilon_d = 0.62$ *eV relative to the molecule in the gas phase*

can be exclusively attributed to the conversion from the intermediate into the final state, as the number of quenched dangling bond orbitals changes from one to two. For a quantitative analysis, the isothermal measurements are plotted on a logarithmic scale in Fig. 1 (right) and fitted with the exponential decay law $\Delta\chi_s^{(2)}(t) = \Delta\chi_s^{(2)}(t=0)\exp(-k_a t)$ of a first order chemical reaction, with k_a being the dissociation rate of Et_2O. The inset in Fig. 1 (right) shows the decay rates k_a plotted as a function of inverse surface temperature. The data points are well described by the Arrhenius law $k_a(T_S) = \nu_a \exp(-\varepsilon_a/K_B T)$ with activation energy $\varepsilon_a = 0.38\pm0.05$ eV and a pre-exponential factor $\nu_a = 10^{4\pm1}$ s^{-1}.

We combined these results with a molecular beam experiment in order to also get access to the binding energy of the intermediate state ε_d. The initial sticking coefficient s_0 of diethyl ether on Si(001) stays close to unity up to surface temperatures of 300 K; for higher temperatures, s_0 drops to values below 0.1 (not shown). This temperature dependence is well described within the Kisliuk model taking into account an adsorption process via an intermediate state. Once trapped in the intermediate state, the molecules can either convert into the final state via ε_a or desorb back into the gas phase via ε_d and the energy barrier difference ε_d-$\varepsilon_a = 0.24\pm0.03$ eV ($\nu_d/\nu_a = (7\pm3)\times10^2$) is extracted. Combining both experiments, the binding energy of the intermediate state is determined to $\varepsilon_d = 0.62\pm0.08$ eV ($\nu_d = 10^{7\pm1.3}$ s^{-1}) and thus the main parameters of the potential energy curve of diethyl ether on Si(001) are experimentally extracted.

Conclusion and Outlook

In conclusion, the main parameters of the potential energy curve of diethyl ether on Si(001) were experimentally determined (Fig. 2). Temperature-dependent measurements of reaction rates by means of optical SHG were combined with molecular beam experiments to deduce both conversion barrier and binding energy. In future, we aim to extend the SHG experiments to a wider range of systems in more systematic studies. In addition, we will study the ether cleavage reaction in more detail; e.g. by triggering the surface reaction electronically by fs-laserpulses.

References

[1] G. Mette, M. Reutzel, R. Bartholomäus, S. Laref, R. Tonner, M. Dürr, U. Koert, U. Höfer, *ChemPhysChem* **15**, 17 (2014).

[2] M. Lipponer, M. Dürr, U. Höfer, *Chem. Phys. Lett.* **624**, 69 (2015).

[3] M. Reutzel, G. Mette, S. Stromberger, U. Koert, M. Dürr, U. Höfer, *J. Phys. Chem. C* **119**, 6018 (2015).

An Introduction to Nuclear Magnetic Resonance at Surfaces

Lars P. Kraft

Department of Physics, NMR at surfaces ,Philipps-Universität Marburg

Nuclear magnetic resonance (NMR) at surfaces combines three areas of physical research:

(1) Surface Science
(2) NMR
(3) Optical Pumping

Each area brings along techniques that are used to get on track of particular mechanisms:

(1) Dynamics of atoms/molecules on crystal surfaces, crystal growth, catalysis
(2) Molecular bindings, bond strength, molecular structures
(3) Laser/Maser, excitation of commonly weak electronic processes

The combination of these 3 areas is tricky since the requirements for one application often compromises the requirements for the other application and vice versa. For example, experiments on surfaces are usually situated in ultra high vacuum (UHV) chambers consisting of stainless steel. In contrast the homogeneity of an NMR magnet, necessary for NMR experiments, is affected by the magnetic iron located in the steel. The other way round a mass spectrometer cannot be used in the fringe field of an NMR magnet. Besides, to perform NMR experiments on a crystal surface "NMR-probes" must be present in a sufficient quantity, only this way signals can be acquired. But this cannot be assumed in general.

Despite all constraints the 3 areas are united in fact. Experiments can reveal molecular bonds on crystal surfaces. In the near future, even structures that are inaccessible to common surface methods are planned to be investigated; for example an internal interface between two crystal structures.

NMR is able to uncover inner structures of solids in a nondestructive way. But if just a few nuclei serve as probes, which is the case on surfaces (10^{14} atoms), the signal strength is too low to lift the signal above the noise background (10^{19} atoms are needed).

The signal strength is proportional to the polarization of the nuclear spin ensemble, i.e. the effective amount of spins that is aligned parallel to the external magnetic field. In thermal equilibrium the polarization is near zero (10^{-6} for ^{129}Xe at room temperature). But it can be enhanced (hyperpolarized) by 5 orders of magnitude: By Laser optical pumping the spin abundant states of the valence electrons of rubidium atoms are populated, and thus polarized. Via hyperfine interaction the polarization is transferred to ^{129}Xe nuclei. This way it is possible to enhance the polarization to more than 50%. In the same way the signal strength rises and the sufficient magnitude for signal detection is reached.

Similar to the transfer between electrons and nuclei it is possible to transfer polarization among nuclei, or to be more precise, between different species of nuclei. Hence it is thinkable to make internal interfaces visible by methods of NMR.

Creation of a Double Resonance Probe Head For Ultra High Vacuum Usage

Lars P. Kraft

Department of Physics, NMR at Surfaces ,Philipps-Universität Marburg

Introduction

One possibility to transfer polarization from one ensemble of nuclei to another one is the "Cross Polarization by Hartmann-Hahn Matching" (CPHH). I.e. by applying two oscillating magnetic fields perpendicular to the static magnetic field and resonant to both species of nuclei respectively the magnetization of each ensemble is precessing in the according effective field. Each magnetization is quantized in its effective field whereby the energetic differences between the nuclear Zeeman levels are dependent on the amplitudes of the oscillating fields. By setting the amplitudes to suitable values it is possible to equalize the Zeeman energies of the two different nuclear species (Hartmann-Hahn matching condition) and thus a passage for spin transfer is opened.

For CPHH experiments a double resonant probe head is a premise. Since the single resonant probe head attached to the UHV chamber is still in use and cannot be changed without excessive effort it is favored to extend it rather than to change it. The solution is to use established principles of double resonant electric circuits and adapt them to our situation, i.e. two electric circuits are connected by a cable. It will be shown that the presence of the cable will not affect the principle severely.

Results

The second resonance providing extension was built and connected to the existing probehead via cable. Tuning and reflectivity were tested with a network analyzer. NMR experiments were performed with ^{11}B situated in the glass work of the UHV chamber and signals were acquirered at two different frequencies shown in fig.1.

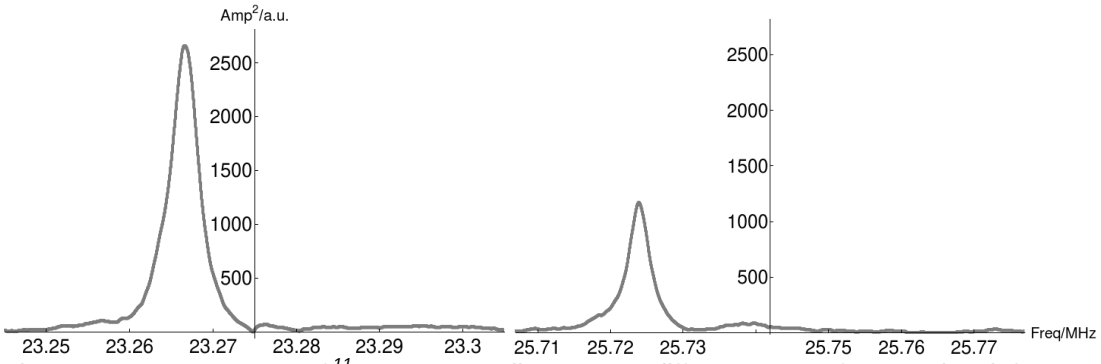

Fig.1: Frequency spectra of ^{11}B resonance lines at two different center frequencies. left: 23.275 MHz, right: 25.742 MHz.

Outlook

The probe head extension was created for CP experiments using hyperpolarized ^{129}Xe as a polarization source at a Larmor frequency of 25.742 MHz while the target nucleus is ^{13}C at a frequency of 23.275 MHz. An isotopically enriched graphene layer on a single crystal substrate like Ir(111) could be a first probe analyzed with this setup.

THEORY TO GENERATION, TRANSPORT, AND RECOMBINATION OF CHARGE CARRIERS IN DISORDERED MATERIALS

Martin Wiemer

Faculty of Physics and Materials Science Center, Philipps-Universität Marburg

This work subdivides into three different studies resulting from collaborations between the groups of Prof. Dr. M. Koch, Prof. Dr. S. Baranovski, Prof. Dr. K. Volz and Prof. Dr. W. Stolz from the Faculty of Physics and Materials Science at Philipps University Marburg, as well as the groups of Prof. Dr. U. Lemmer from LTI at the Karlsruhe Institute of Technology, Prof. Dr. A. V. Dvurechenskii from the Novosibirsk State University and Prof. Dr. P. J. Klar from the Faculty of Physics at Justus-von-Liebig University Gießen.

i) Thermal quenching of photoluminescence in Ga(As,Bi).

We studied the thermal quenching of photoluminescence (PL) intensity in Ga(As,Bi)/GaAs heterostructures [1]. This material shows an unusual plateau in the temperature dependence of PL intensity at low excitation densities (see Fig. 1 c).
Starting from a well-known analytical approach, we were able to show that such a plateau cannot be caused by any monotonous energy distribution of localized states (DOS) in the conduction band tail. As a consequence, the plateau points at a non-monotonous DOS with at least two energy scales. We figured out four different possible energy shapes of the DOS, of which each can well reproduce experimental data. Fig. 1 c) shows exemplarily the resulting PL thermal quenching for the DOS shown in Fig. 1 d), which consists of an exponential and a deeper Gaussian part.

ii) Efficiency of exciton dissociation at internal organic interfaces.

A challenging question in the study of heterojunction organic solar cells is, why the photogenerated electron-hole pairs can dissociated efficiently despite the strong Coulomb interactions in these materials.
A model with discrete dipoles along the internal interface between the different material components appears suitable in order to account for the high exciton-dissociation efficiency [2]. However, the dissociation efficiency in the framework of this model has been so far calculated only within the harmonic approximation.
We have calculated the dissociation efficiency in the dipolar model beyond the harmonic approximation and shown that the exciton dissociation probability appears drastically larger than assumed so far. This can be seen in Fig. 2, where the electric-field dependent dissociation probability is plotted with and without harmonic approximation as well as with and without dipole moments at the heterojunction. We also considered the effect of a finite spatial extent of the dipole charges and showed that if the charges cannot be treated as point-like species, harmonic approximation is not applicable anymore.

iii) Large positive magnetoresistance effects in the dilute magnetic Semiconductors (Zn,Mn)Se in the regime of electron hopping.

We studied the phenomenon of large positive magnetoresistivity, i. e. the increase of resistivity when an external electric field is applied, for the n-type doped dilute magnetic semiconductor (DMS) (Zn,Mn)Se:Cl at temperatures below 10K [4,5]. From the temperature

dependence of resistivity, hopping via localized chlorine states was identified as the dominant charge transport mechanism at the temperature range of interest [4].
Energy levels of Cl donors are affected by the magnetization of Mn atoms in their vicinity via the s-d exchange interaction. Compositional disorder, in particular, the random distribution of magnetic atoms (namely Mn), leads to a magnetic-field induced broadening of the donor energy distribution. This broadening of the donor energy distribution is largely sufficient to account for the experimentally observed magnetoresistance effects in n-type (Zn,Mn)Se with donor concentrations below the metal–insulator transition.
We also demonstrated, that the shift of Cl localized states cue to the s-d exchange interaction with Mn spins can be well estimated with a Gaussian distribution for Mn concentrations about or above 1 % as expected from the central limit theorem.

For the future research, we plan to study recombination processes under various conditions taking into account the fractal structure of the samples. This technique will help us to understand recombination and transport processes in molecular, polycrystalline and other complex structures. Also, we plan to extend the theory of carrier localization due to compositional fluctuations in multicomponent semiconductors.

References

[1] M. K. Shakfa, M. Wiemer, P. Ludewig, K. Jandieri, K. Volz, W. Stolz, S. D. Baranovskii, and M. Koch, J. Appl. Phys. 117, 025709 (2015).
[2] S. D. Baranovskii, M. Wiemer, A. V. Nenashev, F. Jansson, and F. Gebhard, J. Phys. Chem. Lett., Perspectives, 3, 1214 (2012).
[3] M. Wiemer, M. Koch, U. Lemmer, A. B. Pevtsov, S. D. Baranovskii, Org. Electronics 15, 2461 (2014).
[4] F. Jansson, M. Wiemer, A. V. Nenashev, S. Petznick, P. J. Klar, M. Hetterich, F. Gebhard, and S. D. Baranovskii, J. Appl. Phys. 116, 083710 (2014).
[5] A. V. Nenashev, F. Jansson, S. Petznick, M. Wiemer, P. J. Klar, A. V. Dvurechenskii, F. Gebhard, and S. D. Baranovskii, J. Magn. Magn. Mater. 383, 44 (2015).

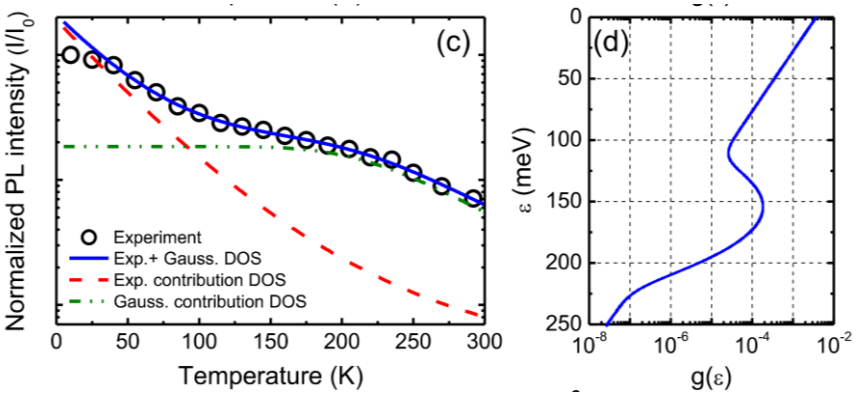

Fig. 1 Panels c) and d) from Fig. 3 in [1]. For the legend – see the text.

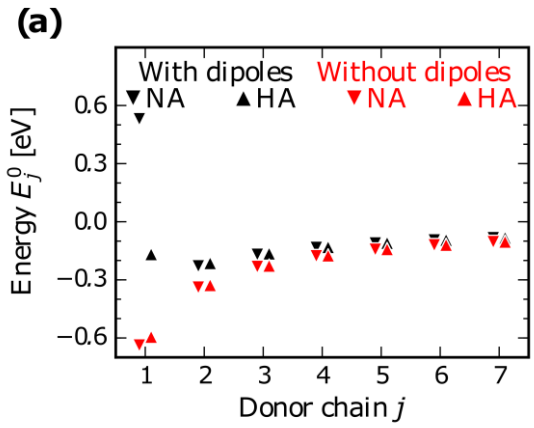

Fig. 2. Dissociation probability of excitons at interfaces with (black) and without (red) dipole moments as a function of electric field [1]. Downward and upward triangles represent the data derived with (HA) and without (NA) harmonic approximation for the electron energy on polymer chains.

Mn doped CdS/ZnS Core/Shell Nanoparticles: Synthesis & characterization

Nadeem Sabir, Pablo del Pino, Wolfgang J. Parak

Faculty of Physics and Material Sciences Center,Philipps-Universität Marburg

Introduction

In last decade, Mn doped CdS/ZnS nanocrystals (NCs) have attracted much attention due to its optical and opto magnetic properties. Magnetic doped based NCs are suitable for different technological applications, in numerous fields such as biomedical diagnosis, solar cells, spintronics, light emitting diodes (LED) [1-7]. Mn dopants cause new photoluminescence features in nanocrystals, enabling particles with duel emission [1-8]. Doping with just few Mn^{2+} ions inside the ZnSe, ZnS and CdSe nanocrystals have been demonstrated to produce a large Zeeman effect [1-9].

Results

With and without Mn-doped CdS/ZnS core-shell nanocrystals were synthesized in organic phase, as described in previously reported methods [9,10]. Mn ions were incorporated into the ZnS shell followed by an additional ZnS shell which was grown on top of the doped shell. The synthesis steps of CdS/Mn:ZnS/ZnS core-shell nanocrystals are shown in the figure 2. Synthesis and characterization of Mn-doped CdS/ZnS core/shell nanocrystals, using a method described previously by Yang et al., are discussed. The mean diameter of CdS/Mn:ZnS/ZnS nanocrystals was determined by TEM micrograph (dc = 4.4 ± 0.7 nm). Mn ions incorporated with QD core-shell structure was confirmed by a clearly observable emission band around 580 nm, which is due to the typical Mn transition.

Conclusions

The synthesis of with and without Mn doped CdS/ZnS core/shell nanocrystals was performed with minor changes. A four-step high temperature colloidal route was used, and the nanocrystals were characterized subsequently [9,10].

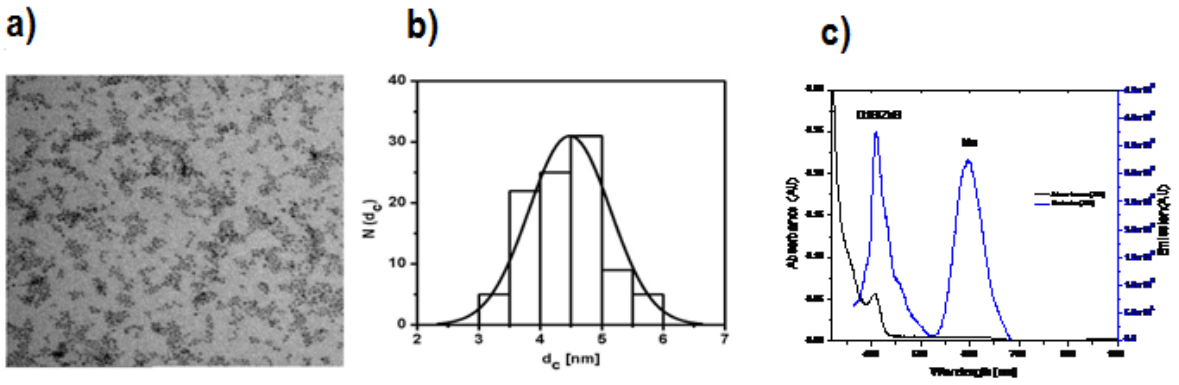

Figure 1: a) TEM micrograph of CdS/Mn:ZnS/ZnS NPs b) From the histogram of the size distribution $N(d_c)$, which refers to the total counts of NPs with a diameter d_c of their inorganic part, the mean NP diameter was determined to be d_c = 4.4 ± 0.7 nm. c) UV-Vis absorption and emission spectra of NPs

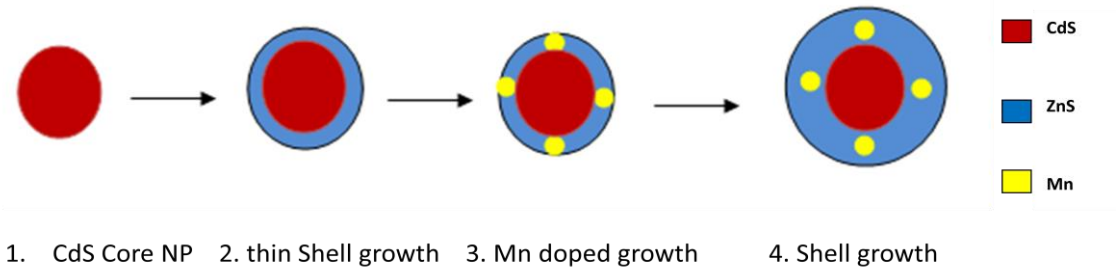

Figure 2. (1) CdS nanocrystals, (2) CdS/ZnS nanocrystals (2ML), (3) Mn-dopant growth, and (4) Mn doped CdS/ZnS nanocrystals (4ML) [9]

References

1. M. Shim, C. Wang, D. J. Norris, P. Guyot-Sionnest, MRS Bull.2001, 1005.
2. J. D. Bryan, D. R. Gamelin, Prog. Inorg. Chem. 2005, 54, 47.
3. D. J. Norris, A. L. Efros, S. C. Erwin, Science 2008, 319, 1776.
4. D. Magana, S. C. Perera, A. G. Harter, N. S. Dalal, G. F. Strouse, J. Am. Chem. Soc. 2006, 128, 2931.
5. N. Pradhan, D. Goorskey, J. Thessing, X. Peng, J. Am. Chem.Soc. 2005, 127, 17586.
6. D. J. Norris, N. Yao, F. T. Charnock, T. A. Kennedy, Nano Lett. 2001, 1, 3.
7. A. Nag, S. Chakraborty, D. D. Sarma, J. Am. Chem. Soc. 2008,130, 10605.
8. S. E. Irvine, T. Staudt, E. Rittweger, J. Engelhardt, S. W. Hell, Angew. Chem. 2008, 120, 2725; Angew. Chem. Int. Ed. 2008, 47, 2685.
9. Y. A. Yang, O. Chen, A. Angerhofer, Y. C. Cao, Chem. Eur. J.2009, 15, 1386.
10. Yang et. al., *J. Am. Chem. Soc*; 2008, *130* (46), Pages: 15649–15661

Intermixing Effects of GaP Grown on Si-(001)

J. O. Oelerich, A. Beyer, A. Stegmüller, K. Jandieri, K. Werner, W. Stolz, R. Tonner, K. Volz, S. D. Baranovskii

Faculty of Physics and Material Sciences Center, Philipps-Universität Marburg

Introduction

III/V semiconductors, combinations of elements from the third and fifth group of the periodic table of elements, are promising candidates for the integration of optoelectronic properties with silicon (Si). While Si itself is an indirect semiconductor, and therefore not optically excitable, many III/V semiconductor compounds have direct bandgaps that can often be tuned by changing the elementary composition. Due to the similarity in lattice constants between Si and gallium phosphide (GaP), the latter is a perfect candidate for buffer layers between the Si substrate and optically active alloys, e.g., Ga(N,As,P) quantum well structures. As device dimensions are decreased to increase the density of components integrated on chips, the interface morphology between the different material layers becomes increasingly important. Recently, it was observed that GaP grown by metalorganic vapour phase epitaxy (MOVPE) on atomically flat Si-(001) substrates exhibits strong intermixing of the materials at the GaP/Si interface. The intermixing structures appear as pyramidally shaped Si clusters within a layer thickness of more than seven monolayers (ML).
We were able to reproduce these effects with kinetic Monte Carlo (KMC) computer simulations of the growth procedure and identify kinetic aspects of the growth as the main driving force of intermixing. The energy barriers necessary for the interdiffusion and formation of the structured interface have been confirmed in density functional theory (DFT) calculations. Our findings suggest that such intermixing behaviour is a general effect of the growth of P-containing heterostructures on Si. The results are submitted for publication to the Journal: Chemistry of Materials [1].

Simulation Method

To simulate the observed structural effects, we employed the bond counting KMC method, in which energy barriers for atomistic events are determined by summing up energy contributions of existing nearest- and second-nearest neighbor bonds. These contributions depend on atomic species of the two participants in the bond, and on their distance. They are the main input parameters to the simulation and were varied in order to reproduce the intermixing effects. Two atomistic events are present in the simulation: An adsorption event, in which a new atom arrives at an unoccupied lattice position on the substrate, and a diffusive event, in which an atom performs a thermally activated transition from one lattice position to an unoccupied site within the second coordination sphere. The parameters for the adsorption events were chosen to match the growth rates used in the experiments. All atoms are at all times constrained to the zincblende lattice structure and lattice strain was not taken into account. The simulated system contained 55 x 55 x 60 unit cells, i.e., in total 1452000 lattice sites. The growth temperature was chosen as 775 K.
First, 25 ML of Si were grown onto two fixed substrate layers. The resulting Si substrate was atomically flat, with only some adatoms and small islands on the surface. Then, P and Ga were provided layer by layer in pulsed growth mode, with a relaxation pause of 1 s after each phase, until a total of 20 ML of GaP were present in the system.
The energy contributions of the nearest- and second-nearest neighbor bonds were chosen as 0.3 eV and 0.15 eV, respectively, for all pairs of atomic species except Si-P. The Si-P bond strengths were chosen as 0.6 eV for a nearest neighbor and 0.2 eV for a second-

nearest neighbor bond. This strong bond between P and the Si substrate is necessary to reproduce the observed significant intermixing (see Results).

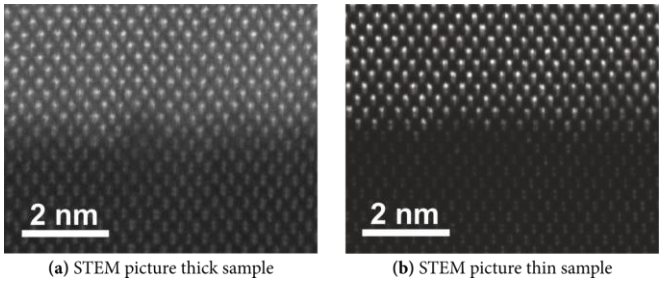

Figure 1: The GaP/Si interface as measured with STEM, at 20 nm (a) and 8 nm (b) thick regions. The dark atomic columns in the bottom half resemble the Si substrate, and the upper half is the GaP overlayer.

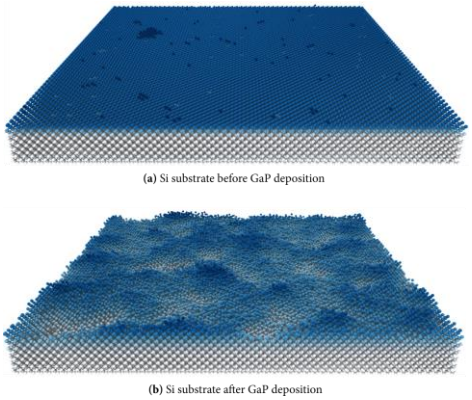

Figure 2: The simulated Si substrate before (a) and after (b) arrival of Ga and P atoms. Higher atoms are shown in darker color.

Results

For the comparison with the experimental measurements, which were performed as scanning transmission electron microscopy (STEM) measurements on 20 nm and 8 nm thick regions of the sample, slices of similar width were cut out from the simulated system. The measured interfaces for both thicknesses are shown in Fig. 1. It is clearly visible, that intermixing of about 7-8 ML occurred at the interface. In addition, the interface is faceted, as pyramidally shaped Si clusters are visible at the interface. The Si substrate before and after growth of GaP (in the latter case, Ga and P atoms are hidden in the picture) is shown in Fig. 2. The initially flat substrate is clearly faceted after GaP growth and exhibits significant intermixing.

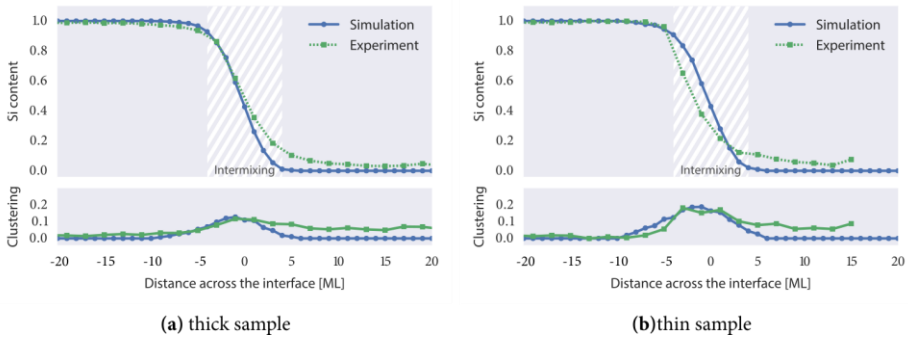

Figure 3: Si content versus distance across the interface for the thick (a) and thin (b) sample regions, compared to the simulated data. The clustering is the standard deviation of Si content of different atomic columns in a single ML and thereby a measure of the faceting at the interface.

The Si content of the MLs with respect to growth direction was determined via iterative frozen phonon simulations from the experimental measurement data and can therefore be compared quantitatively to the theoretical data. The results are shown in Fig. 3. Clearly, the simulations and the experimental measurements agree nicely and produce similarly strong intermixing. In addition, the faceting (clustering) at the interface agrees well.

Conclusion

We were able to show that one slow atomic species, i.e., one species bound more strongly to the Si substrate than the other species, induces strong intermixing effects. The assumption of P atoms being more strongly bound to Si atoms was confirmed in DFT calculation. The remarkable agreement between experiment, KMC simulations and DFT calculations shows that the strong interface intermixing is an inherent effect of the GaP/Si interface and suggests, that this is a general behaviour of P containing heterostructures on Si substrates.

[1] A. Beyer, A. Stegmüller, JOO, K. Jandieri, K. Werner, W. Stolz, SDB, R. Tonner, K. Volz, **submitted**.

Polymorph-Selective Preparation of Perylene Single-Crystals by Liquid-Mediated Growth

André Pick, Gregor Witte

Faculty of Physics, Philipps-Universität Marburg, D-35032 Marburg, Germany

Introduction

Organic semiconductors occurring in polymorphic structures represent excellent model systems for fundamental studies of optoelectronic excitations in different crystalline configurations. Perylene is an archetypal polycyclic aromatic hydrocarbon appearing in two phases known as α- and β- phases which reveal various molecular packing motifs. However, the growth of high quality single-crystals with appropriate sizes and polymorph selectivity remains challenging. In this study [1], we compare various approaches to prepare polymorph-selective perylene single-crystals, which are analyzed in terms of morphology and structure. We demonstrate that organic molecular beam deposition onto silicone-oil covered substrates enables the fabrication of high quality crystals of both phases. By carefully tuning the deposition parameters the relative occurrence of the individual polymorphs can be controlled. While pyramidal crystals reveal screw-dislocations, platelets exhibit molecularly flat surfaces and thus enable detailed fluorescence studies without any defect related emission signals.

Results

Thin-films of silicone-oil spin-coated onto a substrate have been used to grow large single-crystals polymorph-selectively (cf. Fig.1). The different polymorphs are distinguishable by the characteristic crystal shapes:

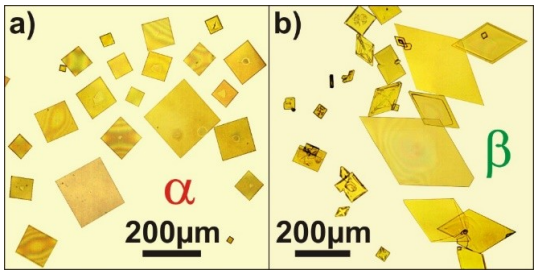

Fig.1: Optical micrographs of perylene single-crystals grown in oil:
a) α-phase (35nm @ 300K & 4Å/min)
b) α- and β-phase (235nm @ 290K & 2Å/min)

This is confirmed by out-of-plane XRD with appropriate single-crystals grown from toluene-solution:

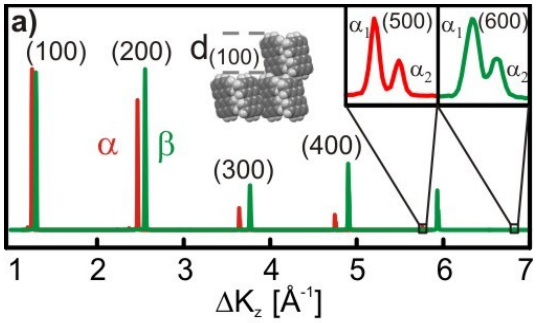

Fig.2: Bragg-Brentano scans confirming a slight difference in the (100) lattice spacings of the two different polymorphs.

To identify crystallographic directions within a single-crystal, in-plane measurements were performed (cf. Fig.3). This information is crucial for the interpretation of polarization resolved spectroscopy data.

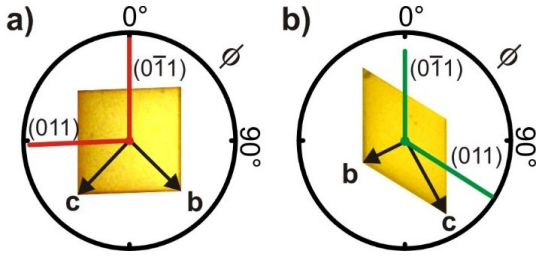

Fig.3: Polar plots of in-plane XRD scans together with the azimuthal orientation of the unit cells within the (100)-planes

A morphological analysis of single-crystallites obtained from sublimation of the perylene-powder between two substrates shows that platelets of both phases are molecularly flat over a distance of more than 20µm (cf. Fig.4). In contrast to this, pyramidal shaped single-crystals exhibit screw-dislocations of different complexity, which may affect UV/vis-spectra (cf. Fig.5).

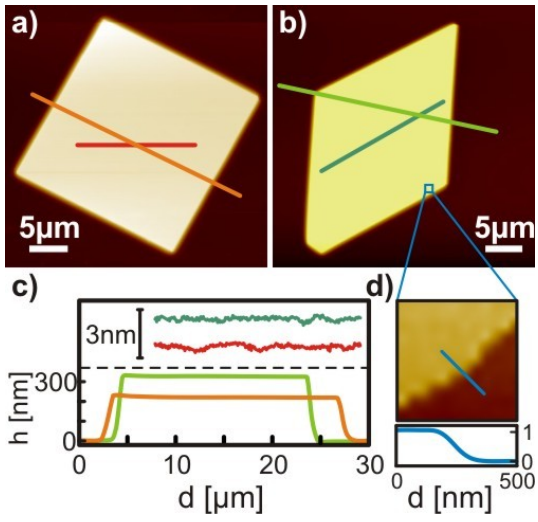

Fig. 4: AFM-analysis of perylene-platelets of both phases, the β-phase crystal in b) possesses one single monomolecular step.

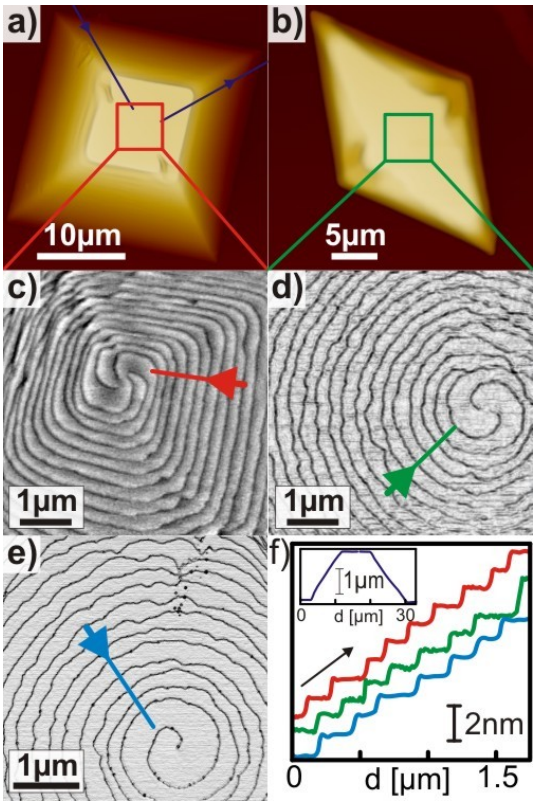

Fig.5: AFM-analysis of pyramidal single-crystals: The spirals are shown as derivative of the topography together with their cross-sections.

The photoluminescence-spectra of perylene-platelets are shown in Fig.6. The different crystalline phases can easily be distinguished using Confocal Laser Scanning Fluorescence Microscopy: While the α-phase appears red, the β-phase emits green light (insets).

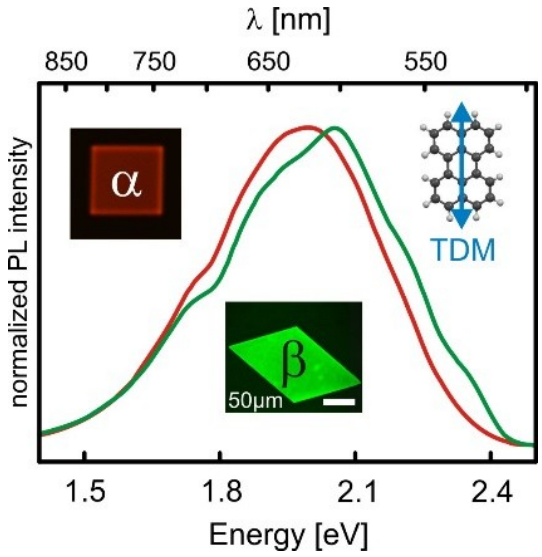

Fig.6: PL-spectra and CLSF-micrographs together with the transition-dipole-momentum which is oriented nearly perpendicular to the (100) planes

In addition parasitic emission at defects is found which also affects their spectral signature. Moreover we show that consideration of the spectral sensitivity of the detection system is important as it distinctly affects the true fluorescence spectrum.

Summary

Polymorph-selective crystal growth of perylene is achieved by means of liquid mediated molecular beam deposition. By choice of temperature of the supporting oil and growth rate the relative occurrence of both crystalline phases can be adjusted, hence demonstrating that polymorph selection is mainly kinetically controlled. Crystals of both polymorph exhibit characteristic base areas (rhombic vs. near rectangular) which have been thoroughly characterized by means of AFM, optical microscopy and XRD and allow an unambiguous distinction solely based on their crystalline shape. Liquid mediated grown crystals of both polymorph are disc-shaped with a thickness of less than 300nm and exhibit almost atomically flat surfaces. By contrast pyramidal shaped crystals grown by re-sublimation of powder or from solution are substantially thicker and frequently exhibit defects like screw-dislocations or steps and micro-facets. Finally we have examined also the fluorescence signature of the various crystals. Though the different color impression of both polymorphs enables their easy distinction, the fluorescence emission is spatially rather anisotropic.

Outlook

The exceptional high quality of platelet crystals in combination with their low thickness that makes them semitransparent enables in particular optical studies in transmission geometry without disturbing influence of defects. Previous work has shown that this approach can provide detailed information on the excitation dynamics in crystalline organic semiconductors [2] and will be applied also to the various polymorphs of perylene in future studies.

Furthermore, differently functionalized self-assembled monolayers can be used to control the nucleation of perylene (cf. Fig.7). The focus of such studies is on the understanding of the mechanism of position selective nucleation of perylene that is achieved by stamping patterns of self assembled monolayers of different chemical termination.

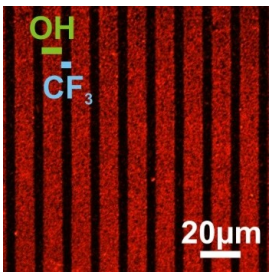

Fig.7: CLSF-micrographs of perylene-patterns on different SAMs.

References

[1] Pick, A.; Klues, M.; Rinn, A.; Harms, K.; Chatterjee, S.; Witte, G. submitted to *Crystal Growth & Design*

[2] Kolata, K.; Breuer, T.; Witte, G.; Chatterjee, S. *ACS Nano*, **2014**, 8, 7377-7383.

Organic functionalization of discrete Sn/Se clusters with the aim of functionalizing semiconductors

By Niklas Rinn

AK Dehnen, Faculty of Chemistry, Philipps-Universität Marburg

Both SnSe and $SnSe_2$ are semiconductor materials with interesting properties for different applications.[1,2] In the group of Prof. Dehnen, the possibility for organic functionalization of discrete Sn/Se Clusters was first showcased, opening up pathways for further ligation to other (semiconducting) compounds and surfaces.[3] This creates a synthetic approach to well defined model systems for electronic interaction between Sn/Se based systems and other materials.

Continuing from the results of my master thesis, I started my research by synthesizing and investigating the synthesis of different simple Sn/Se-clusters and their reactivity towards hydrazines. Through a condensation reaction involving the keto-functionality in the organic ligand, I was able to attach simple molecules to my compounds in this way (figure **1**).

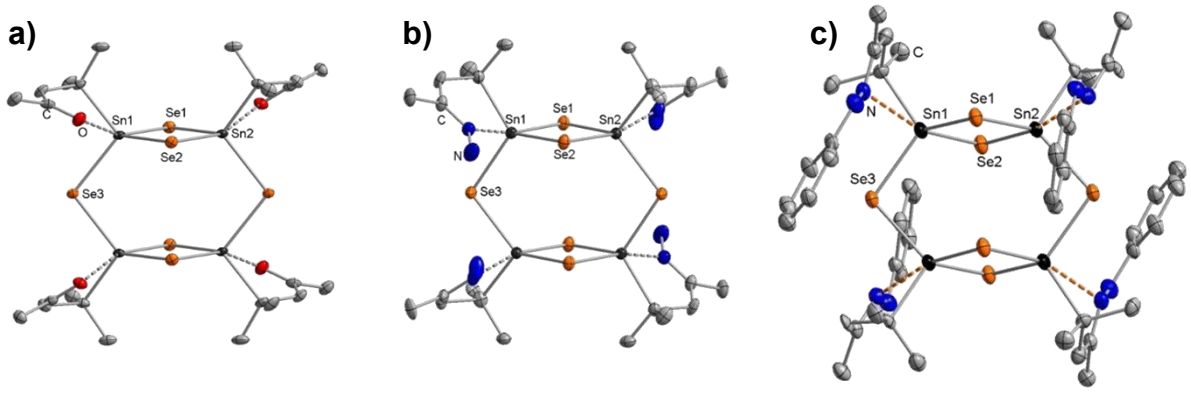

Figure 1: Simple Sn/Se-clusters (**a**) and condensation products upon hydrazine hydrate (**b**) and phenylhydrazine (**c**) addition.

Another possibility for tuning of Se/Sn Clusters is the introduction of further metals to the inorganic cluster core. A variety of metal complexes with the general composition $[M(PPh_3)_xCl_y]$ (M = Cu, Ag, Pd) were used to successfully synthesize compounds with ternary cluster cores. Again, a linkage to hydrazine compounds could be carried out in most cases, albeit sometimes leading to a rearrangement of the Cluster topology. When introducing silver to a one of my compounds, formation of an Ag/Se core surrounded by an organically shielded Sn/Se shell could be observed (figure **2**), which is especially interesting considering the semiconducting nature of Ag_2Se.

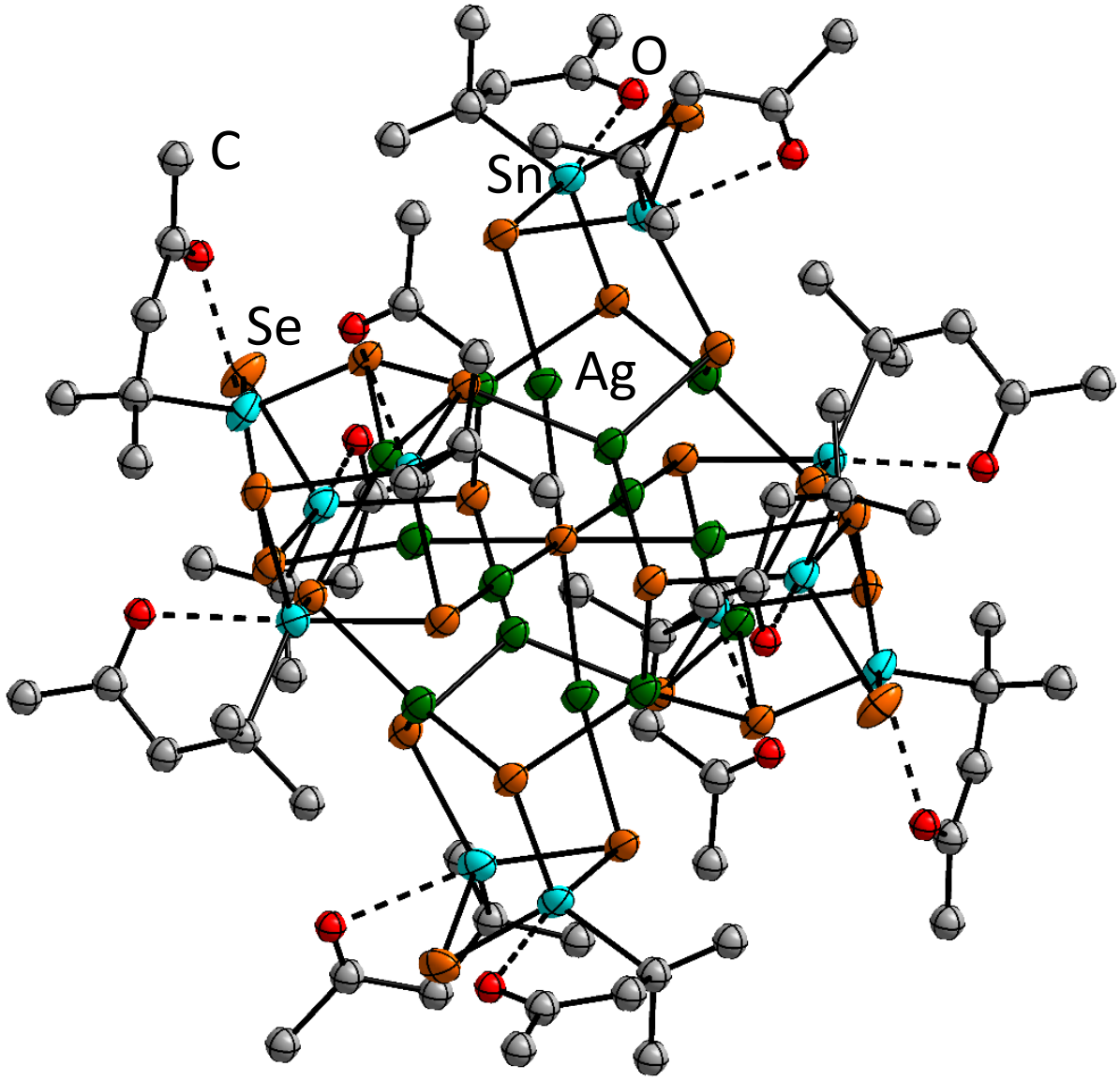

Figure 2: Sn/Se/Ag Cluster showing distinct Ag/Se and Sn/Se domains.

Building up from these results, my research goal for my time in the GRK is to investigate the electronic properties of my cluster and investigate the interaction with other compounds, either to other Sn/Se clusters or semiconducting surfaces, through organic linkers. In the next 6 month, it is my goal to first link Sn/Se/(M) clusters to each other via multifunctional linkers using the complementary reactivity of hydrazines and carbonyls. My remaining time will be used to develop new organic Ligands to attach my compounds to surfaces like Si(001), a chemistry that was shown for similar Sn/S compounds in the Dehnen group recently.

[1] B. Pejova, I. Grozdanov, *Thin Solid Films*, **2007**, *515*, 5203-5211.
[2] K. Bindu, P. Nair, *Semicond. Sci. Technol.*, **2004**, *19*, 1348-1353.
[3] J. P. Eußner, B. E. K. Barth, E. Leusmann, Z. You, N. Rinn, S. Dehnen, *Chem. Eur. J.* **2013**, *19*,13792−13802.

Micro structuring of light-addressable biosensors

Johannes Völkner and Gregor Witte

Molecular Solid State Physics, Faculty of Physics, Philipps-Universität Marburg

Introduction

Biosensing systems for applications in life sciences have gained significant interest in recent years. One concept in this field is a light-addressable biosensor that incorporates quantum dots (QDs) linked to a metal support. Charge carriers that are generated in the QDs upon illumination can flow towards a supporting electrode in an electrochemical cell while the resulting current can be used to monitor the concentration of chemical agents within the cell. In this frame my project focusses on the linking of nanoparticles to a gold surface *via* organic molecules. Sufficient conductivity and stability of the linking layer is required in order to effectively transduce the created charge carriers. Furthermore, the capability to stably bind to both, the QDs and the electrode is requisite. Molecules with two thiol terminations seem to be promising candidates to fulfill latter request. Aromaticity and the feasibility of forming a well-ordered monolayer lead to the application of stilbenedithiol (StDT)[1]. My work concerns the quality and stability of such self-assembled monolayers (SAMs). A second topic regards the QD-immobilization as stable thiol-QD-binding is reported rather contradictory in literature[2-3].

Results

SAMs of StDT were prepared wet chemically, *i.e.*, at elevated temperature a gold surface (evaporated on mica) was immersed in a solution containing the molecule, that subsequently covalently binds to the metal and over time self-assembles in a well-ordered monolayer. Additional molecules on top are after extraction rinsed away and the achieved monolayer is at this state either subject of investigation or undergoes further modification with QDs.

In X-ray photoelectron spectroscopy electrons leaving a sample upon X-ray irradiation are counted in dependence of their kinetic energy that in turn reflects their binding energy and thus origin. Deconvolution of obtained high-resolution data in the S2p region into doublets of different specific binding energies enables one to deduce the chemically neighborhood of the sulfur atoms. It can be part of an intact thiol group, bound to the gold surface as part of the molecule (thiolate) or singularly or present in an oxidized fashion (cf. inset in Fig. 2, left)[1]. Optimally, a predominating thiol and weaker thiolate feature can be recognized. However, as seen in Fig. 2, a not negligible fraction of the obtained signal is to attribute to oxidized thiol groups and ripped off sulfur. This observation is intensified for films prepared from toluene solution in contrast to dichloromethane. A heat series of second sample (recorded sequentially after cooling) showed peculiar persistency of both, the thiol and oxide species, whereat latter evolved to become predominant with higher temperature up to its sudden disappearance from 700 to 800K. This behavior stands in contrast to previous observations where the oxidized sulfur appeared to be rather unstable with temperature (data not shown). A depth profiling of the molecular film did not allow an indisputable spatial localization, however, data let us exclude that the oxide is not solely located at the film-substrate interface.

It is noteworthy that the binding energy correlated to the presence of thiol (~163.5eV) can alternatively be assigned to dithiols that readily form between different molecules[4]. In particular, a conversion from thiol to

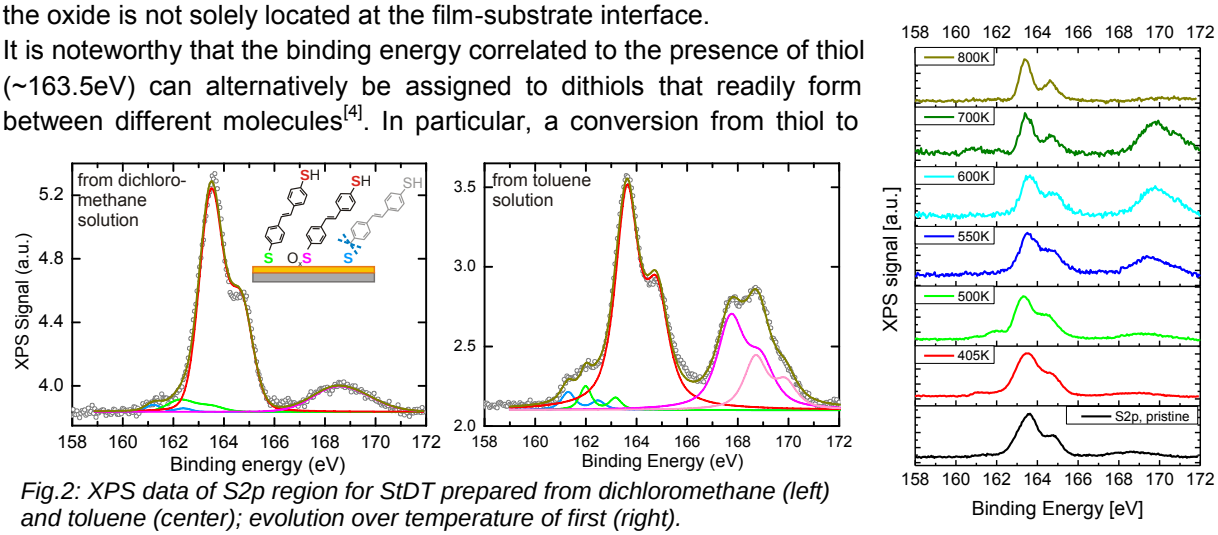

Fig.2: XPS data of S2p region for StDT prepared from dichloromethane (left) and toluene (center); evolution over temperature of first (right).

dithiol is imaginable and not to reveal from present data.

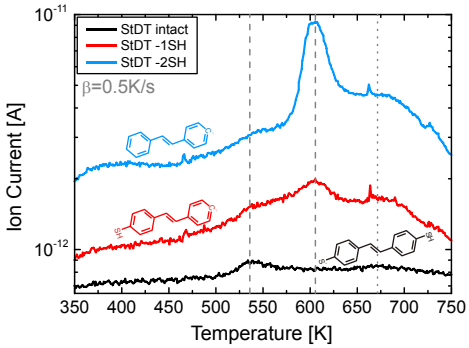

Fig.3: Thermal desorption spectrum of StDT-SAM with three mass fragments.

Stability of the SAM was further investigated by analyzing the thermal desorption of the molecules. A typical TD spectrum is shown on Fig. 3. Different detection traces are each attributed to a specific fragment of the molecule. According to the spectrum, a small fraction of molecules desorbs intact at about 535K, whereas dissociative de-sorption of the majority, *i.e.*, leaving behind the sulfur, takes place at about 605K. Above 650K signal spikes are to correlate to irregularities in the measurement, the increased intensity at 670K more likely originates from a general increase of material in the chamber than surface desorption of particularly StDT.

Another side-study addresses the capability of the dithiol layer to bind QDs from solution. The strategy chosen for this purpose was quartz crystal microbalance (QCM), where the adsorption of material specifically changes the resonance frequency of the oscillating quartz crystal. Upon assembling of molecules on the surface as expected a slight decrease in frequency was observed. In contrast, results upon immersion in QD-solution showed no significant and reproducible effect.

Conclusions

XPS data show that the used toluene is unsuitable regarding the formation of high-performance SAMs from solution. The occurring oxidation of thiol groups is highly detrimental to film order and when it comes to the application as it causes trapping of charge carriers that in turn cannot contribute to the photocurrent. Still, the point of time of ongoing oxidation is not revealed as well as the location and role in the film (formation). The origin is most likely oxygen and water residues in the toluene. StDT dissolved in dichloromethane yields films of better quality, however, preparation is less practical as due to higher vapor pressure the solvent readily evaporates through the sealed crucibles used at elevated temperature.

Stability of the monolayers in terms of heating appears high as compared to other (mono-)thiols. While the measured temperature values in the XPS-setup might be defective, values observed in TDS seem more realistic. Lying-down of molecules upon desorption of intact species and binding to the gold with both thiol groups could be an explanation for the two observed desorption channels and high thermal stability. I would hereby neglect the argumentation of different adsorption sites (microterrace vs. step edge) due to the essential difference in intensity of 535 and 605K peak. One might apply this explanation to the bump visible at about 670K in data provided one wants to associate this to StDT desorption. Regarding the QCM-investigation of QD-attachment on functionalized gold surfaces it is to mention that used QD-solution was highly diluted as compared to other studies[2] and results are potentially sophisticated by the necessity of dismounting the QDM-setup between each experimental step.

Outlook: what is planned?

The preparation protocol of the dithiol layers needs to be reconsidered. The application of “dry” and degassed toluene seems inevitable, furthermore the relocation of entire procedure into a glove box might be beneficial. However, one further (or first) has to rethink the employment of dithiols to form the linking layer. QCM studies with a more suitable setup are underway to test the amount of QDs immobilized on such, in comparison with SAMs that do not exhibit a thiol termination (*i.e.*, specific vs. non-specific QD adsorption). A flow cell will be used to monitor the crystal’s frequency while QD-solution constantly flows over the chip. If no thiol-assisted attachment can be proved efforts towards the pre-treatment of QDs with dithiol ligands will have to be tackled. By now, the nanocrystals are from synthesis capped with an extensive organic layer that to our perception hinders external molecules to reach the core. Apart from these plans, the incoherent XPS results deserve further investigation and eventually the lateral patterning of sensor structures has to be tackled.

References

[1] Khalid *et al.*, ACS Nano **5** (12), 9870 (2011)
[2] Pernik *et al.*, J. Phys. Chem. C **115**, 13511 (*2011*)
[3] Sambur et al., Langmuir **26** (7), 4839 (2010)
[4] Turchanin *et al.*, Langmuir **25** (13), 7342 (2009)

Quantitative Investigations of Local Lattice Distortions in Crystalline Semiconductors by C_s-Corrected (Scanning) Transmission Electron Microscopy

Jürgen Belz, Andreas Beyer, Kerstin Volz

Faculty of Physics and Material Sciences Center, Philipps-Universität Marburg

Introduction

Transmission electron microscopy (TEM) is undoubted the most advanced microscopy technique when atomic scale information is sought. Nevertheless, for many years the resolution of the TEM was far beyond its theoretical wave optical limit due to severe lens aberrations present in magnetic lenses. With the advent of aberration correction the limiting aberration called spherical aberration could be compensated and a routine operation with sub-Angstrom resolution is achievable. Furthermore, the incorporation of stable multipole correctors made the residual aberrations measureable opening the door for highly reliable atomic measurements. These advances made both conventional (CTEM) and scanning TEM (STEM) increasingly popular for material science applications.

With a resolving power in the order of most crystal lattice spacings the TEM is the most suitable device for investigation of atom scale irregularities in highly ordered crystalline material systems.

The present work focuses on the quantitative measurement of compositions in multinary materials like the compound semiconductor (GaIn)(NAs) as well as the investigation of interfaces of semiconductor heterostructures.

Furthermore, focus is laid on the quality of sample preparation because of its severe effect on thin TEM samples. Therefore, the damaging effect of ion milling processes are explored. Additionally, the effect of thin foil relaxation is investigated and its influence on CTEM and STEM imaging is considered.

Results

In order to distinguish material composition of complex material systems on the atomic scale the artifacts presumably introduced by the preparation have to be considered (cf. figure 1). Therefore, the standard thinning process has to be investigated with high precision.

The focus was set to two main artifacts, which are known to have considerable effects on the imaging processes in the TEM. Both arise from the need of having thin samples in the TEM (< 100 nm) due to the very strong electron matter interaction. The first artifact is the resulting damage of the thinning process, which is inevitable when i.e. cross-sections of semiconductor heterostructures are investigated. The conventional approach is to produce sandwich structures, which are first mechanically thinned to a few microns thickness. The final thinning is carried out by using ion milling under shallow angles in order to produce flat and thin samples. This process not only produces surface amorphization but also damages the material under investigation by ion implantation and (sub-) surface damage. The magnitude of these effects are usually estimated from the amorphous layers only.

In contrast to this, a different approach is used in the context of this research. After carrying out a standard argon ion thinning procedure, the sample was furthermore sectioned by the use of a focused gallium ion beam milling device. With this device it is possible to prepare high quality samples from any position of a target. It itself is similar to the conventional ion beam thinning but due to its focusing capability an actual TEM sample can be sectioned to produce a cross-section of a TEM sample.

From such a cross-section it can be seen that the sub-surface damage extends much further into the crystal than initially assumed, even for the low argon ion energies. The implantation damage is revealed by annular dark field imaging in the STEM mode. The increase of intensity with respect to the GaAs matrix (cf. figure 2) indicates a disorder effect, which is described in [1].
A second effect, which is to be investigated is the elastic thickness relaxation in coherently strained heterostructures, which are used e.g. for the laser device fabrication.
Whereas during epitaxial growth of coherently strained materials with different lattice constants the resulting stress results in a pure elongation of the unit cell in growth direction ("tetragonal distortion"), which is not the case for TEM sample foils anymore. In contrast to the huge lateral dimension of the wafers compared to the unit cell during growth, the preparation of cross-sectional samples reduces the lateral dimensions drastically. The size of the thinned sample is therefore only several times bigger than the lattice constant and the strained layers relax elastically into the surrounding space. This causes lattice bending and reduces the strain state of the layer [2] (cf. figure 3).
It is known that this artifact introduces smooth contrast irregularity perpendicular to the strained quantum well layers and its effect can be mistaken for changes in composition. In order to model this geometric effect, finite element simulations are carried out solving the equations of linear elastic theory for anisotropic materials.
By utilizing the inelastic scattering and measuring the electron energy loss spectrum (EELS) in the TEM, the transmitted thickness could be derived by using the Kramers-Kronig-Analysis [3]. In addition, the (revised) semi-empirical method provided by Iakoubovskii et al. [3,4] is used to ensure data consistency. As a complementary method the absolute fraction of ADF-intensity in the STEM was used to measure the thickness by data matching with image simulations [5]. All three methods provide a consistent thickness estimation and are strongly encouraging the use of the ADF signal because of its relatively simple acquisition.
The results are used to estimate the strain reduction in low dimensional materials from simulations and to reconstruct the volume strain value.

Conclusions

The investigation of preparation artifacts revealed ion implantation damage in the range of 10 nm for GaAs-based materials below the fully amorphous surface layer. The damage distribution is linearly decreasing and could be investigated with ADF-STEM.
The effects of elastic strain relaxation were modeled and simulated successfully via finite element relaxation and show, even without image simulation, good agreement with CTEM measurements under certain imaging geometries. Therefore, the validity of the approach is shown.

Outlook

The results derived from the aforementioned projects will be used to reduce the artifacts introduced by sample preparation. New methods of thinning are sought and precise mechanical grinding to the nanometer scale is investigated. The effect of elastic strain relaxation on composition determination is under current research by coworkers and a correction scheme of its influence is under development. The accuracy and reliability of the ADF-thickness measurements is further explored for different scattering regimes and corrections of the projection system on the ADF detection are under consideration.
Additionally, the research is extended to the investigation of the gallium phosphide / silicon interface.

References

[1] V. Grillo, K. Mueller, K. Volz, F. Glas, T. Grieb, A. Rosenauer, Strain, composition and disorder in ADF imaging of semiconductors, J. Phys. Conf. Ser. 326 (2011) 012006. doi:10.1088/1742-6596/326/1/012006.

[2] M.M.J. Treacy, The effects of elastic relaxation on transmission electron microscopy studies of thinned composition-modulated materials, J. Vac. Sci. Technol. B Microelectron. Nanom. Struct. 4 (1986) 1458–1466. doi:10.1116/1.583473.

[3] R.F. Egerton, Electron energy-loss spectroscopy in the TEM, Reports Prog. Phys. 72 (2009) 016502. doi:10.1088/0034-4885/72/1/016502.

[4] K. Iakoubovskii, K. Mitsuishi, Y. Nakayama, K. Furuya, Thickness measurements with electron energy loss spectroscopy., Microsc. Res. Tech. 71 (2008) 626–31. doi:10.1002/jemt.20597.

[5] A. Rosenauer, M. Schowalter, STEMSIM—a New Software Tool for Simulation of STEM HAADF Z-Contrast Imaging, Springer Netherlands, Dordrecht, 2008. doi:10.1007/978-1-4020-8615-1.

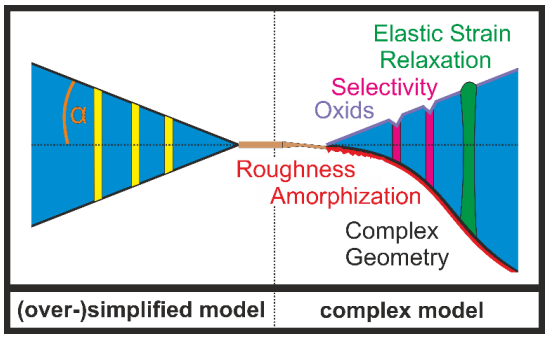

Fig.1: Illustration of the different artifacts, which might occur during ion beam milling. The samples are usually wedge shaped with a semi-angle related to the sputtering geometry.

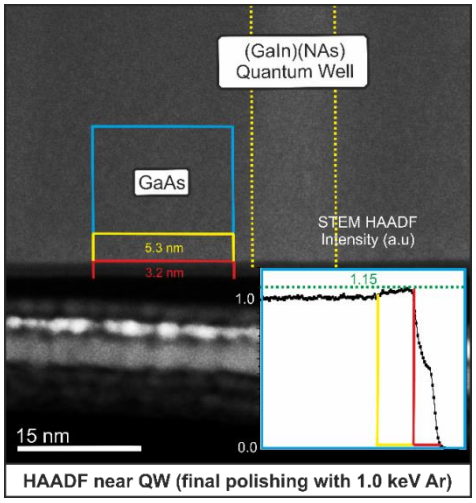

Fig.2: The disorder effect near the surfaces by argon ion beam damage presumably increases the ADF-STEM intensity in this region with respect to the surrounding gallium arsenide matrix.

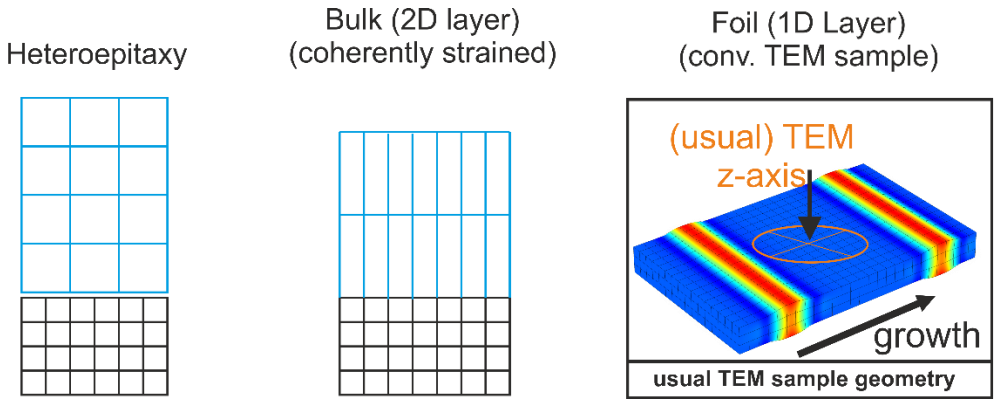

Fig.3: Strained quantum well layers cannot reduce their strain in any except the growth direction while they form a thin film over the wafer. In a cross section of such a stack additional surfaces provide the elastic relaxation into the surrounding environment, generally reducing the strain state.

Spectral Properties of FWM Signals from (GaIn)As Quantum Wells under strong THz fields

M. Drexler, R. Woscholski, S. Lippert, W. Stolz, A. Rahimi-Iman, M. Koch

Faculty of Physics and Material Sciences Center, Philipps-Universität Marburg

In order to reveal the features of a THz-induced intra-excitonic reversible transfer as it has been predicted by microscopic theory in Ref. [1], a four-wave-mixing (FWM) experiment in transmission geometry was combined with strong THz fields as it has been described in Ref. [2]. The experimental details as well as the description of the sample can be found in Ref. [2]. Here, we extend the discussion to the spectral properties of the THz-FWM-experiment described in that reference, as the FWM signals have been spectrally resolved by a spectrometer and a (GaIn)As detector as described in Ref. [3].

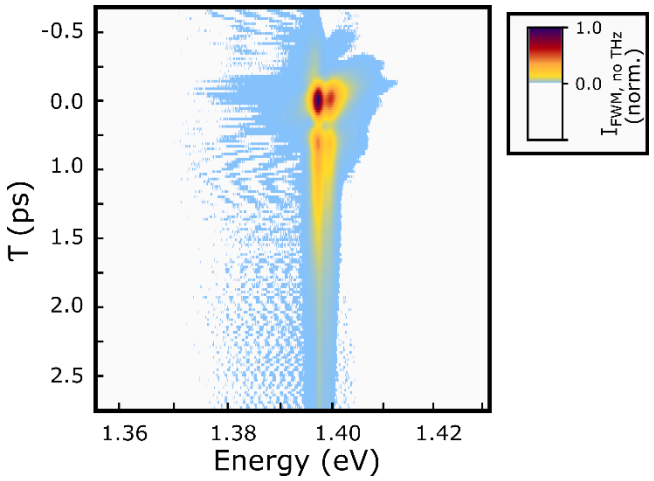

Fig. 1: *Two-dimensional spectra encoded in false-colors of the normalized undisturbed FWM intensity as a function of the delay τ between both optical FWM pulses.*

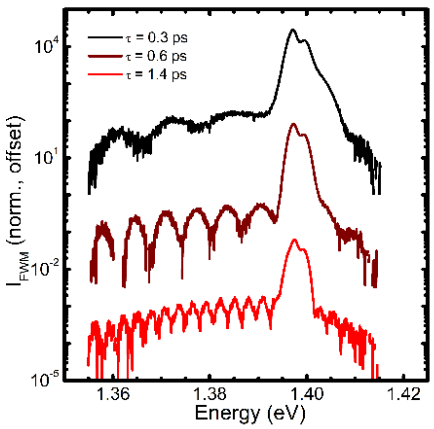

Fig. 2: *Normalized spectra of the undisturbed FWM intensity in logarithmic scaling. The three delay times (black, dark red, red) are shifted vertically and horizontally. In correspondence with Fig. 1, an oscillatory structure appears which exhibits a large energy difference of the oscillations when approaching time-zero.*

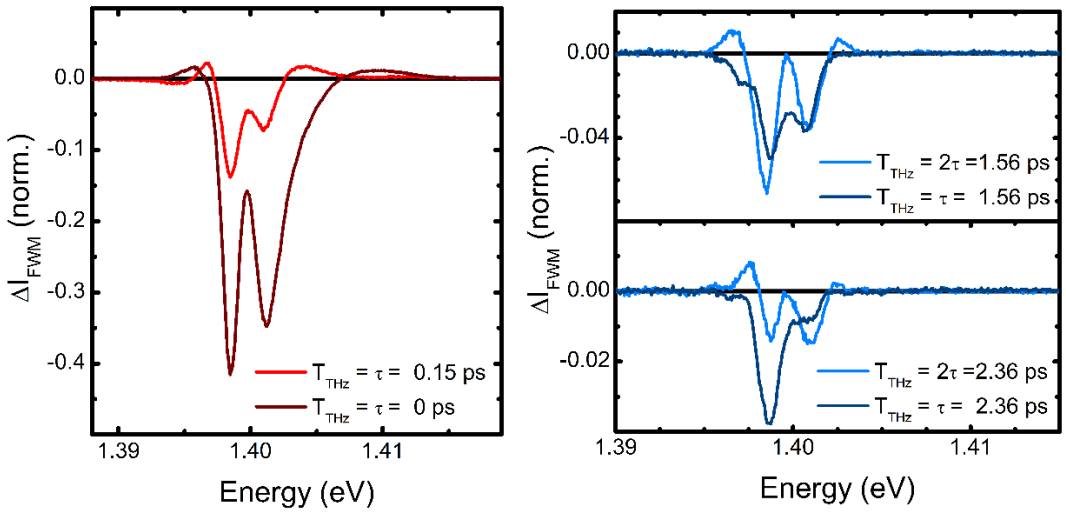

Fig. 3: *Differential spectra of the FWM intensity with THz and without THz at a field strength of 9 kV/cm. The delay times T_{THz} and τ correspond to the two-dimensional plot in Fig. 1 (c) of Ref. [2].*
(Left) For the case of small delay times τ (delay between optical pulses), at a THz delay of T_{THz}=τ (delay between THz pulse and first optical pulse) the spectra exhibit signatures of a broadening caused by the ionization of the excitonic polarization by the incident THz field.
(Right) For larger delay times τ, the signatures of broadening only appear in the spectra at a THz delay of T_{THz}=2τ. Only at the exact point in time where the radiation of the FWM signal occurs, the signatures of THz induced ionization become apparent.

Fig. 1 and Fig. 2 show the spectra of the averaged undisturbed FWM signals as a function of the time-delay τ from data shown Fig. 1 (c) of Ref. [2]. An oscillatory signature appears at very low intensities compared to the main FWM signal. Additionally, the energy difference of the oscillation increases when the time-delay approaches time-zero.
When analyzing the THz-induced changes in differential-intensity spectra, one can recognize a spectral broadening (Fig. 3) which is consistent with previous FWM experiments under the presence of static electric fields [4].

[1] B. Ewers, N. S. Köster, R. Woscholski, M. Koch, S. Chatterjee, G. Khitrova, H. Gibbs, A. Klettke, M. Kira, and S. Koch, “Ionization of coherent excitons by strong terahertz fields,” *Phys. Rev. B*, vol. 85, no. 7, pp. 1–5, Feb. 2012.

[2] M. J. Drexler, R. Woscholski, S. Lippert, W. Stolz, A. Rahimi-Iman, and M. Koch, “Disturbing the coherent dynamics of an excitonic polarization with strong terahertz fields,” *Phys. Rev. B*, vol. 90, no. 19, p. 195304, 2014.

[3] K. Kolata, S. Imhof, N. S. Köster, S. Cecchi, D. Chrastina, G. Isella, J. E. Sipe, A. Thränhardt, and S. Chatterjee, “Hole system heating by ultrafast interband energy transfer in optically excited Ge/SiGe quantum wells,” *Phys. Rev. B*, vol. 85, no. 16, pp. 1–5, Apr. 2012.

[4] von Plessen G, T. Meier, M. Koch, J. Feldmann, P. Thomas, S. Koch, E. Göbel, K. Goossen, J. Kuo, and R. Kopf, “Exciton ionization induced by an electric field in a strongly coupled GaAs/AlxGa1-xAs superlattice.,” *Phys. Rev. B. Condens. Matter*, vol. 53, no. 20, pp. 13688–13693, May 1996.

ZnO nanoparticle characterization and surface optimization with a look on toxicity

Karsten Kantner

Faculty of Physics, Biophotonics Workgroup, Philipps-Universität Marburg

ZnO nanoparticles were synthesized by colloidal routes and their physicochemical properties were investigated in detail. Three different surface modifications were investigated, involving coatings with amphiphilic polymer poly(isobutylene–*alt*–maleic anhydride)–graft–dodecyl, mercaptoundecanoic acid, and L-arginine, which provide the nanoparticles with either a negative or a positive ζ-potential. The hydrodynamic diameters and ζ-potentials of all three nanoparticle species were investigated at different pH values and NaCl concentrations by means of dynamic light scattering and laser Doppler anemometry, respectively.

While in general different physicochemical properties are entangled, specially designed model series of NPs allow for unravelling the impact of individual physicochemical properties. As surface charge and state of agglomeration of NPs are highly interconnected, for the investigation of both effects a series of NPs with different charge as well as with different states of agglomeration is required. There is a general agreement that in most experimental scenarios positively charged NPs are more toxic than negatively charged ones.

This type of nanomaterial is one of the mostly employed NP species, finding numerous applications such as in sun cream, solar cells, *etc*. Toxic effects of ZnO NPs are well studied in literature but not their origins. One possible source of their apparent toxicity lies in the release of Zn^{2+} ions due to the NPs' corrosion.

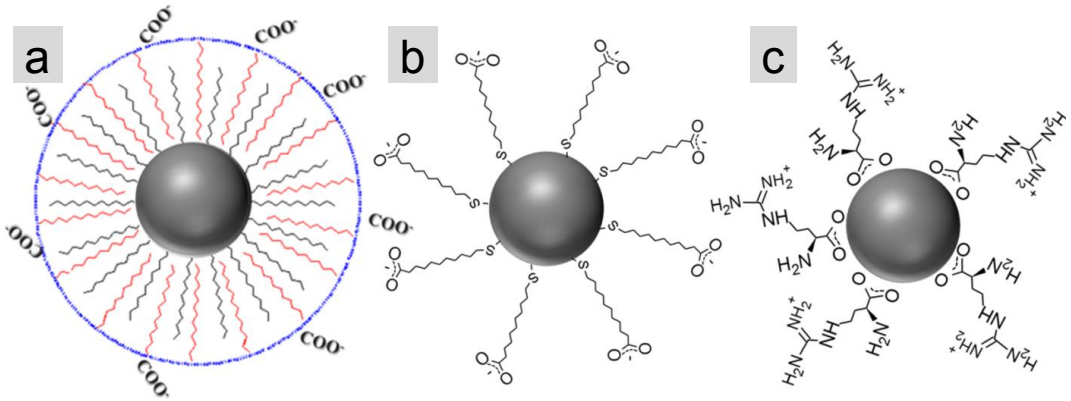

Figure 1: a) PMA, b) 11-mercaptoundecanoic acid, c) arginine capped ZnO nanoparticles

The band edge emission peak of all the NPs is located in the UV, whereby in all cases there is also an additional emission peak, which is associated to trap state emission.

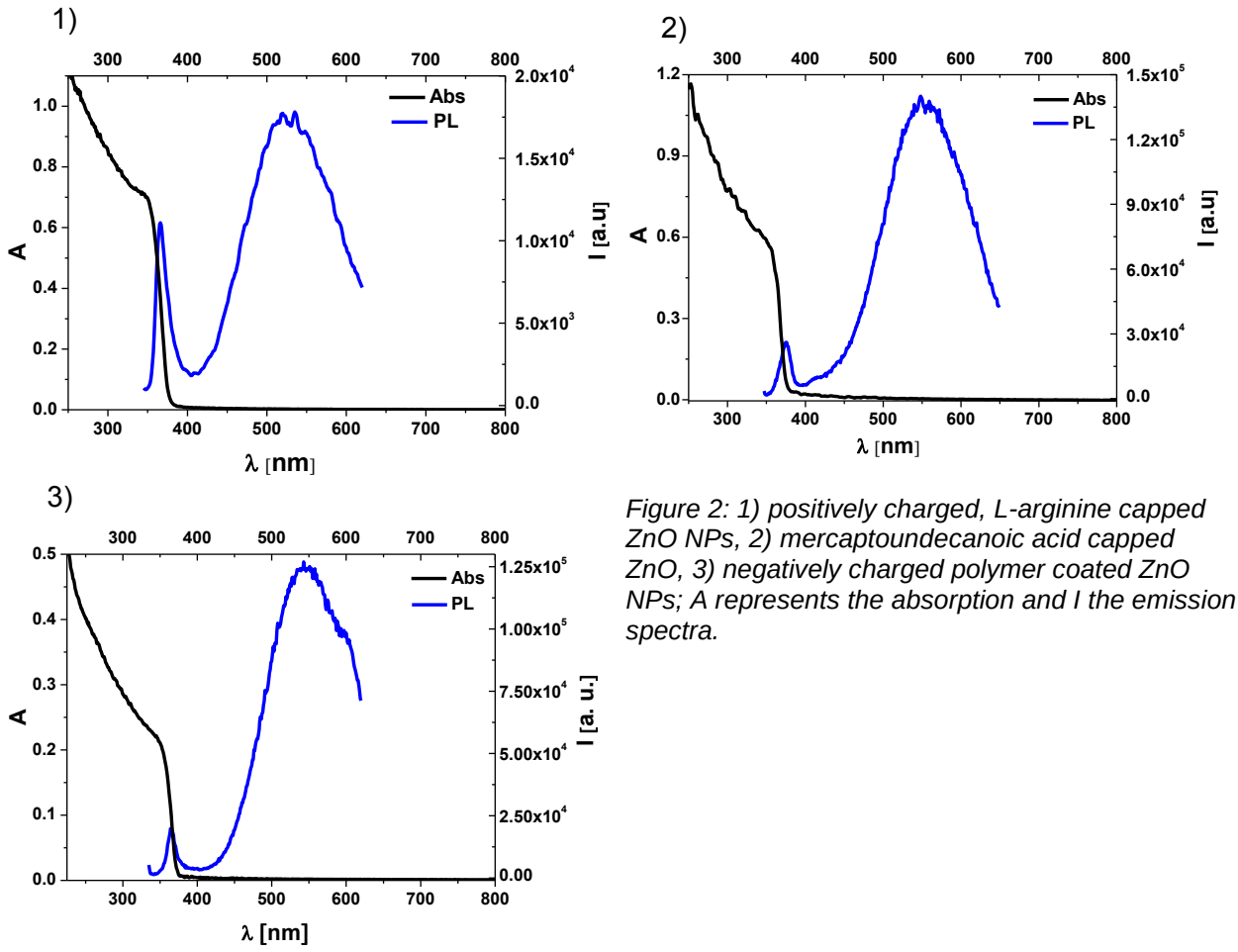

Figure 2: 1) positively charged, L-arginine capped ZnO NPs, 2) mercaptoundecanoic acid capped ZnO, 3) negatively charged polymer coated ZnO NPs; A represents the absorption and I the emission spectra.

While the first peak in the near UV is attributed to the typical fluorescence as a result of the recombination of the photo-excited electrons in the conduction band with holes in the valence band or to near-band-edge emission resulting from the recombination of the photo-excited electrons in the conduction band with the holes trapped near the valence band, the photoluminescence in the visible, *i.e.* the second peak, might be attributed to the presence of oxygen vacancies.

	ZnO-PMA	ZnO-MUA	ZnO-Arg
λ_{abs} [nm]	345	355	349
$\lambda_{em,1}$ [nm]	364	374	365
$\lambda_{em,2}$ [nm]	543	546	521
ζ [mV]	-35.2 ± 3.6	-19.8 ± 2.9	+26.6 ± 0.4
d_c [nm]	6.8 ± 1.5	6.8 ± 1.5	6.8 ± 1.9
d_h (0 mM NaCl) [nm]	18.4 ± 1.0	50.4 ± 5.1	18.1± 0.4
d_h (100 mM NaCl) [nm]	16.7 ± 2.0	117.2 ± 10.2	1314.0 ± 83.2

Table 1: Conclusion of nanoparticle characterization.

High resolution STEM HAADF investigations of Bi- ordering in MOVPE- grown Ga(AsBi)

Nikolai Knaub, Andreas Beyer and Kerstin Volz

Faculty of Physics and Material Sciences Center, Philipps-Universität Marburg

Introduction

Dilute bismide Ga(AsBi) based III-V semiconductors are promising candidates for the next generation of optoelectronic devices. A major reason for this is the fact that the incorporation of Bi in GaAs leads on the one hand to a strong reduction of the band gap by 80 meV per % Bi and on the other hand it shifts the spin orbit split of band towards lower energies [1]. However, the growth of Ga(AsBi) by metal organic vapor phase epitaxy (MOVPE) takes place under metastable conditions and thus is very challenging, since metallic droplets can occur during growth [2].
In this summary we will show by means of high resolution scanning electron microscopy (HR STEM) measurements that even under optimized growth conditions and droplet free Ga(AsBi) layers [3], Bi atoms show the tendency to order on an atomic scale.

Results

High resolution measurements were performed in a double- spherical aberration (C_S) corrected JEOL JEM 2200 FS field emission transmission electron microscope operating at 200 kV. We used the high angle annular dark field (HAADF) method for the Ga(AsBi) sample's investigation which allows us an uncomplicated interpretation of the HR images, since the measured intensity is proportional to $Z^{1.7}$ (Rutherford-like scattering), where Z is the atomic number. Figure 1a depicts a HR- HAADF image of a $Ga(As_{0.952}Bi_{0.048})$ layer, at this point it is worth to mention that the image in figure 1a is a sum of seven independent images of the equal position which were recorded with a fast scan rate. Thus we obtain a much better signal to noise ratio and specimen drift as well as scan distortions do not have a huge effect on the image's quality compared to a slower scan rate image. Afterwards we aligned the images by using the non-rigid **MATLAB** written **Smart Align** code [4].

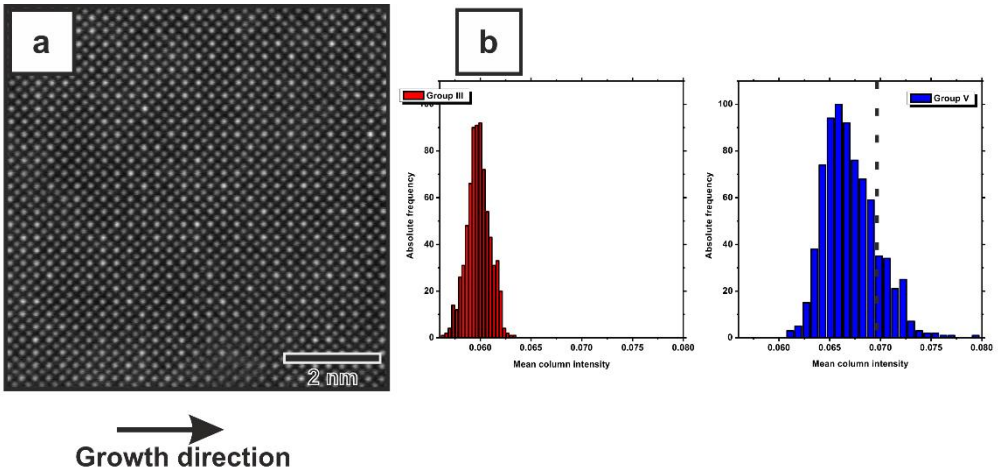

Fig.1: (a) STEM HR HAADF image of $Ga(As_{0.952}Bi_{0.048})$ layer and corresponding histograms (b) which depict the intensity distribution of group III (Ga) and group V (As+Bi) columns.

In the next steps we normalized the aligned image to the impinging electron beam and separated the group III and group V sublattices, which allows us to plot the mean column intensity distribution for each sublattice (figure 1b). The histograms in figure 1b describe a narrow and Gaussian- like distribution for the Ga- containing columns, while the group V histogram describes a broadened intensity distribution with a “shoulder” in the region of the higher intensities. This is expectable, since some group V columns contain more Bi atoms than others and thus provide higher column intensities. Therefore we defined a region for the higher intensities in the histogram (dashed line) and plot the corresponding group V columns in the HAADF image (figure 2a). In this plot it is possible to see columns with the highest intensity (red circles) as well as columns which seem to arrange in a certain way (“chain”- like structures in growth direction and perpendicular to it). For this reason we wrote a **MATLAB** code which performs a Hough- transform [5] of the image (figure 2b). The Hough- transform has the property that every single peak (blue squares in figure 2b) in the Hough- space corresponds to a line in the original image. Hence we have chosen those peaks which correspond to lines in growth direction and perpendicular to it and perform a back-transformation to detect the “chain”- like structures as lines in the original image which is depicted in figure 2c. Judging from the result in figure 2c one can argue that Bi atoms seem to prefer the surrounding of other Bi atoms which arrange them to appear mostly pairwise in growth direction (and perpendicular to it) and also to create longer “chain”-like structures.

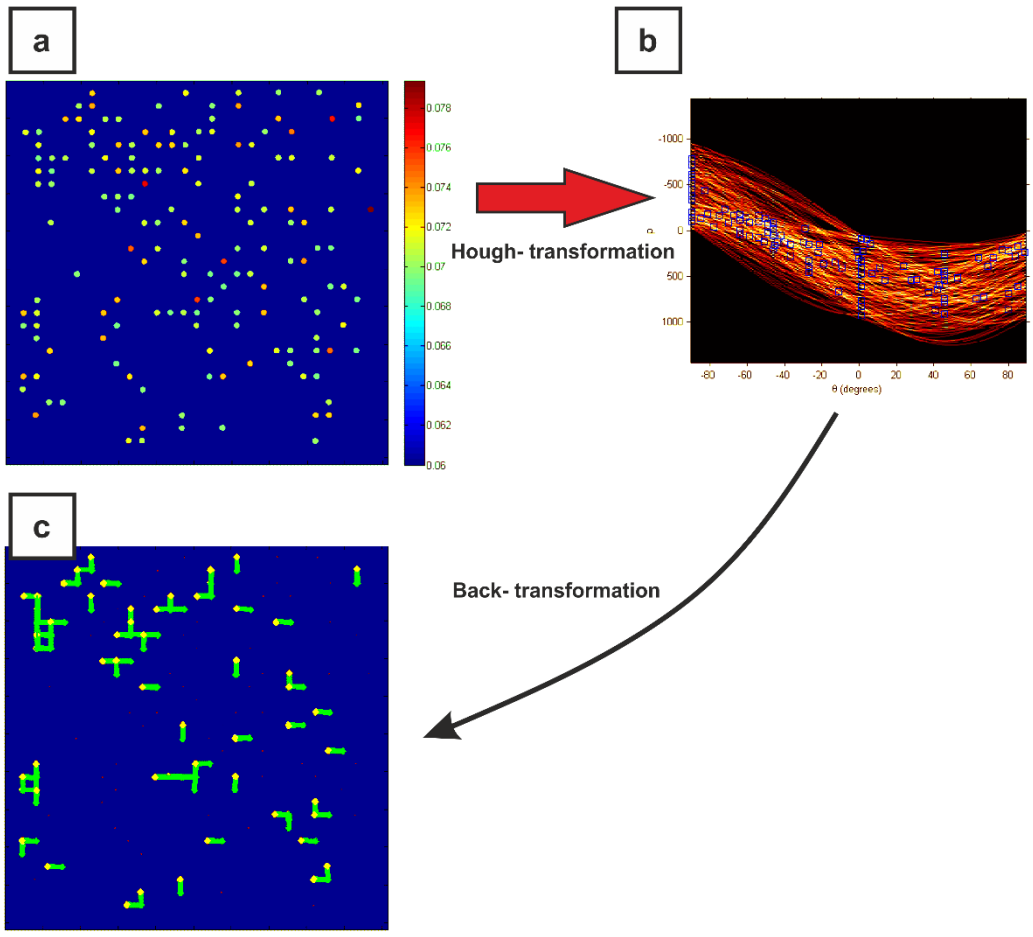

Fig.2: (a) Position plot of group V columns with the highest intensity (defined by dashed line in the histogram figure 1 (b)) and corresponding Hough- transformation (b). The blue squares mark the Hough- peaks which are used for the back- transformation to detect lines in the position plot (c).

Summary & Outlook

We developed a method for STEM HR HAADF measurements which allows us to detect ordering of Bi atoms in dilute bismide Ga(AsBi) layers on an atomic scale. This method is based on the Hough- transform and allows us to detect Bi pairs as well as “chain”- like structures in growth direction and perpendicular to it. The next step is to decide what kind of Bi ordering is present in the Ga(AsBi) layers, because one has to keep in mind that STEM HAADF measurements are always a two dimensional projection of three dimensional layers. Therefore there are many possibilities how Bi atoms could order in a three dimensional layer and real “chain”- like ordering, where the Bi atoms are in the same plane next to each other, is not automatically the only one possibility. For this reason we will construct supercells with different kind of Bi- “chains” and perform STEM HAADF simulations, to compare and to find the best fit between experiment and simulation.

References

[1] K. Alberi et al., *Phys. Rev. B* **75**, 04523 (2007)
[2] E. Sterzer et al., *J. Cryst. Growth* **408** (2014), pp. 71-77
[3] P. Ludewig et al., *J. Cryst. Growth* **396** (2014), pp. 95-99
[4] L. Jones et al., *Advanced Structural and Chemical Imaging* (2015) 1:8
[5] P. Hough, *U.S. Patent* 3 069 654 (1962)

Optical Spectroscopy on Organic-Inorganic Hybrids

Ingo Meyenburg, Jane Falgenhauer**, Christian Prinzisky*, Nils Rosemann, Andrea Karthäuser, Tobias Breuer, Jörg Sundermeyer*, Derck Schlettwein**, Gregor Witte, Wolfram Heimbrodt

Faculty of Physics and Material Sciences Center, Philipps-Universität Marburg
**Department of Chemistry, Philipps-Universität Marburg*
***Institute of Applied Physics, Justus-Liebig-University Gießen*

Introduction

In recent years organic semiconductors have attracted considerable attention because of their unique optical, electronic and mechanical properties. It has been shown for example that organic-inorganic hybrids like p-type Pentacene on ZnO are feasible to prepare p-n-junction. Understanding interface processes is crucial for improvements of existing and new functional materials based on organic-inorganic hybrids. Optical measurements help to understand the properties of hybrid structures including the interface.

Results

Dye sensitized solar cells are based on an efficient charge transfer (CT) from organic molecules to inorganic semiconductors after photon absorption. In the project we study the resulting CT excitons. Promising hybrid systems are indoline [1][2] and anthraquinone [3] based dyes on inorganic substrates.

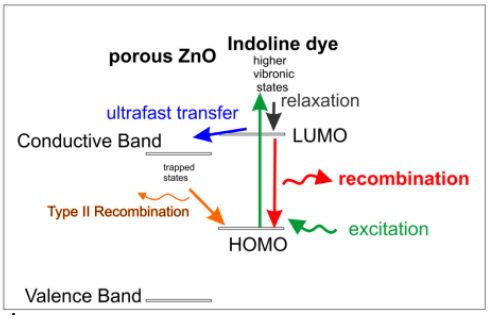

Fig. 1: Level alignment of indoline dye on mesoporous ZnO.

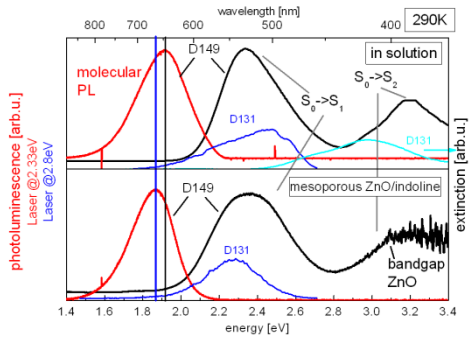

Fig. 2: Comparison of indoline dyes D149 and D131 in absorption and photoluminescence.

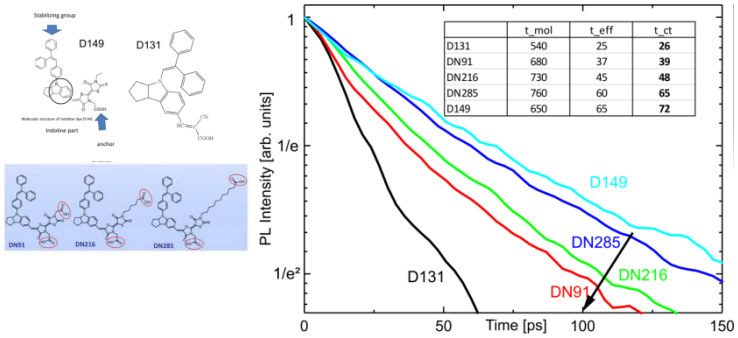

	t_mol	t_eff	t_ct
D131	540	25	26
DN91	680	37	39
DN216	730	45	48
DN285	760	60	65
D149	650	65	72

Fig. 3: (left) Molecular structures of indoline, prepared by J. Falgenhauer (AG Schlettwein, Uni Giessen)
(right) Time resolved photoluminescence of various indoline dyes. The decay is determined by the fast electron transfer across the organic inorganic interface. D131 injects a lot faster than D149. Obviously, the longer the molecular anchor the slower the electron transfer time.

*Fig. 4: (a) The optical absorption and photoluminescence spectra of **Anthraphenol** molecules in solution and on mesoporous TiO_2.*
(b) PL and absorption of a single crystal. The crystal formation results in red-shifted PL spectra. In the absorption spectra a strong linear polarization of the excitonic band was found.

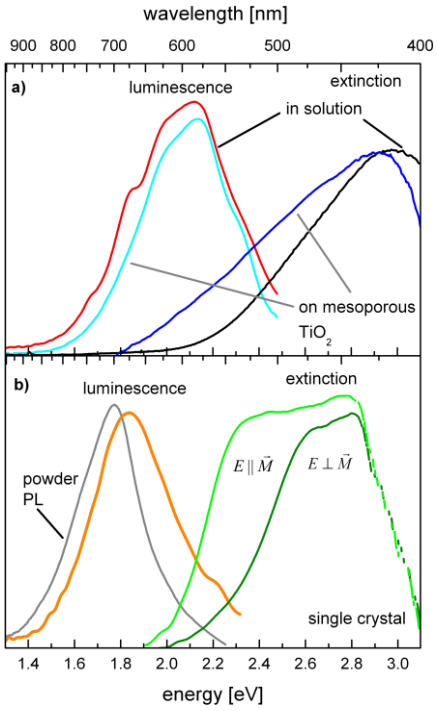

Synthesization of Anthraquinone based molecular variations done by C. Prinzisky (AG Sundermeyer) [3].

Different crystallographic phases of pentacene either as layer on ZnO or as bulk crystal have been studied.

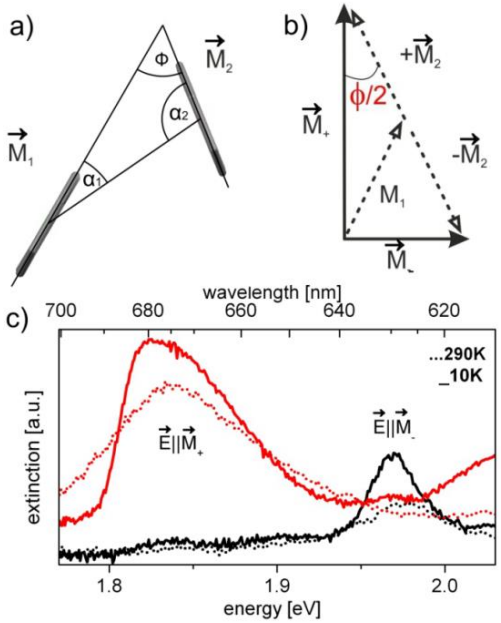

Fig. 5: (a) The herringbone angle Φ between both molecules in the unit cell. (b) Schematic formation of the dimer moments, which are perpendicular to each other. (c) The polarized absorption spectra for the pentacene Siegrist phase at room temperature and 10K.

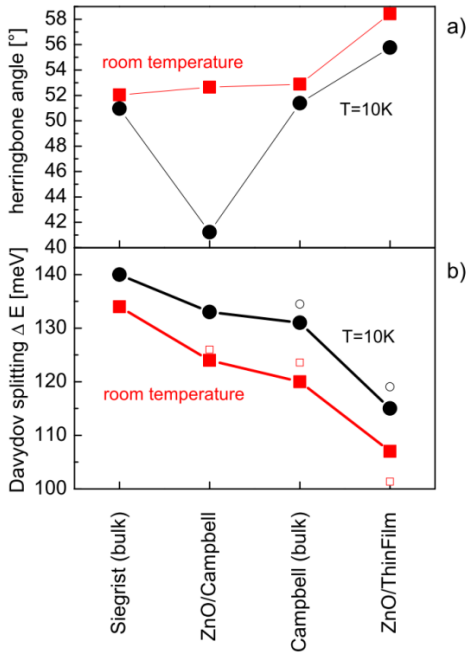

Fig. 6: (a) The herringbone angle for the different crystalline phases of pentacene. (b) The excitonic Davydov splitting at T=300K (red) and T = 10 K (black). experimental (full symbols); calculated in a dipole model (open symbols)

Conclusions and outlook

Time resolved PL allows for the determination of the level alignment at the interface. The LUMO of D131 lies higher above the ZnO conductive band compared with D149. The influence of the anchoring carboxylate chain length on the charge transfer has been revealed. Next we will search for the spatially indirect type II excitons, which will enable a detailed study of the organic-inorganic Interface.

References

[1] E. Rohwer, ChemPhysChem, 14 (2013) 132 and 16 (2015) 943
[2] M. Rudolph, J. Phys. Chem. C 119 (2015), 1298
[3] C. Prinzisky, submitted (2015)

Development and application of a combined energy and density decomposition method to analyze chemical bonding for extended systems

Marc Raupach, Ralf Tonner

Faculty of Chemistry, Philipps-Universität Marburg

The knowledge about chemical bonding and reactivity helps to understand and predict reactions mechanisms in molecular systems. Here, the investigation of chemical bonds by means of an energy decomposition analysis (EDA) allows the partition of the interaction energy ΔE_{int} into chemical and physical meaningful parts. Thereby ΔE_{int} is defined as the energy difference between a compound A-B and its structurally unrelaxed fragments A and B.

Ziegler and Rauk proposed an EDA scheme, based on the transition state (TS) method, which decomposes ΔE_{int} into a Pauli repulsion part, ΔE_{Pauli}, an electrostatic, ΔE_{elstat}, and an orbital relaxation term, ΔE_{orb}.[1] Recently, the dispersion energy term, ΔE_{disp}, was introduced to take van-der-Waals type interactions between fragments into account.

$$\Delta E_{int} = \Delta E_{Pauli} + \Delta E_{elstat} + \Delta E_{orb} + \Delta E_{disp} \quad (1)$$

The EDA method was later extended by Mitoraj and Ziegler to include natural orbitals for chemical valence (NOCV), in order to decompose the orbital relaxation term into principal contributions.[2] This leads to quantification of σ and π symmetric orbital interactions by means of the associated NOCV deformation densities, $\Delta\rho_i$, and the energies ΔE_i. (See Scheme 1) The combined method is called EDA-NOCV.

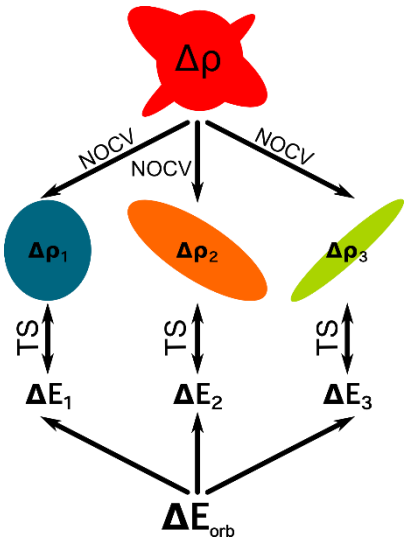

Scheme 1: *Schematic description of the energy and density decomposition of the orbital interaction term within the EDA-NOCV scheme.*

With the aim to transfer the capabilities of the EDA and EDA-NOCV methods from molecular to extended systems, we developed the periodic EDA (pEDA)[3] and the periodic EDA-NOCV (pEDA-NOCV)[4], which are implemented in the density functional theory (DFT) based program package BAND[5].

Now the analysis of chemical bonding for one, two and three dimensional systems is possible. As an example of a surface-adsorbate interaction, the bond between of acetylene and a Si(001) substrate was analysed. (See Fig. 1a) Here, the interaction energy amounts

to -660 kJ mol^{-1} (PBE-D3/TZ2P). According to the pEDA results, the chemical bond is dominated by covalent character (-1153 kJ mol^{-1}), compared to the electrostatic term (-817 kJ mol^{-1}). The dispersion interaction is negligible (-12 kJ mol^{-1}). These attractive energy terms are opposed to the repulsive Pauli repulsion term, which amounts to +1321 kJ mol^{-1}.

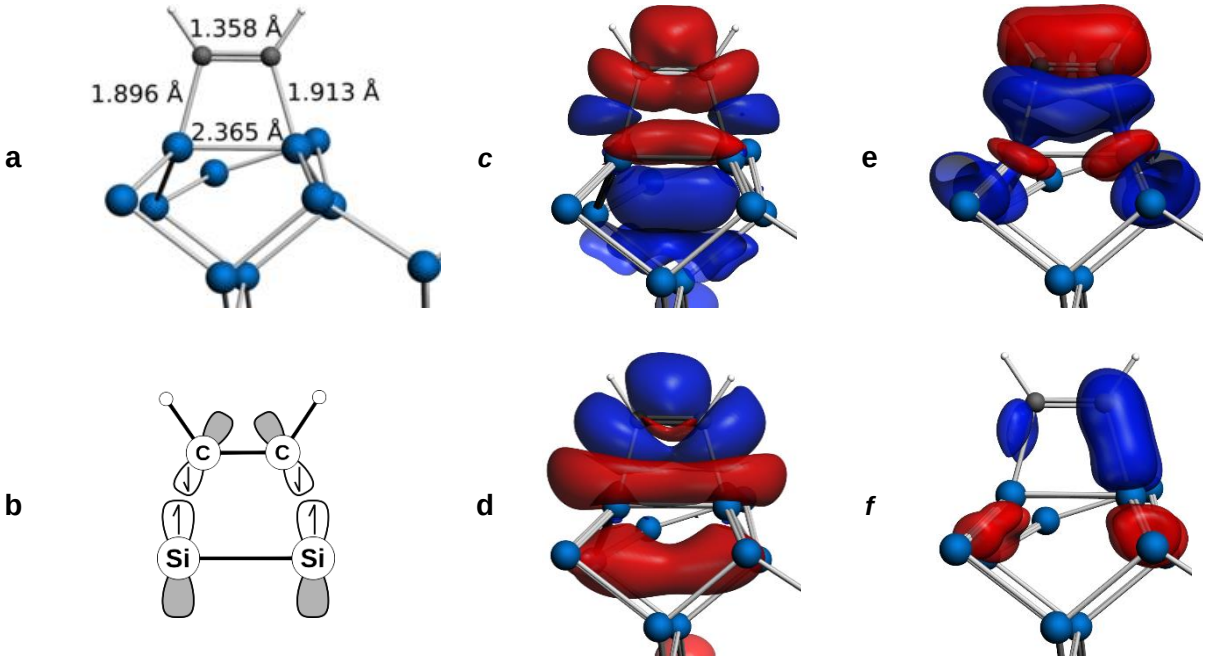

Fig. 1: *(a) Adsorption of acetylene on a Si(001) surface and (b) fragmentation for the pEDA-NOCV. Deformation densities for σ (c and d) and π (e and f) symmetric interactions between acetylene and the Si surface (charge flow from red to blue).*

The pEDA-NOCV result shows that the covalent interaction between molecule and surface is dominated by the σ symmetric shared electron bond (-1003 kJ mol^{-1}, Fig. 1c and 1d) compared to the π symmetric donor acceptor interactions (-96 kJ mol^{-1}, eg. Fig. 1e and 1f). Here, the deformation densities show that molecule and surface exhibit two shared-electrons σ bonds. In the case of the π bonds, solely the acetylene fragment is donating electrons into the bonding region.

The new methods, pEDA and pEDA-NOCV, allow for a detailed analysis of the chemical bond for extended systems. Especially the visualization and discussion of the deformation densities, and theirs associated energies, will improve the understanding of surface reactivity and will lead to rationalization of known reactions and prediction of yet unknown compounds.

References

[1] T. Ziegler and A. Rauk, *Inorg. Chem.* **18**, 1558 (1979).
[2] M. Mitoraj, A. Michalak and T. Ziegler, *J. Chem. Theo. Comp.* **5**. 962 (2009).
[3] M. Raupach and R. Tonner, *J. Chem. Phys.* **142**, 194105 (2015).
[4] M. Raupach, T. Ziegler and R. Tonner, *in preparation*.
[5] P. H. T. Philipsen, G. teVelde, E. J. Baerends, P. L. de Boeij, J. A. Groeneveld, E. S. Kadantsev, R. Klooster, F. Kootstra, P. Romaniello, D. G. Skachkov, J. G. Snijders, G.Wiesenekker and T. Ziegler, BAND2012 (developer version), SCM, Theoretical Chemistry, Vrije Universiteit, Amsterdam, The Netherlands.

Thermal quenching of photoluminescence in disordered Ga(AsBi)

M. K. Shakfa, M. Wiemer, P. Ludewig, K. Jandieri, K. Volz,
W. Stolz, S. D. Baranovskii, and M. Koch

Department of Physics and Material Sciences Center, Philipps-University of Marburg, Renthof 5, 35032 Marburg, Germany

Introduction

Ga(AsBi) ternary semiconductor alloys have attracted increasing attention in the scientific community because of their interesting physical properties. In particular, a large reduction of the energy band gap as high as 62-88 meV/%Bi is possible for a very small amount of Bi introduced into GaAs [1]. This makes Ga(AsBi)-based structures attractive for long-wavelength optoelectronic applications such as optically pumped- [2] and electrically injected [3] laser diodes. On the other hand, the incorporation of Bi atoms into GaAs results in a certain degree of disorder. The latter results in an increase in the density of localized states (DOS) and, hence, lead to a significant change in carrier dynamics which can be translated in, e.g., peculiar photoluminescence (PL) characteristics.

we present a comparative study of the experimental and theoretical thermal quenching of the PL intensity in $Ga(As_{1-x}Bi_x)/GaAs$ heterostructures measured under relatively low excitation conditions. The structures used in this study were grown by metal-organic vapour-phase epitaxy (MOVPE) at a growth temperature of 400 °C. The Bi content is varied from 2.9% to 4.5%. The PL excitation source is a pulsed Ti:sapphire laser tuned to 780 nm. The PL emission signal is detected using a streak camera.

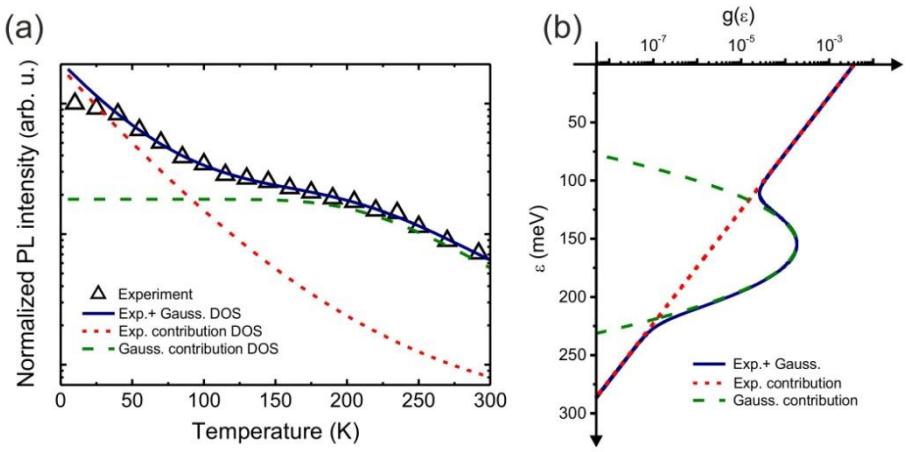

***Fig.1**: (a) Temperature-dependent PL intensity of a $Ga(As_{0.958}Bi_{0.042})/GaAs$ heterostructure. Open triangles indicate experimental results. The solid line is theoretically calculated assuming a combination of exponential (Exp.) and Gaussian (Gauss.) distribution of localized states. (b) Density of localized states as a function of the energy difference from the mobility edge.*

Results

The temperature dependences of the PL intensity in disordered semiconductors usually demonstrate three distinct regions: a relatively weak temperature dependence at low temperatures, a considerable decrease of the PL intensity in a middle temperature range followed by the saturation at room temperature. This common behavior has been observed also in Ga(AsBi), though under high excitation powers [4]. In our experiments performed at a relatively low excitation power, the PL intensity decreases with increasing temperature in a different way: a pronounced plateau appears in the intermediate temperature range as illustrated in Fig. 1(a). The thermal quenching of the PL intensity in Ga(AsBi) at high

excitation powers has been explained by employing a theoretical model with a single-scale monotonously energy-dependent DOS [5]. In contrast, our theoretical analysis [6], based on the well approved theoretical approach, shows that the observed anomalous plateau in the PL thermal quenching cannot be reproduced assuming such monotonous DOS. Experimental data clearly point at a non-monotonous DOS with at least two energy scales illustrated in Fig. 1(b) by the solid line. The solid line in Fig. 1(a) shows an example of the theoretical simulation for the DOS given in Fig. 1(b).

Conclusions

The PL thermal quenching in MOVPE-grown Ga(AsBi)/GaAs heterostructures with different Bi contents has been studied experimentally and theoretically. Under relatively low excitation conditions, the PL intensity is nearly temperature-independent in the intermediate temperature range. Our theoretical study demonstrates that a two component DOS of the band-tail is indispensable in order to reproduce this plateau in the temperature-dependant PL intensity.

Outlook: what is planned

It is planned to study the influence of the Bi content on some other disorder-induced PL features in $Ga(As_{1-x}Bi_x)/GaAs$ heterostructures, e.g. the temperature-dependent PL peak energy. Since disorder affects the optical properties of a semiconductor, such a study is very important in order to quantify the disorder degree in Ga(AsBi) alloys.

References

[1] M. K. Shakfa, D. Kalincev, X. Lu, S. R. Johnson, D. A. Beaton, T. Tiedje, A. Chernikov, S. Chatterjee, and M. Koch, “Quantitative study of localization effects and recombination dynamics in GaAsBi/GaAs single quantum wells,” J. Appl. Phys. 114, 164306 (2013).

[2] Y. Tominaga, K. Oe, and M. Yoshimoto, “Low Temperature Dependence of Oscillation Wavelength in GaAs1-xBix Laser by Photo-Pumping,” Appl. Phys. Express 3, 062201 (2010).

[3] P. Ludewig, N. Knaub, N. Hossain, S. Reinhard, L. Nattermann, I. P. Marko, S. R. Jin, K. Hild, S. Chatterjee, W. Stolz, S. J. Sweeney, and K. Volz, “Electrical injection Ga(AsBi)/(AlGa)As single quantum well laser,” Appl. Phys. Lett. 102, 242115 (2013).

[4] S. Imhof, A. Thränhardt, A. Chernikov, M. Koch, N. S. Köster, K. Kolata, S. Chatterjee, S. W. Koch, X. Lu, S. R. Johnson, D. A. Beaton, T. Tiedje, and O. Rubel, “Clustering effects in Ga (AsBi),” Appl. Phys. Lett. 96, 131115 (2010).

[5] O. Rubel, S. D. Baraovskii, K. Hantke, W. W. Ruhle, P. Thomas, K. Volz, and W. Stolz, “Model of temperature quenching of photoluminescence in disordered semiconductors and comparison to experiment,” Phys. Rev. B 73, 233201 (2006).

[6] M. K. Shakfa, M. Wiemer, P. Ludewig, K. Jandieri, K. Volz, W. Stolz, S. D. Baranovskii, and M. Koch, “Thermal quenching of photoluminescence in Ga(AsBi),” J. Appl. Phys. 117, 025709 (2015).

Synthesis of charge transfer self-complementary Pentacenes

F. Wagner, U. Koert

Institute of organic Chemistry, Philipps-Universität Marburg

Introduction

Based on the staggered orientation of 1,3,5-trinitrobenzene with N^1,N^1,N^3,N^3,N^5,N^5-hexamethylbenzene-1,3,5-triamine, we envisioned a substituted pentacene derivative which could unify this structural motif in a single molecule. The synthesis of molecule **1** (Fig. 1) is the target of this work.

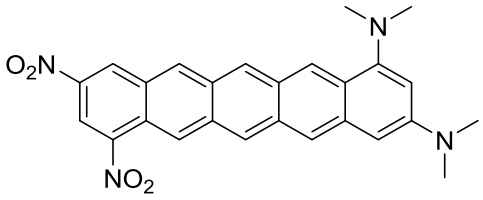

1

*Fig.1: target molecule **1**.*

Our retrosynthetic approach is based on the coupling of two naphthalene derivatives **3** and **4** which are both formed by derivatisation of naphthalene **2**. Later, aromatization of pentacene quinone **5** has to be achieved (Fig 2).

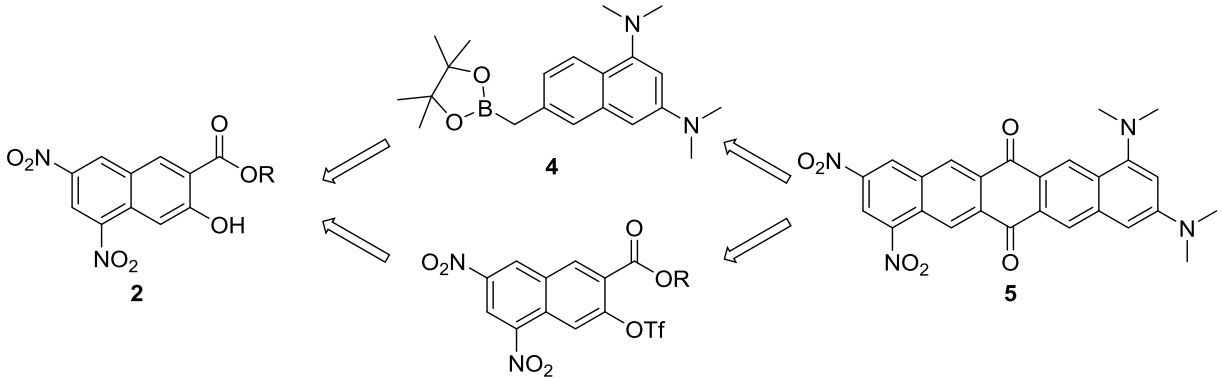

Fig.2: retrosynthetic approach.

Results

The synthesis of **2** was achieved by reduction and re-oxidation of commercial available benzoic acid **6**. The resulting aldehyde **7** was protected as acetal **8**. This acetal was subjected to a novel cross-coupling protocol with a bis silyl enol ether **9** to yield the dicarbonyl compound **10**. Cleavage of the acetal under acidic conditions results in naphthalene **2** (Fig. 3).

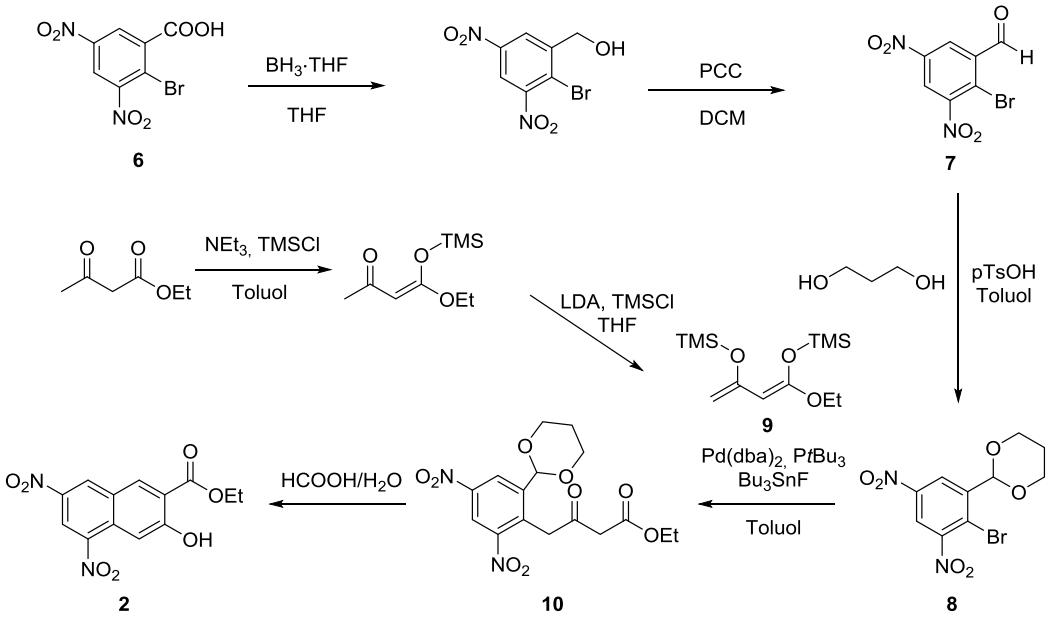

*Fig. 3: synthesis of **2**.*

Naphtalene **2** is then converted into the triflate, to yield the electron deficient building block **3**. This can be reduced to the diamine **11**. Removal of the triflate by hydrogenolysis and reductive amination yields **12**, which can be reduced to a precursor (**14**) of the electron rich building block **4**.

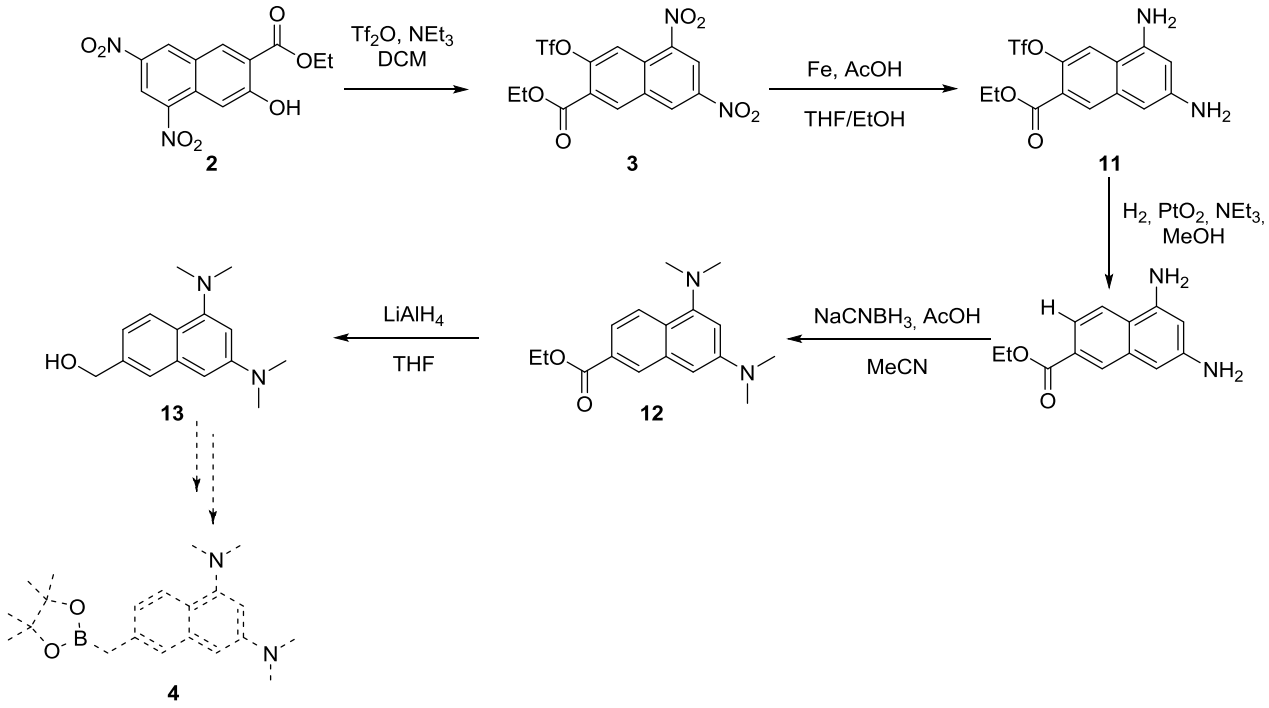

*Fig. 4: Derivatisation of **2**.*

Conclusions

Until now, the synthesis and derivatisation of substituted naphtalenes was successful. A novel cross-coupling protocol which can be applied to several substrates was also developed.

Outlook

Our plan is now to connect both building blocks via cross-coupling chemistry. While **2** already bears a suitable functional group (triflate) for this kind of transformation, the synthesis of the transmetallating species of **4**, bearing for a example a boronic ester moiety, has not been achieved yet.

Ga(NAsP)-layers in Si-based Laser Structures Investigated by HRSTEM

T. Wegele[1], A. Beyer[1], P. Ludewig[1], K. Jandieri[1], P. Rosenow[2], R. Tonner[2], W. Stolz[1] and K. Volz[1]

1. *Material Sciences Center and Faculty of Physics, Philipps-Universität Marburg*
2. *Faculty of Chemistry and Materials Science Center, Philipps-Universität Marburg*

Introduction

Our investigations in the framework of the GRK „Functionalization of Semiconductors“ are focused on the quantitative analysis of such dilute quaternary semiconductor materials as Ga(NAsP) grown by metal organic vapour phase epitaxy (MOVPE) under metastable growth conditions. This material is of particular interest because it can be grown lattice-matched to Si and has a tunable band-gap [1,2]. Lasing of structures containing Ga(NAsP)-layers on GaP-substrates up to room temperature as well on (001) Si substrates at low temperatures was already reported in [3,4], what reveals very promising potential of Ga(NAsP) as an active layer of an efficient and stable laser on (001) Si. The quality of an active layer is very strongly connected to the performance of optoelectronic device and should be optimized by variation of growth conditions. One of the most important characterization techniques is the scanning transmission electron microscopy (STEM), which allows comparison of the layers grown at different conditions at atomic scale.

Results

To be able to compare different layers some characteristics should be defined. Here we restricted the comparison to two of possible characteristics: interface roughness and compositional fluctuation in dependence on nominal quantum well (QW)-thickness and growth temperature.

The investigations were fulfilled using double-Cs-corrected JEOL JEM 2200 FS in scanning mode at 200 kV. In order to distinguish the impact of QW-components with different atomic numbers Z on the intensities in STEM-micrographs [5] and to describe their distribution separately different ranges of the detector angles, starting at low, middle and high inner detector angles, were chosen for the measurements.

For the evaluation of the experimental results a program was written, which includes normalization to the electron beam according to [6], thickness gradient correction, detection of the QW-region in the STEM-micrograph, determination of the mean thickness and standard deviation from this thickness defined as absolute roughness, calculation of standard deviation of mean QW-intensity in each pixel of a STEM-image visualized in compositional fluctuation map (Fig.1).

According to this evaluation interface roughness, absolute as well relative, and compositional fluctuation show just negligible dependence on the QW-nominal thickness. However, the variation of the growth temperature has more influence on the characteristics of the quality of a layer: on the one hand, higher growth temperature leads to a higher absolute and relative interface roughness; on the other hand, the QWs grown at higher temperatures have more homogeneously distributed components. Furthermore, the investigations at different ranges of detector angles reveal that N-atoms are distributed more inhomogeneously than As-atoms in the Ga(NAsP)-QWs.

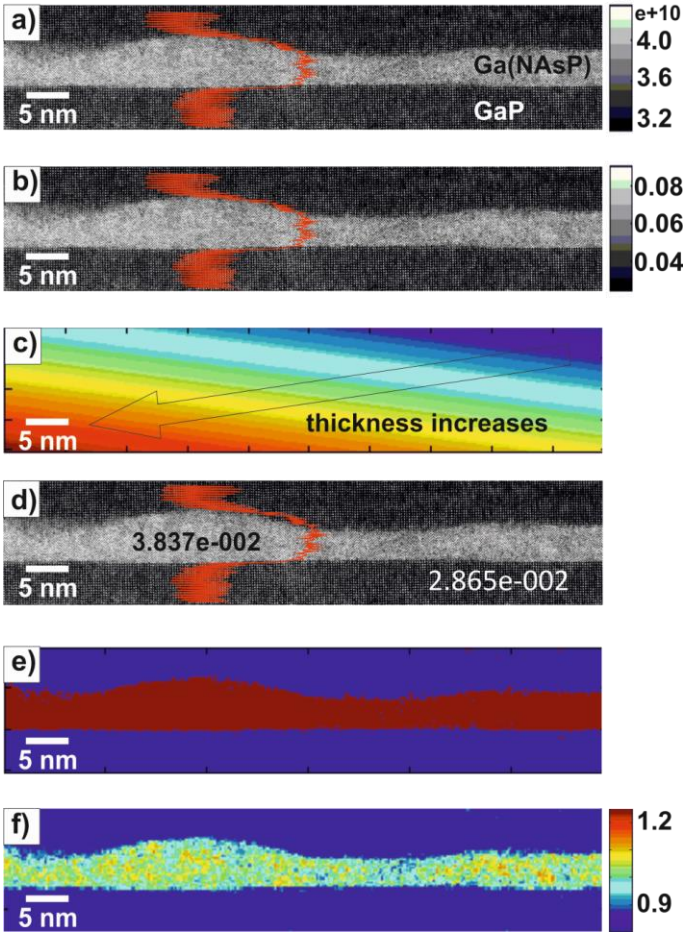

Fig.1: Step-wise evaluation of ADF-STEM images: a) The raw STEM-image (in this case at 50 mrad inner detector angle) is normalized b) to the electron beam intensity. The grey scale units are then fractions of the impinging beam intensity. The red intensity profiles parallel to the growth direction visualize the higher intensity in the Ga(NAsP)-QW and lower intensity in neighbouring GaP-barriers as well as thickness increase from top to bottom. c) The 2-D thickness gradient is detected, visualized and corrected. d) The STEM-image without a thickness gradient can be used for quantitative evaluation. e) The Ga(NAsP)-QW region is detected (red) as well as the GaP-barriers are identified (blue). f) Shows the according quantitative map of composition fluctuation. The growth direction is in all images from bottom to top.

Conclusions

In contrast to the nominal QW-thickness the growth temperature has significant and very interesting influence on the interface roughness and compositional fluctuation. The first one increases for higher growth temperature, whereas the letter decreases so the QWs become more homogeneous. That reveals the change of the metastable character of Ga(NAsP)-material what was verified by DFT calculations.

Outlook

On further interest is to obtain knowledge about the width of the intermixing layer between Ga(NAsP)-QW and GaP-barrier and to prove using DFT-calculations whether it is an energetically most favourable one. Moreover, the use of STEMsim-software [7] and optimization of specimen preparation will allow to determine the composition of each atomic column in the Ga(NAsP)-QW.

References

[1] B. Kunert, K. Volz, J. Koch, W. Stolz, Direct-band-gap Ga(NAsP)-material system pseudomorphically grown on GaP substrate, Appl. Phys. Lett. 88 (2006) 1–4. doi:10.1063/1.2200758.

[2] B. Kunert, S. Zinnkann, K. Volz, W. Stolz, Monolithic integration of Ga(NAsP)/(BGa)P multi-quantum well structures on (001) silicon substrate by MOVPE, J. Cryst. Growth. 310 (2008) 4776–4779. doi:10.1016/j.jcrysgro.2008.07.097.

[3] N.W. Rosemann, B. Metzger, B. Kunert, K. Volz, W. Stolz, S. Chatterjee, Temperature-dependent quantum efficiency of Ga(N,As,P) quantum wells, Appl. Phys. Lett. 103 (2013). doi:10.1063/1.4852575.

[4] S. Liebich, M. Zimprich, A. Beyer, C. Lange, D.J. Franzbach, S. Chatterjee, et al., Laser operation of Ga(NAsP) lattice-matched to (001) silicon substrate, Appl. Phys. Lett. 99 (2011) 10–13. doi:10.1063/1.3624927.

[5] V. Grillo, K. Müller, F. Glas, K. Volz, A. Rosenauer, Toward Simultaneous Assessment of In and N in InGaAsN Alloys by Quantitative STEM-ADF Imaging, Microsc. Microanal. 17 (2011) 1862–1863. doi:10.1017/S143192761101018X.

[6] J.M. LeBeau, S. Stemmer, Experimental quantification of annular dark-field images in scanning transmission electron microscopy, Ultramicroscopy. 108 (2008) 1653–1658. doi:10.1016/j.ultramic.2008.07.001.

[7] A. Rosenauer, M. Schowalter, STEMSIM - A New Software Tool for Simulation of STEM, Microsc. Semicond. Mater. 2007. 120 (2008) 170–172. doi:10.1007/978-1-4020-8615-1_36.

Carrier Dynamics in (BGa)(NAsP)-materials on silicon

R. Woscholski, K. M. Shafka, S. Gies, A. Rahimi-Iman, W. Stolz, W. Heimbrodt, M. Koch

Faculty of Physics and Material Sciences Center, Philipps-Universität Marburg

Introduction

The goal of my work performed in the framework of the GRK *functionalization of semiconductors* is to investigate the carrier dynamics of metastable nitrogenous and boracic III/V semiconductors on Silicon, fabricated in the framework of the GRK.

Work and Results

Due to its quaternary nature this material system is very prone to disorder. Compositional fluctuations and nitrogen related clusters as well as imperfect interfaces and varying quantum well width can raise the disorder potential. This can affect the carrier dynamics of the semiconductor and, hence, its performance in devices applications. The disorder in a material is determined by its growth conditions, composition and the annealing process. During the last year I have been investigating by means of time-resolved photoluminescence (TR-PL) spectroscopy both, the effects of different temperatures during rapid thermal annealing (RTA) and the effects of different growth temperatures, on the optical properties and carrier dynamics in Ga(NAsP) Multi-Quantumwells (MQWHs) grown on silicon substrate.

The measurements for the samples annealed at different temperatures in the range of 850°C to 975 °C show an enhancement in the PL efficiency when the annealing temperature is increased up to 925 °C. However, when the annealing temperature is further raised, the PL intensity dramatically decreases. This is explained by the variation of the disorder degree in the studied structures. The analysis of the low-temperature emission-energy-dependent PL decay time can be used to characterize the disorder in the Ga(NAsP) MQWHs with the (very much simplified) model suggested by Gourdon and Lavallard. The theoretically extracted energy-scales of disorder confirm the experimental observations.

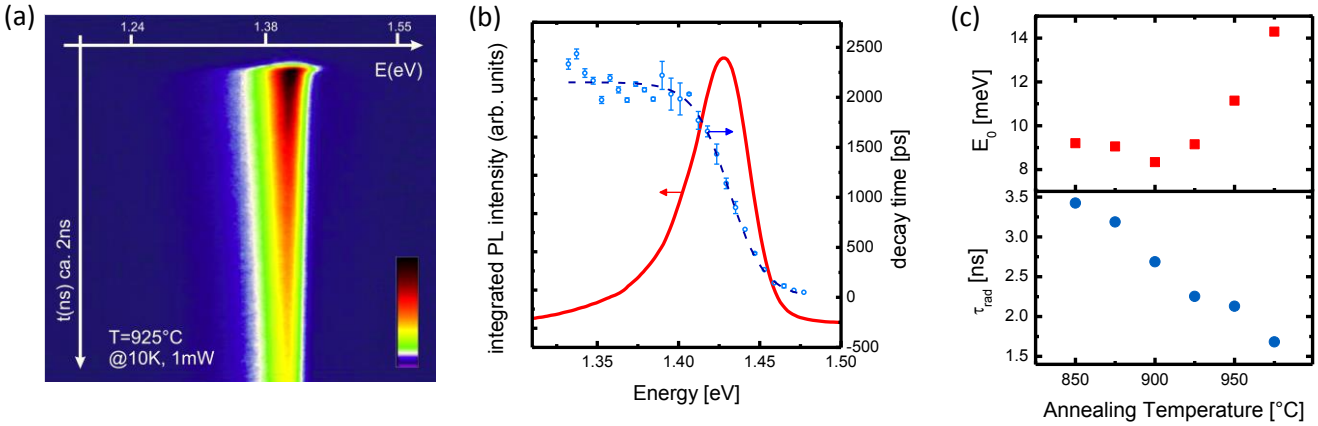

Figure 1: *(a) timeresolved photoluminescence spectrum*
(b) emission energy dependence of the decay time
(c) theoretically extracted parameters from the model suggested by Gourdon and Lavallard for different annealing Temperatures: E_0 *is a characteristic energy for the density of states and* τ_{rad} *is the radiative recombination lifetime*

The use of different growth temperatures leads to different As and P contents in the QW material, while the N content stays nearly constant at 8% between 565°C - 650°C. The variation in composition leads to a blueshift of the PL maximum. The optimal growth temperature with respect to high PL intensity, small linewidth and small disorder energy scale was found between 575°C - 605°C. The disorder-energy-scale parameters were extracted from the characteristic temperatures of the s-shape for the short range disorder, which is mainly due to compositional fluctuations, and from the rise of the exponential slope of the lower-energy side of the PL spectrum for the long-range disorder which is attributed to interface imperfections.

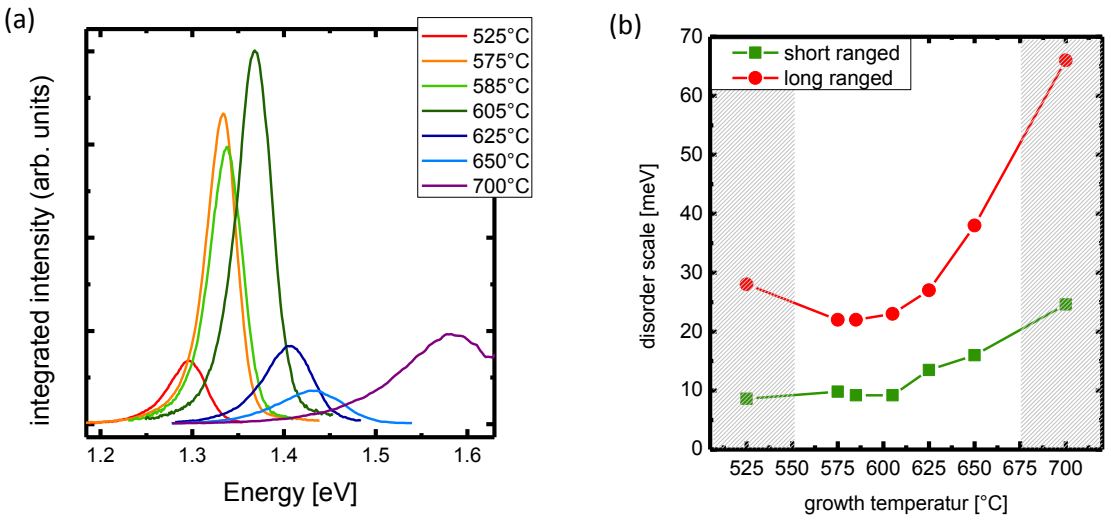

Figure 2: (a) time-integrated photoluminescence spectrum for different growth temperatures
(b) disorder energy scales for different growth temperatures

Conclusion and Outlook

The time resolved photoluminescence measurements reveal a strong connection between the carrier dynamics on the one hand and the sample composition as well as the disorder energy scale on the other hand. For a better understanding, different scattering processes and carrier loss channels must be taken into account. Further TR-PL-measurements are planned to identify the influence of the nitrogen content, as well as pump-probe measurements on GaNAsP QW structures to observe the carrier dynamics by means of transient-absorption.

Teilnehmer GRK-Seminar
vom 07.10. - 09.10.2015 in Hofheim

Beyer	Andreas	Dr.
Bo Hamud	Taman	
Dobener	Florian	
Duschek	Lennart	
Eußner	Jens	
Finger	Lars	
Gies	Sebastian	
Gupta	Shalini	
Kraft	Lars	
Lammers	Christian	
Nattermann	Lukas	
Oelerich	Jan Oliver	
Ostapenko	Alexandra	
Pick	Andre	
Prinzisky	Christian	
Pulz	Susanne	
Reutzel	Marcel	
Ringler	Benjamin	
Rinn	Niklas	
Röder	Johannes	
Rosemann	Nils	
Rosenow	Phil	
Rotter	Paul	
Sabir	Nadeem	
Springer	Phillip	
Stegmüller	Andreas	Dr.
Sterzer	Eduard	
Valkovski	Vitalii	
Völkner	Johannes	
Wagner	Frederic	
Werner	Katharina	
Wiemer	Martin	
Wilhelm	Mikko	

Chatterjee	Sangam	PD Dr.
Dehnen	Stefanie	Prof. Dr.
Dürr	Michael	Prof. Dr.
Eckhardt	Bruno	Prof. Dr.
Göbel	Ernst O.	Prof. Dr.
v. Hänisch	Carsten	Prof. Dr.
Heimbrodt	Wolfram	Prof. Dr.
Höhnsdorf	Falko	Dr.
Koert	Ulrich	Prof. Dr.
Mogilatenko	Anna	Dr.
Stolz	Wolfgang	Dr. habil.
Sundermeyer	Jörg	Prof. Dr.
Tonner	Ralf	Dr.
Volz	Kerstin	Prof. Dr.
Witte	Gregor	Prof. Dr.

Schnepf	Andreas	Prof. Dr.
Schulz	Axel	Prof. Dr.